

Long liquid slugs in horizontal tubes

Development study and characterisation
with electrical conductance techniques

Long liquid slugs in horizontal tubes

Development study and characterisation
with electrical conductance techniques

PROEFSCHRIFT

ter verkrijging van de graad van doctor
aan de Technische Universiteit Delft,
op gezag van de Rector Magnificus prof. dr. ir. J. T. Fokkema,
voorzitter van het College voor Promoties,
in het openbaar te verdedigen op
vrijdag 21 december 2007 om 12.30 uur

door

Marco Leendert Zoetewij

natuurkundig ingenieur
geboren te Goes

Dit proefschrift is goedgekeurd door de promotoren:

Prof. dr. R.V.A. Oliemans

Prof. dr. R.F. Mudde

Samenstelling promotiecommissie:

Rector Magnificus, voorzitter

Prof. dr. R.V.A. Oliemans

Technische Universiteit Delft, promotor

Prof. dr. R.F. Mudde

Technische Universiteit Delft, promotor

Prof. dr. B.J. Azzopardi

University of Nottingham, UK

Prof. dr. ir. G. Ooms

Technische Universiteit Delft

Prof. dr. ir. G.J.F. van Heijst

Technische Universiteit Eindhoven

Prof. dr. ir. H.E.A. van den Akker

Technische Universiteit Delft

Prof. dr. ir. H.W.M. Hoeijmakers

Universiteit Twente

The work in this thesis was supported by Technologiestichting STW

Cover design by:

SRP Strategie in Reclame en Promotie

Johan van Reigersbergstraat 41

4336 XB Middelburg

www.srp.nl

Printed by:

PrintPartners Ipskamp

Postbus 333

7500 AH Enschede

www.ppi.nl

ISBN 978-90-9022512-8

Keywords: two-phase flow, gas-liquid, long slugs, hydrodynamic slugging

© 2007 M.L. Zoetewij

All rights reserved. No part of the material protected by this copyright notice may be reproduced or utilized in any form or by any means, electronic or mechanical, including photocopying, recording, or by any information storage and retrieval system without written permission from the publisher.

Yesterday is history, tomorrow is a mystery

Today is a gift, that's why we call it present

Summary

Long liquid slugs in horizontal tubes

Development study and characterisation with electrical conductance techniques

In many industrial applications, two phase flows are present. Depending on the velocities of the two phases, different flow patterns may occur. One of these types is the slug flow pattern, in which the liquid is transported as blocks with high velocity. In the current study air and water are used.

Within the regime of the liquid slugs, a distinction can be made between the short hydrodynamic slugs, with lengths of 40 tube diameters ($40D$) at maximum, and the longer slugs, which can reach lengths of over $400D$. A lot of research is done in the last decades on the short slugs, of which the behavior is quite regular and relatively easy to predict. The other type of slugs, which can reach much larger lengths, can give more problems in industry, since the behavior of these kind of slugs is difficult to predict. This study focuses on the understanding of the processes in the long slug regime, which has not been studied in such detail before.

In a 137 m long ($L/D = 2740$) set-up with 5.2 cm inner diameter (2"), experiments were done with air (atmospheric pressure) and water for flow conditions in both the hydrodynamic and the long slug region. For gas velocities $U_{sg} \geq 2.5$ m/s, the transition goes directly from stratified flow to the short hydrodynamic slugs. For lower gas velocities, the transition goes via the long slug regime. For increasing liquid velocity, the slug length decreases, and the short slugs will be formed for sufficiently high liquid velocities.

With electrical conductance techniques, the properties of the slugs are determined. The tail of the slug moves with constant velocity through the pipe. This velocity is the same for all slugs being formed, and is independent of the position along the tube.

The slugs can grow by picking up liquid at the front from the stratified layer they move over. The front of a growing slug moves faster than its tail. As long as liquid is available at the slug front, the slug can grow. There is a minimum liquid level, indicated by the minimum hold-up environment, below which the slug can not take up any more liquid from the stratified layer. When the liquid level in front of the slug drops to this minimum level, the slug length can not increase any longer and the slug has reached its maximum length.

In literature, many relations for slug length distributions and the slug frequency are derived. Some of these are based on the physics behind the slug formation process, others are empirical relations fitted through experimental data without any physical background. Most of these relations are derived for the short hydrodynamic slug regime, and have no meaning when treating the situation of the long slugs.

In the current study, relations are derived from the experimental results, showing that both the maximum possible slug length and the slug frequency can be fitted with algebraic expressions including only the superficial gas and liquid velocities, which are valid for both the short and the long slug regime. For the slug length, this expression is validated with a simple slug model, which shows nice agreement with the experimental observations. The first slug after a change in the inlet conditions behaves differently, since this slug encounters a different environment. As long as the liquid in front is higher than at the tail (minimum hold-up), the slug can continue growing, in theory to infinite length. From the many experiments carried out during this study, regularities were observed in the slug pattern in time. These qualitative observations show clearly that the slug process is not random, but has a fixed structure. The quantitative investigation of these patterns and structures is recommended as a future study.

The critical liquid velocities and the minimum and maximum hold-up, corresponding to the different environments were determined experimentally as a function of the gas velocity. The maximum hold-up showed nice agreement with the Viscous Long Wavelength theory, while the minimum hold-up differs considerably from the hold-up calculated by Slug Stability. For the latter, the trend is correct, but the theoretical values are higher than the experimental data. The slugs which are already formed can also be present in an environment with lower hold-up than calculated based on the Slug Stability. The critical liquid velocity is predicted lower with Slug Stability than observed in the experiments.

With the instrumentation used, the structure of the liquid slug can be measured, allowing the estimate of the content of gas bubbles inside the liquid slug body. For a quantitative study of the bubble size and distribution inside the liquid slug, a non-linear data-reconstruction algorithm should be implemented. The level of the stratified flow before and after the slugs is easy to measure, since the stratified layer is assumed to be free of gas bubbles. The average gas void fraction inside the liquid slug body is found to be a function of the mixture velocity. Although some researchers claim that the gas bubbles only occur above a certain mixture velocity, in the current study bubbles were also observed for small mixture velocities, and the data showed good agreement with the used correlation for the whole range of mixture velocities investigated.

On the slug initiation several stages were observed, ranging from (roll-)waves to (pseudo-)slugs. Since only four measurement locations were used during the experiments, the slug formation mechanisms could not be studied in more detail.

Marco Zoetewij

Samenvatting

Lange vloeistof slugs in horizontale buizen

*Onderzoek naar de ontwikkeling en karakterisatie
met meettechnieken op basis van elektrische geleiding*

Tweefasenstromingen zijn te vinden in vele industriële toepassingen. Verschillende stromingspatronen kunnen ontstaan, afhankelijk van de snelheden van de beide fasen. In deze studie is gekeken naar stromingen van lucht en water. Een van de patronen die op kan treden is die van slug-stroming, waarbij de vloeistof door de leiding wordt getransporteerd in de vorm van blokken, die met hoge snelheid door de leiding bewegen.

Binnen het gebied van de slug stroming kan onderscheid worden gemaakt tussen de korte hydrodynamische slugs, met lengten van hooguit 40 buisdiameters ($40D$), en de lange slugs, welke (veel) langer zijn en lengten tot boven $400D$ kunnen bereiken. De afgelopen decennia is er veel onderzoek gedaan naar de korte slugs, waarvan het regelmatige gedrag relatief eenvoudig te voorspellen is. De lange slugs kunnen vanwege hun enorme lengte voor veel meer problemen zorgen, aangezien het gedrag van deze structuren moeilijk te voorspellen is. Bij dit onderzoek ligt de nadruk op deze lange slugs, om een beter begrip te krijgen van de processen in dit gebied, iets wat tot dusverre niet eerder zo nauwkeurig is gedaan.

Voor gassnelheden van $U_{sg} \geq 2,5$ m/s gaat de overgang direct vanuit de gelaagde stroming naar de korte hydrodynamische slugs. Voor lagere gassnelheden gaat de overgang via het gebied van de lange slugs. Voor toenemende vloeistofsnelheid neemt de sluglengte af en voor voldoende hoge vloeistofsnelheden zullen er weer korte slugs ontstaan.

In de 137 m lange opstelling ($L/D = 2740$) met 5,2 cm buizen zijn experimenten gedaan met lucht en water, waarbij zowel naar de korte als de lange slugs is gekeken. Met behulp van elektrische geleidingsensoren zijn de eigenschappen van de slugs bepaald. De staart van de slug beweegt met een constante snelheid. Deze snelheid is constant voor alle slugs bij vaste stromingscondities, en is ook onafhankelijk van de positie waar de slugs zich bevinden.

De voorkant kan sneller bewegen dan de staart. De lengte neemt toe doordat water wordt opgenomen aan de voorkant. Deze vloeistof wordt opgenomen van de laag water die zich voor de slug bevindt. Zolang er voldoende water beschikbaar is in de gelaagde stroming aan de voorkant, zal de slug kunnen blijven groeien. Zodra de minimale vloeistof hoogte van de gelaagde stroming is bereikt, zal er geen water meer kunnen worden opgenomen, en zal de slug verder bewegen met constante lengte.

In de literatuur zijn er vele relaties bekend die de lengte of de frequentie van de slugs voorstellen. Sommige daarvan zijn gebaseerd op fysische modellen, andere zijn empirische relaties die afkomstig zijn uit experimentele gegevens. Veel van deze relaties zijn afgeleid en ook alleen geldig voor de korte, hydrodynamische slugs. In het geval van de langere slugs hebben deze relaties geen betekenis.

In dit onderzoek is aangetoond dat zowel de sluglengte als de frequentie waarmee de slugs voorbij komen, kunnen worden beschreven met algebraïsche vergelijkingen die zowel voor de korte als de lange slugs geldig zijn. Deze relaties zijn alleen afhankelijk van de gas- en vloeistofsnelheden bij de ingang van de leiding. De uitdrukking voor de sluglengte is vergeleken met de uitkomsten van een eenvoudig fysisch model, waarbij goede overeenstemming is gevonden. De eerste slug die ontstaat na een verandering van de stromingscondities gedraagt zich anders in vergelijking met de andere slugs, aangezien deze slug in een afwijkende omgeving komt. Zolang de vloeistofhoogte aan de voorzijde hoger is dan aan de achterzijde van de slug (minimum hoogte), zal de slug blijven groeien, theoretisch tot een oneindige lengte. Tijdens de vele experimenten zijn verschillende patronen van slugvorming in de tijd gezien. Dit geeft duidelijk aan dat het ontstaan van slugs niet iets willekeurigs is, maar dat er een zekere regelmaat aanwezig is. Het ontstaan en kwantificeren van deze tijdsintervallen tussen de slugs kan nog nader worden onderzocht.

De kritische vloeistofsnelheden en de minimale en maximale vloeistofhoogte, overeenkomstig met de verschillende omgevingen, zijn experimenteel vastgesteld als een functie van de gassnelheid. De maximale vloeistofhoogte komt goed overeen met een viskeuze golftheorie (VLW), terwijl de minimale hoogte duidelijk afwijkt van de slug stabiliteits theorie (SS). In het laatste geval is de trend overeenkomstig met de theorie, maar de theoretische waarden zijn hoger dan de experimentele gegevens. Slugs die al eerder gevormd zijn kunnen blijkaar blijven bestaan in een omgeving met een vloeistofhoogte die lager is dan die volgt uit de SS-theorie. De kritische vloeistofsnelheid wordt door de SS-theorie lager voorspeld dan gemeten in de experimenten.

Met de instrumenten die zijn gebruikt bij de experimenten is het mogelijk om de structuur van de waterslugs te bepalen. Hieruit kan de hoeveelheid gas (lucht) die zit opgesloten in de slug worden afgeschat. Voor een kwantitatief onderzoek naar de afmetingen en de verdeling van de bellen zal een niet-linear gegevens-reconstructie model moeten worden ontwikkeld. Met de huidige reconstructie techniek kan alleen een kwalitatieve uitspraak worden gedaan over deze bellen. De hoogte van de gelaagde stroming voor en achter de vloeistof slug kan nauwkeurig worden bepaald, aangezien deze waterlaag geen luchtbellen bevat.

De gemiddelde hoeveelheid gasbellen in de vloeistofslug blijkt afhankelijk te zijn van de mixsnelheid. Ondanks dat andere onderzoekers beweren dat gasbellen alleen bestaan boven een bepaalde snelheid, zijn er ook bellen gemeten bij lagere snelheden. De bellenfractie bleek aan de correlatie te voldoen voor het hele snelheidsgebied wat bekeken is.

Betreffende het ontstaan van de slugs zijn er verschillende tussenvormen gezien bij de experimenten, variërend van (rol-) golven tot (pseudo-) slugs. Aangezien er slechts op vier locaties gemeten is, was het niet mogelijk om het initiatie proces van de slugs in detail te onderzoeken.

Marco Zoetewij

Contents

| | |
|--|-----------|
| Summary | i |
| Samenvatting | v |
| Nomenclature | xv |
| 1 Introduction | 1 |
| 1.1 Background : Gas production industry | 1 |
| 1.2 Regimes in horizontal 2-phase flow | 4 |
| 1.3 How to handle slug flow : separators and slug catchers | 6 |
| 1.4 Research goal : Better understanding of slug flow occurrence | 8 |
| 1.5 Outline of the thesis | 8 |
| 2 Literature Review | 9 |
| 2.1 Two phase flow patterns in horizontal tubes | 10 |
| 2.2 Flow transitions and slug initiation | 12 |
| 2.2.1 Kelvin-Helmholtz | 12 |
| 2.2.2 Viscous long wavelength | 13 |

| | | |
|----------|--|-----------|
| 2.2.3 | Slug stability | 13 |
| 2.2.4 | Slugs, Plugs and Pseudo slugs : the differences | 15 |
| 2.2.5 | The effect of waves on flow transitions | 16 |
| 2.3 | The effect of pipe geometry on the behavior of the flow | 18 |
| 2.3.1 | Undulations and inclinations enhance the formation of liquid slugs | 18 |
| 2.4 | Different mechanisms for slug length increase | 19 |
| 2.4.1 | Slug growth due to merging of small slugs | 19 |
| 2.4.2 | Hold-up up- and downstream of the slug : local environment | 20 |
| 2.4.3 | Difference in front and tail velocity | 21 |
| 2.4.4 | Time interval between successive slugs | 21 |
| 2.5 | Slug frequency | 22 |
| 2.6 | Literature review on experimental work | 31 |
| 2.6.1 | Multiphase flow experiments with different inlet conditions | 31 |
| 2.6.2 | Two phase experiments in the hydrodynamic slugging region | 32 |
| 3 | Experimental Set-up | 35 |
| 3.1 | Overview of the different parts of the used set-up | 36 |
| 3.2 | Different inlet geometries | 39 |
| 3.3 | The effect of the bend halfway the pipeline | 41 |
| 3.4 | The effect of the alignment of the pipeline | 42 |
| 3.5 | Conclusions | 44 |
| 4 | Experimental techniques; possibilities and limitations | 45 |
| 4.1 | Different types of instrumentation | 45 |
| 4.1.1 | Slug detectors for slug development measurements | 46 |

| | | |
|----------|---|-----------|
| 4.1.2 | Data processing for the slug detector signals | 48 |
| 4.1.3 | Slug development length | 50 |
| 4.2 | Wire-mesh sensors for detailed flow imaging in stratified and slug flow | 50 |
| 4.2.1 | Data acquisition with the wire-mesh | 51 |
| 4.2.2 | What is actually measured. Different approaches to the measurement volume | 52 |
| 4.2.3 | The amount and distribution of gas bubbles in the liquid slug | 55 |
| 4.3 | Measuring the liquid level | 58 |
| 4.3.1 | Design of the level sensors | 58 |
| 4.3.2 | From sensor data to slug properties | 59 |
| 4.4 | Stability of the signal and drift effects | 64 |
| 4.4.1 | Electronic drift in the wire-mesh data acquisition equipment | 65 |
| 4.5 | Data acquisition systems | 66 |
| 4.5.1 | Measuring analogue signals from the flowloop | 66 |
| 4.5.2 | Slug detector units, data storage and reconstruction | 67 |
| 4.6 | Conclusions | 68 |
| 5 | Slug development in different regimes | 69 |
| 5.1 | Different flowtypes investigated | 70 |
| 5.2 | Which flow type for which inlet conditions : the flow map | 71 |
| 5.3 | Slug development, changes in slug length | 74 |
| 5.3.1 | Slugs with increasing length, the behavior | 78 |
| 5.3.2 | A special case, the first slug | 81 |
| 5.4 | Slug behavior in time : slug frequency | 88 |
| 5.4.1 | Regular occurring long slugs; a constant slug frequency | 93 |

| | | |
|----------|--|------------|
| 5.4.2 | Slug patterns with two characteristic frequencies | 98 |
| 5.4.3 | Slugs with an irregular pattern in time | 99 |
| 5.4.4 | Initiation of slugs for slightly upward flow | 100 |
| 5.5 | The relation between slug length and slug frequency | 104 |
| 5.6 | Conclusions | 107 |
| 6 | Slug structure and initiation processes | 109 |
| 6.1 | Different growth behavior depending on the local hold-up environment | 109 |
| 6.2 | Liquid hold-up at flow transition, minimum and maximum hold-up situation . | 113 |
| 6.3 | The effect of gas bubbles inside the liquid slug body | 115 |
| 6.4 | The distribution of bubbles in the slug, front or tail bubbles | 118 |
| 6.5 | Intermediate stages during slug formation : Waves and Pseudo slugs | 122 |
| 6.6 | Conclusions | 125 |
| 7 | Model comparison | 127 |
| 7.1 | Development of slug length and slug frequency | 127 |
| 7.2 | Simple slug length model | 131 |
| 8 | Conclusions and Recommendations | 141 |
| 8.1 | Conclusions | 141 |
| 8.2 | Recommendations | 145 |
| A | The length over which slug development can be measured | 147 |
| B | Friction factors | 149 |
| B.1 | A simple case, friction at a smooth wall | 150 |

| | |
|---|-------------|
| Contents | xiii |
| B.2 Pressure drop and interfacial friction | 151 |
| C Overview of the detector positions | 153 |
| D Calibration data | 155 |
| D.1 Liquid flowmeters | 155 |
| D.2 Gas flowmeters | 156 |
| E Wire mesh electronics : details and schemes | 157 |
| E.1 Electronics device for measurement control and data logging | 157 |
| E.2 Measurement principle | 159 |
| E.3 Measurement data, different data formats and conversion | 164 |
| References | 167 |
| Dankwoord | 171 |
| Curriculum Vitae | 173 |

Nomenclature

Roman symbols

| | | |
|------------------------|--------------------|----------------------------|
| <i>A</i> | area | m^2 |
| <i>D</i> | diameter | m |
| <i>D_H</i> | hydraulic diameter | m |
| <i>Fr</i> | Froude number | - |
| <i>f</i> | frequency | s^{-1} |
| <i>f</i> | friction factor | - |
| <i>H</i> | hold-up (liquid) | - |
| <i>h_l</i> | liquid height | m |
| <i>h_{i,j}</i> | local hold-up | - |
| <i>L</i> | length | m |
| <i>P</i> | contact area | m |
| <i>p</i> | pressure | Pa |
| <i>Q</i> | volume flux | $\text{m}^3 \text{s}^{-1}$ |
| <i>Re</i> | Reynoldsnumber | - |
| <i>s</i> | slip ratio | - |
| <i>T</i> | temperature | $^{\circ}\text{C}$ |
| <i>t</i> | time | s |
| <i>U</i> | velocity (gas/liq) | m s^{-1} |
| <i>u</i> | velocity | m s^{-1} |
| <i>V</i> | volume | m^3 |
| <i>v</i> | velocity (slug) | m s^{-1} |
| <i>w_{i,j}</i> | weight factor | - |
| <i>x</i> | position | m |

Greek symbols

| | | |
|---------------|-------------------------|----------------------------|
| α | hold-up | - |
| β | velocity ratio | - |
| ε | gas void fraction | - |
| η | dynamic viscosity | Pa s |
| θ | angle to horizontal | ° |
| ν | kinematic viscosity | $\text{m}^2 \text{s}^{-1}$ |
| ρ | density | kg m^{-3} |
| σ | surface tension | kg s^{-2} |
| τ | timeshift | s |
| τ | wall shear stress | kg m s^{-2} |
| μ | mean value (statistics) | - |
| σ | std error (statistics) | - |

Sub scripts

| | |
|-----------------|------------------------|
| <i>b</i> | bubble |
| <i>cm</i> | center of mass |
| <i>d</i> | downstream |
| <i>f, front</i> | front |
| <i>g</i> | gas |
| <i>i</i> | interface |
| <i>i, j</i> | grid indices |
| <i>l</i> | liquid |
| <i>m, mix</i> | mixture (velocity) |
| <i>s</i> | superficial (velocity) |
| <i>t, tail</i> | tail |
| <i>u</i> | upstream |
| <i>w</i> | wall |
| <i>w</i> | water (temperature) |

Constants

| | | |
|---|--------------------|------------------------|
| g | grav. acceleration | 9.81 m s ⁻² |
|---|--------------------|------------------------|

Abbreviations

| | |
|-----|--------------------------------|
| AC | Alternating Current |
| ADC | Analogue to Digital Converter |
| DC | Direct Current |
| KH | Kelvin-Helmholtz theory |
| USB | Universal Serial Bus |
| SS | Slug Stability theory |
| VLW | Viscous Long Wavelength theory |

CHAPTER 1

Introduction

1.1 Background : Gas production industry

All over the world, oil and gas are the most used energy supplies for heating, electricity production and transportation. Since many oil and gas fields have reached the mature stage, the increasing amount of water being produced is one of the major concerns of the oil and gas business. Shell, one of the major oil and gas producers in the world, produces about 1 million cubic meters of water per day. Another important player, Total, produces 3 m³ of water for each 1 m³ of oil (Zitha (2000)). The presence of this water changes the flow in the pipelines dramatically.

The dutch energy supply relies for an increasing part on gas from offshore gas production fields. Based on data from the dutch energy research center (<http://www.energie.nl/>), it can be concluded that over the last 20 years the off-shore production has increased from 20% to 40% of the total national production, as shown in figure 1.1.

Together with the gas, large amounts of water or oil/water mixtures are produced, resulting in multi-phase flow conditions in the transporting pipe system between the source and the production platform. When the fields grow older, the produced gas contains an increasing amount of water, giving rise to different mixture compositions. Up till recently, usually a stratified flow pattern occurred for the gas/liquid flow, where the two phases flow separately, but increased liquid loading triggers the formation of liquid slugs. Slug flow is an intermittent type of flow, where the liquid is transported in packages instead of in a continuous way.

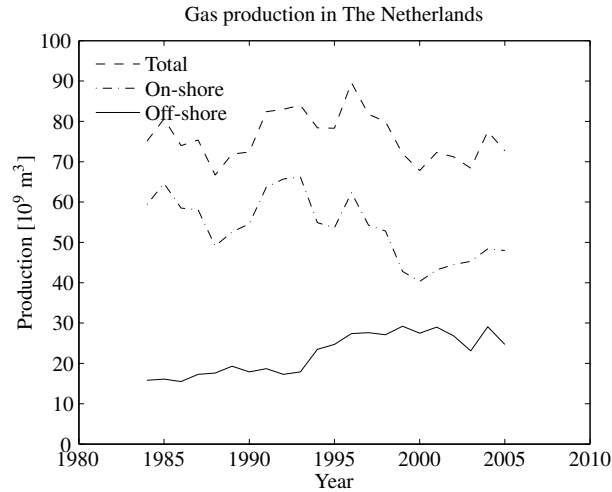


Figure 1.1: Gas production in The Netherlands over the last 20 years. The contribution of the off-shore production increased considerably. Data from : <http://www.energie.nl/>

The liquid slugs can be initiated from topological effects, *e.g.* kinks and bends, and from instabilities in the flow, *e.g.* due to changing flow conditions. The presence of liquid slugs in the flow system gives an irregular output in terms of gas and liquid flow at the outlet of the system, or at the next processing stage. The irregular nature of slugs makes it highly unpredictable. The liquid slugs can reach lengths up to several hundred tube diameters. In the 2" facility used in the current study, slugs were observed with lengths of 20 m, which equals 400D. For large capacity systems in industry, these liquid slugs can even grow longer, carrying large momentum. Often slug catching devices or separators are used to collect the slugs, and prevent any damage to the downstream equipment. For the design of such slug catchers (usually large vessels, or a network of large pipes separating the phases), it is important to know what kind of slugs to expect. The short slugs usually give no serious problems, but also the long(est) slugs should be caught and broken down in a proper way. For that reason, it is important to study the behavior of slug flow in great detail.

Gas-liquid slug flow is a frequently occurring flow pattern in a number of industrial two-phase pipe flows. Not only in gas production, but also in numerous other industrial and chemical applications similar two-phase flows become more and more common. Due to economical push, production rates are increased, which directly implies a higher change of operating in the slug flow regime.

A particular challenge for the petroleum industry is the development of multiphase technology for transportation of oil and gas from sub sea production units at large water depths to processing facilities at nearby platforms or onshore facilities, as shown schematically in figure 1.2. The tubing, between sources on the sea bottom and the riser at the production platform at the left of the figure, is quite long. Since processing is done after the production facility, the flows in the sub-sea pipelines usually contain multiple phases, like water, oil and gas, which composition is not known in advance. Changing composition inside the long sub-sea infra structure can lead to serious operational problems, ranging from non-continuous production to damaged equipment.

Reliable flow models can then contribute to safe and cost efficient design and operation of pipelines with multiphase flows. So far, mainly empirical relations are used in the design and modeling of production and transportation facilities. With the experiments done in the current study, more insight is gained in the physical phenomena behind the slug properties and the way they behave under various flow conditions. A more fundamental approach is used for improving the general knowledge on slug flow.

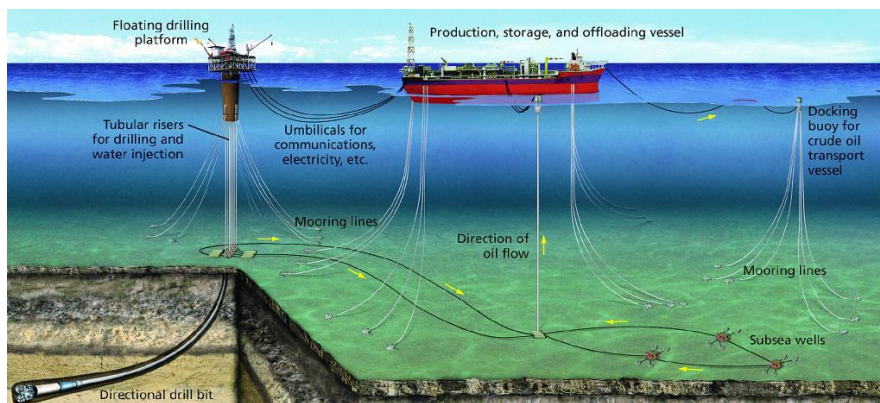


Figure 1.2: A sub-sea drilling facility with production, storage and transportation. The drilling platform at the left drills the hole to reach the oil reservoirs. The vessel in the middle produces the oil from the different sub-sea wells. In the horizontal lines at the sea-bottom, slugs can be initiated, which will cause large variations in the gas and liquid flow rates.
From : <http://www.ehponline.org/>

1.2 Regimes in horizontal 2-phase flow

The most simple flow pattern for a horizontal two-phase flow is stratified flow, where the heavy liquid phase moves through the lower part of the tube, and the lighter gas phase in the top part of the tube. This is schematically shown in figure 1.3(a).

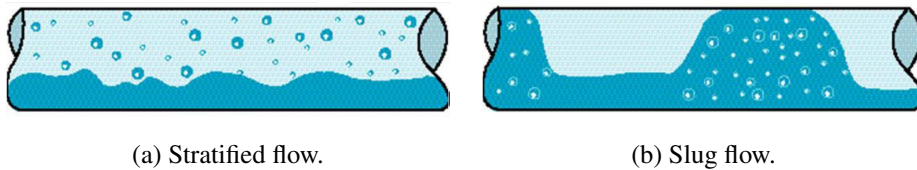


Figure 1.3: Two characteristic flow patterns in two-phase gas-liquid flow. In (a) stratified flow, in (b) slug flow is shown.

Another interesting pattern is slug flow, indicated in figure 1.3(b), where the liquid is moving in liquid blockages. Because of the intermittent nature of the liquid slugs, this flow pattern may cause serious problems in the field. When increasing the production rates, also more liquid will be produced from wet gas wells or sub-sea reservoirs. This increased liquid rate changes the pattern in the pipe from stratified flow to slug flow. In the flowmap in figure 1.4, the different flow regimes are indicated.

For low liquid velocities, the pattern is smooth stratified, or with small waves on the interface as indicated in figure 1.3(a). For larger liquid flow rates, the transition to slug flow is made, as indicated in graph 1.4. The slug regime corresponds to the flowtype shown in figure 1.3(b). Especially just above transition and in the left part of the flowmap, long slugs can be present, which can reach lengths of $L = 400D$. Further to the right, the slug regime contains mainly short, hydrodynamic slugs, which do not cause any serious operational problems. This study focuses on the transition and the long slugs just above transition.

In the current study, the focus is on the long slugs in horizontal tubes, as indicated in figure 1.4. The long slug regime contains slugs which start from small disturbances in the flow, grow when traveling downstream, till they reached their stable or maximum length. Despite the 137 m long experimental set-up, some slugs were observed which had not reached their final length when leaving the set-up after 137 m. The experimental range is small compared to other 2-phase flow studies, as will be shown later on in figure 2.12. This gives the advantage to zoom in on the characteristic growth behavior of these long slugs. The large length of the set-up ($L/D = 2700$) is another major advantage compared to the smaller set-ups used by other groups.

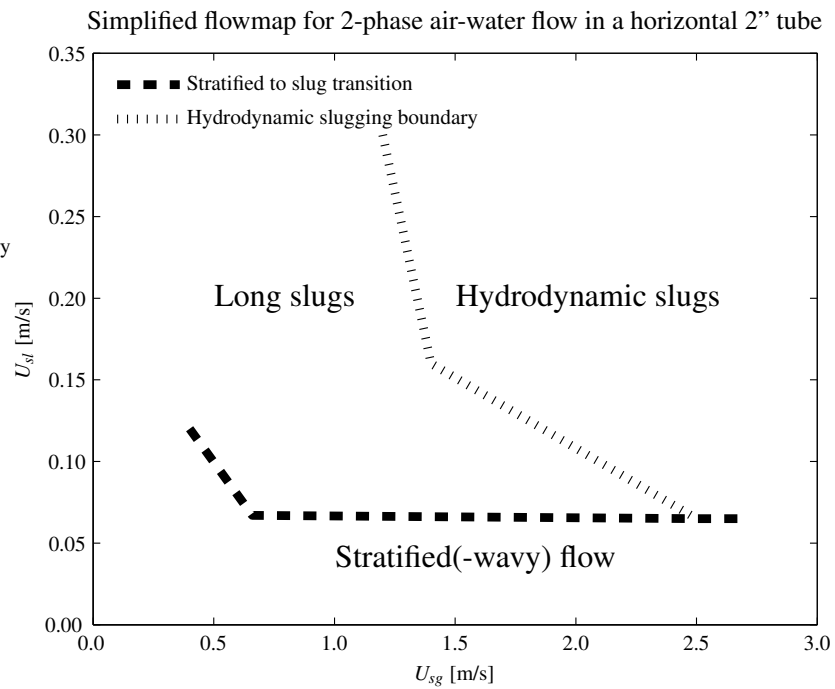


Figure 1.4: Flowmap indicating the different regimes for two-phase gas-liquid flow. On the horizontal axis the superficial gas velocity is shown, on the vertical axis the superficial liquid velocity. The lower regime indicates stratified flow. For higher liquid velocities, slugs start to occur. In the long slug regime on the left, slugs can grow upto several hundred tube diameters. The shorter, hydrodynamic slugs on the right have $L/D < 40$. This simplified flowmap is based on data from 2-phase water-air experiments in a long tube with 2" inner diameter.

1.3 How to handle slug flow : separators and slug catchers

The unwanted effect of slugs can cause damage to the downstream production facilities. To prevent this, separators and slugcatchers are used to separate the gas and the liquid phases. The irregular two-phase flow enters the separator, usually a large vessel, where the liquid is collected at the bottom and the gas phase leaves through an outlet at the top of the vessel, as shown in figure 1.5. These separators are usually designed to handle the hydrodynamic slugs, which are in the order of $L/D \leq 40$. When larger slugs are present, with $L/D \approx 400$, these vessels are too small.

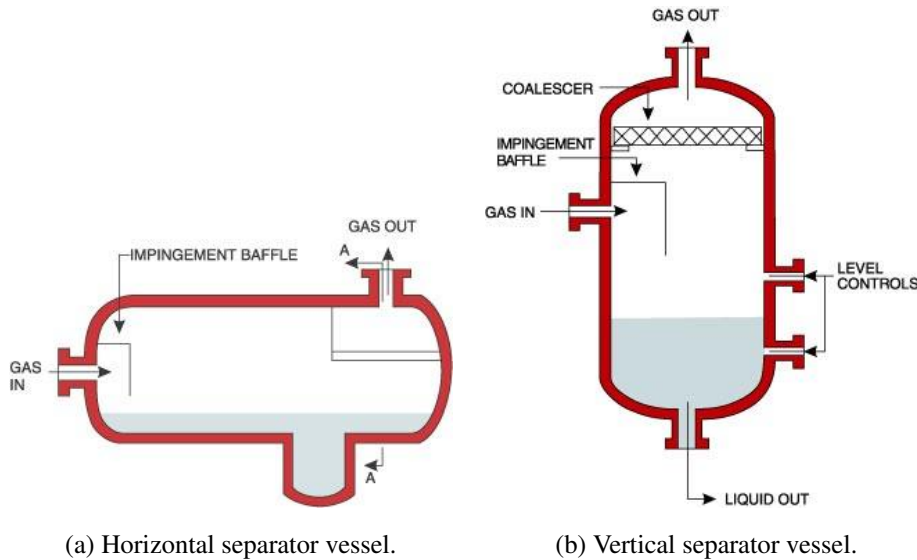


Figure 1.5: Two examples of 2-phase flow separators. From : <http://www.tfes.com/>.

When flushing the pipelines with a sphere, the so-called sphere-generated slugs will be formed, which contain almost the whole liquid content of the line. Since these amounts of liquid can not be separated using a separator, slug catchers are used which have a much larger capacity. In figure 1.6 a slug catcher is shown schematically. The irregular two-phase flow enters in the lower right corner, and both phases are separated in the large tubes. Since the flow is divided over multiple tubes, the flow velocities will decrease. As can be seen from the regimes indicated in figure 1.4, the slug flow will change into stratified flow because of the lower liquid velocity. The liquid flows towards the end (upper left), indicated by L, while the gas (G) is taken off in the upper pipes in the beginning of the catcher.

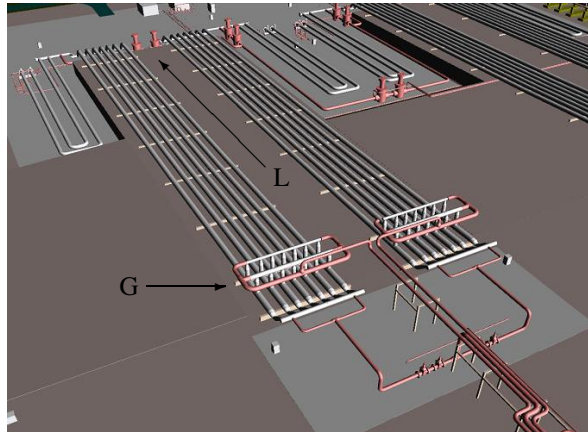


Figure 1.6: Schematic slug catcher. The mixture enters from below, and is separated in the long tubes. The liquid flows towards the end, while the gas is taken out near the inlet.
From : <http://www.hydro.com/>.

In figure 1.7 a slug catcher build in The Netherlands for the Norwegian oil company Statoil is shown. As a consequence of its large size and complexity, these slug catchers are very expensive. The increasing knowledge on slug behavior allows better control of slugs in the upstream pipelines, such that the size and complexity of the slug separators and catchers can be reduced.



Figure 1.7: Large slug catcher, the equipment measures 140 by 36 meters.
From : <http://www.statoil.no/>.

1.4 Research goal : Better understanding of slug flow occurrence

Since only little is known about slug flow, especially for the case of growing slugs, more information is required for accurate flow predictions. In the current study, experiments are performed in the different flow regimes, varying from stratified flow to long and hydrodynamic slugs. Two specific topics have been studied. The different transitions from one regime into another are measured and related to transition mechanisms in literature. The other part of the study focuses on the behavior of the slug which is already present. Different types of slugs are observed and classified based on their properties.

The slug-correlations which are presently available, are for a large extend based on averages of large sets of field data and laboratory experiments. In the current study, the goal is to get a more fundamental analysis of the experimental data, and derive relations which have a solid physical basis.

1.5 Outline of the thesis

After this introducing chapter, the thesis consists of 3 main parts. In the first part, chapter 2, the theory on two-phase flows and relevant studies are discussed.

The second part is on the experimental set-up and the methods used for the experiments. The set-up is illustrated in chapter 3. A special focus on the data acquisition systems and a brief overview of the data processing steps is given in chapter 4. In this chapter, also the properties, possibilities and limitations of the different instruments are shown.

The last part deals with the results, explained in chapter 5 and 6. The behavior and development of the slugs when traveling through the set-up is discussed in chapter 5. The properties of the slugs and the relation between the slug and its surrounding stratified layer are shown in chapter 6. The initiation of slugs from the waves on the stratified flow is also addressed.

In chapter 7, the results on slug development are compared with a simple model. The conclusions of the study are summarized and discussed in chapter 8. For more details on the work, the reader is referred to the appendices and the bibliography at the end of this thesis.

CHAPTER 2

Literature Review

In this chapter the necessary theory on two-phase flows in horizontal tubes are be discussed. The two phases, in this case gas and liquid, give rise to different possible flow patterns, of which an overview is given in section 2.1. Different machanisms for flow transitions from one regime to another are discussed in section 2.2.

After the geometrical effects of the set-up on the flow in section 2.3, the flow instabilities, the start and growth of the slugs are discussed in section 2.4. The slug frequency, the pattern of slugs in time is treated in section 2.5, where different models from literature are discussed in detail.

Comparison with other experimental studies is made in section 2.6, where similarities and differences are mentioned. This section also explains the advantages of the current study compared to the work done by other investigators.

2.1 Two phase flow patterns in horizontal tubes

In situations where gas and liquid phases flow concurrently in a single horizontal tube, many different flow patterns may occur. The most common patterns are shown in figure 2.1. The flows can be divided into several categories, as indicated in the figure. In the upper two images, the two phases are separated. The heavy liquid phase is on the bottom of the pipe, while the lighter gas phase flows on top. For low velocities, the interface will be flat, resulting in a stratified smooth flow. For higher velocities, small waves may occur, which is called stratified wavy flow.

In the intermittent regime, irregular packages of liquid may block the whole area of the pipe. One of these patterns is slug flow, which is investigated in detail in this study. The third set of patterns is the annular flow, where the phases are spread in radial direction. In the last regime, the two phases are completely mixed, giving rise to dispersed flow type.

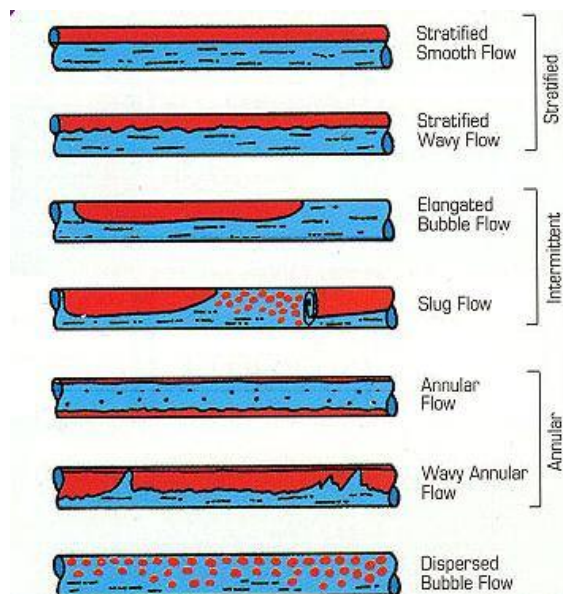


Figure 2.1: Overview of the most common pattern in 2-phase flows. From top to bottom : stratified, intermittent and annular flow pattern. In the current project, only the first two sets of patterns are observed. From : <http://www.pe.utexas.edu/>.

The conditions for which the patterns shown in figure 2.1 are likely to occur, are shown in figure 2.2.

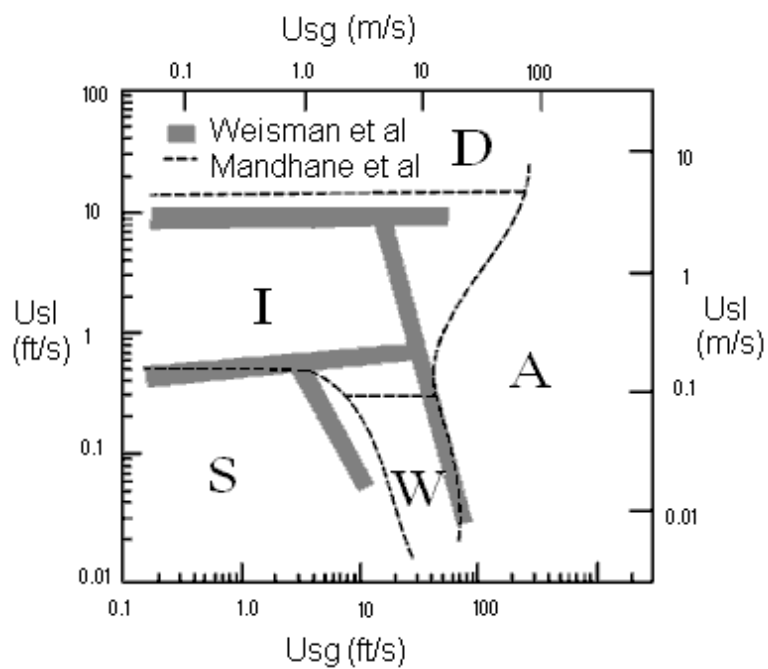


Figure 2.2: Flowmap indicating the different regimes for two-phase gas-liquid flow of figure 2.1. On the horizontal axes the superficial gas velocity is shown, on the vertical axis the superficial liquid velocity for air-water mixture in a 1" tube. From Weisman et al. (1979).

The regimes (S) and (W) indicate stratified and wavy flow. The central part, indicated by (I), is the intermittent region where slugs occur. The other regimes, (A) and (D) which respectively indicate annular and dispersed flow occur only at high velocities which are beyond the scope of this research. The focus is on the slug regime (I), with special interest in the transition between (S,W) and (I), where the long slugs are likely to occur.

2.2 Flow transitions and slug initiation

In this section, the different mechanisms for flow transition are discussed. The transitions are set by the (in)stability of the stratified flow and/or the slug flow. The most important stability theories are

- Kelvin Helmholtz instability (KH), originally by Milne-Thompson.
- Viscous Long Wavelength instability (VLW). The VLW theory predicts the critical heights based on the stability of the stratified flow, as explained in detail by Lin and Hanratty (1987).
- Slug Stability (SS), introduced by Dukler and Hubbard (1975). This theory examines the stability of the slugs themselves instead of looking at the waves. Where the previous two (VLW and KH) look to the transition from stratified to slug flow by analyzing the stability of the stratified flow, the SS predicts the transition from slug to stratified flow based on the stability of the liquid slugs.

2.2.1 Kelvin-Helmholtz

For the prediction of the stability of waves on the stratified flow, a sinusoidal wave with small amplitude is assumed to propagate over the liquid layer

$$h = \bar{h} + \hat{h} \exp[ik(x - Ct)], \quad (2.1)$$

with \bar{h} the average liquid height, \hat{h} the amplitude of the wave and C the propagation velocity of the wave. From the momentum balance (for details, see *e.g.* Hurlburt and Hanratty (2002)), the critical relative velocity and wave number can be calculated as

$$k_{crit} = \left(\frac{\rho_l g \cos \theta}{\sigma} \right)^{1/2}, \quad (2.2)$$

$$(\bar{U} - \bar{u})_{crit}^2 = 2 \left(\frac{\sigma g \cos \theta}{\rho_l} \right)^{1/2} \frac{\rho_l}{\rho_g}, \quad (2.3)$$

which for air-water flow under atmospheric pressure results in a $(\bar{U} - \bar{u})_{crit} = 6.6$ m/s and a wavelength $\lambda_{crit} = 1.7$ cm. For high pressure systems (higher density), these numbers will be smaller and the critical point of transition is reached for lower velocity differences.

2.2.2 Viscous long wavelength

Similar to the KH-theory, waves are assumed on the gas-liquid interface, and the critical gas and liquid velocities are calculated. Since the friction at the interface is included, viscous effects now also play a role. This theory predicts the formation of slugs at low gas velocities (Hurlburt and Hanratty (2002)).

2.2.3 Slug stability

The stability of liquid slugs is studied in detail by Hurlburt and Hanratty (2002) based on the amount of liquid that enters the slug at the front and leaves at the back.

Slugs traveling downstream with a front velocity V_s that is larger than the local liquid velocity u_1 in the stratified layer, will scoop up liquid from the stratified layer in front with a volumetric flow rate

$$Q_{in} = (V_s - u_1)A_{L1}, \quad (2.4)$$

with A_{L1} the area occupied by the liquid in stratified flow upstream of the slug as illustrated in figure 2.3.

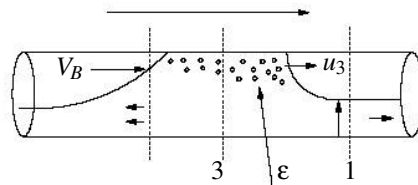


Figure 2.3: Schematic representation of a slug moving over a stratified liquid layer. From Hurlburt and Hanratty (2002).

Inside the slug, the liquid is moving with average velocity u_3 , which is smaller than the velocity of the bubble V_B at the tail of the slug. For higher velocities, bubbles might be present, of which the volume fraction is denoted by ϵ . The volumetric flow rate of liquid that is shed at the tail of the slug equals

$$Q_{out} = (V_B - u_3)(1 - \epsilon)A, \quad (2.5)$$

with $V_B - u_3$ the relative velocity between the bubble and the liquid inside the slug, and $(1 - \epsilon)A$ the area of the liquid slug corrected for the bubbles.

Depending on the values of Q_{out} and Q_{in} , the slug can be stable ($Q_{out} = Q_{in}$), grow ($Q_{out} < Q_{in}$) or decay ($Q_{out} > Q_{in}$). For stable slugs, $Q_{out} = Q_{in}$ and $V_s = V_B$, giving the following expression for the critical liquid hold-up (here indicated with the liquid area)

$$\left(\frac{A_{L1}}{A}\right)_{crit} = \frac{(V_B - u_3)(1 - \epsilon)}{V_B - u_1}. \quad (2.6)$$

When the liquid area in front is larger than the expressed $(A_{L1})_{crit}$, slugs will tend to grow.

For calculating the critical hold-up, expressions for u_3 and ϵ are required. From a volume balance between the inlet of the tube and a point in the slug body (indicated with subscript 3), it can be derived that

$$U_{mix} = U_{sg} + U_{sl} = \epsilon U_3 + (1 - \epsilon)u_3, \quad (2.7)$$

with U_3 and u_3 the actual velocities of the gas (bubbles) and the liquid inside the slug. When introducing the slip ratio

$$s = \frac{U_3}{u_3}, \quad (2.8)$$

the liquid velocity u_3 can be expressed as

$$u_3 = \frac{U_{mix}}{1 + (s - 1)\epsilon}. \quad (2.9)$$

The void fraction ϵ is investigated by Bendiksen (1984); Nydal et al. (1992); Woods and Hanratty (1996). For small velocities, $U_{mix} < 2\sqrt{gD}$ the void fraction is negligible. For larger velocities, based on the data by Woods and Hanratty (1996, 1999), the following correlation was derived

$$\epsilon = 0.8 \left[1 - \frac{1}{1 + \left(\frac{U_{mix}}{8.66}\right)^{1.39}} \right]. \quad (2.10)$$

The slip ratio s equals $s = 1$ for low mixture velocities ($U_{mix} < 4$ m/s) according to the observations by Woods and Hanratty (1996) as shown in figure 2.4. For higher mixture velocities, the slip ratio s increases to $s \approx 1.3 - 1.5$.

The liquid velocity u_3 of the liquid inside the slug is lower than the velocity of the propagation velocity of the slug, which equals V_B of the bubble behind the slug. In the experiments shown in figure 2.4, the velocities are in the order of 1 m/s for both gas and liquid superficial velocities. When the liquid velocity is much lower, the bubbles inside the slug will also move to the top due to buoyancy, and gain a larger velocity than the surrounding liquid.

For the bubble velocity V_B , expressions as proposed by Bendiksen (1984) can be used

$$V_B = C_0 U_{mix} + C_1 \sqrt{gD}, \quad (2.11)$$

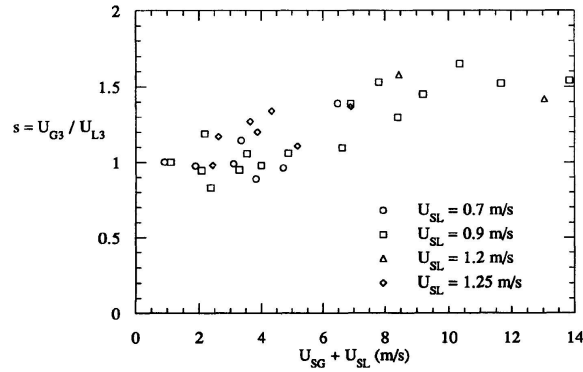


Figure 2.4: The slip ratio s versus mixture velocity for various liquid velocities. From Woods and Hanratty (1996).

with C_0 ranging from $1.05 \leq C_0 \leq 1.2$ depending on the Froude number and $C_1 = 0.54$ for horizontal flow. For higher Froude numbers, the inertia term dominates, and $V_B = 1.2U_{mix}$. These relations are valid for high Reynoldnumber situations $Re = U_{mix}D/\nu_l > 2300$. For the laminar slugs formed for $Re < 2300$, the bubble velocity behaves as $V_B = 2U_{mix}$ (Hurlburt and Hanratty (2002)).

2.2.4 Slugs, plugs and pseudo-slugs : the differences

For a range of liquid flow rates, the waves form foamy bridges (called 'bursts') which may or may not develop into slugs. This phenomenon is known as 'pseudo-slugs', which are characterized by entities having the appearance of slugs, but that do not travel as fast as the normal type of slugs. A more detailed study on pseudo-slugs is performed by Simmons and Hanratty (2001); Soleimani et al. (2002); Soleimani and Hanratty (2003); Kristiansen (2004).

For relatively low gas and liquid flow rates a stratified configuration occurs with the liquid flowing at the bottom and the gas flowing above it. As the liquid rate is increased (at a constant gas rate) waves appear on the interface. At even higher liquid rates the waves can grow to the top of the pipe and, intermittently, form liquid blockages. At low gas velocities this intermittent regime is characterized as a plug pattern, in which the gas flows as steady elongated bubbles along the top of the pipe Hurlburt and Hanratty (2002).

For low gas velocities, the pattern is characterized by series of long gas bubbles flowing along the top of the tube. This regime is called plugflow, where the liquid plugs do not contain any gas bubbles. In situations with higher gas velocities, the liquid is concentrated in liquid slugs, which are (highly) aerated. The front of the liquid is characterised by a hydraulic jump, which entrains gas into the liquid slug body. The slugs move approximately at gas velocity, and the flow between the slugs behaves as a stratified (wavy) flow. The transition from plug to slug flow occurs at a gas Froude number of $Fr_g = U_{sg}/\sqrt{gD} \approx 2$ (Ruder and Hanratty (1990); Woods and Hanratty (1996)).

Within the class of the liquid slugs, a distinction can be made between the short hydrodynamic slugs and the long slugs. The hydrodynamic slugs, usually occurring in a regular pattern (Ujang et al. (2006)), are short with an $L/D \leq 40$. In the second group, the slugs are longer ($L/D > 40$) and can reach sluglengths upto $400D$ each for a sequence of slugs. When flowconditions change at the inlet, slugs can grow upto almost $L/D \approx 800$.

2.2.5 The effect of waves on flow transitions

The liquid slugs which can be present in two-phase flows, usually originate from disturbances in the flow. These triggers can be due to changes in the geometry of the tubes, or from instabilities in the waves.

The gas and liquid, in this study air and water, flow concurrently through the pipes. At low flow rates, the liquid moves over the bottom of the tube and the gaseous phase flows on top, giving a stratified flow pattern. When the gas flow rate is increased (*e.g.* by opening a valve), small waves will occur on the gas-liquid interface, giving rise to a stratified-wavy flow pattern.

When the gas phase is moving faster than the liquid phase, it will exert a force on the crests of the waves. These small waves can grow into larger waves. This forcing has two effects on the dynamics of the waves. The first contribution is the Bernoulli-effect, which creates an upward force on the waves crest. This force is due to a local decrease in pressure as a consequence of the local increase in velocity, as shown in figure 2.5. This effect is balanced by the gravity force acting on the liquid in the wave crest. Depending on the strength of these two forces and the height of the liquid layer, the level can be elevated and reach the top of the tube, initiating a slug.

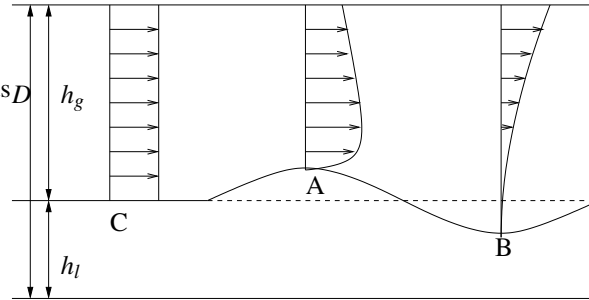


Figure 2.5: Schematic drawing of a wavy interface. Point C is at equilibrium level, A is the wave crest and B represents the wave trough. The total flow rate is constant, so that the actual velocity in point A will be higher since the cross sectional area for the gas is smaller.

The next contribution of the faster moving gas is the forcing in streamwise direction, which makes the crests to move faster than the troughs. This effect is indicated in the velocity profiles in figure 2.5. The waves are not pure sinusoidal any longer, and the wave front steepens. Depending of the upward and streamwise velocities of the wave crest, the waves might collapse into roll waves. When the forward motion is stronger, the crest rolls over the trough of the wave in front, as indicated in figure 2.6. In this situation, no slugs will be formed, since the wave did not reach the top of the tube.

Soleimani and Hanratty (2003) predicted the initiation of roll waves based on the instabilities in the flow. They concluded that the frequency of roll waves increases for increasing liquid flow rates in the pseudo-slug region. The equilibrium height of the stratified liquid film \bar{h}/D is unaffected. Since the volume flow increases for increasing liquid velocity, and the liquid level does not change, the velocity will increase and thus also the frequency of the waves. When the liquid flow rate is increased even more, slugs are likely to appear.

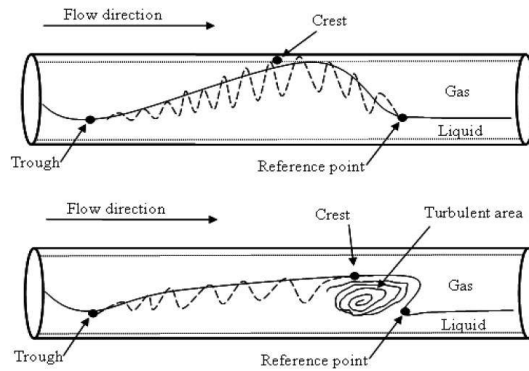


Figure 2.6: Two different motions in the wave crest. The lower image show the forward motion of the crest, which results in a roll wave. In the upper graph, the wave amplitude grows, and the crest touches the top of the tube, initiating a liquid slug, which will be explained in the next section. Depending on the strengths of these two forward and upward motions, roll waves or slugs can occur. From Kadri et al. (2007a).

2.3 The effect of pipe geometry on the behavior of the flow

In horizontal and nearly horizontal pipes, slug flow can be generated from stratified flow by two main mechanisms: natural growth of hydrodynamic instabilities and liquid accumulation due to an instantaneous imbalance between pressure and gravitational forces caused by pipe undulations.

2.3.1 Undulations and inclinations enhance the formation of liquid slugs

In this paragraph the influence of bends, elbows and other kinds of undulations in a pipeline are discussed. All these undulations influence the initiation of slugs and the slug length.

The presence of gas and liquid flowing simultaneously in pipelines made of several uphill and downhill sections, can lead to the formation of long liquid slugs which are blown from one pipeline section to the next due to the gas pressure. Slugs can be generated at low elbows, dissipate at top elbows and shrink or grow in length as they travel along the pipe, as shown by Zheng et al. (1993); De Henau and Raithby (1995).

The effect of bottom topography on roll waves is discussed by Mandre (2001) for a periodic varying bottom height. Also the influence of wall-roughness (Hoogendoorn (1957)) and a slug generator tested by Pols and Oliemans (1995) influence the stability of the stratified flow.

When a pipeline is inclined the liquid phase can accumulate in the low elbows of the tube, forming long liquid bridges. This is shown in figure 2.7. Therefore, the occurrence of slug flow is possible for lower liquid velocities as predicted for the horizontal situation, as illustrated by De Henau and Raithby (1995); Cook and Behnia (2000); Kristiansen (2004); Simmons and Hanratty (2001); Zheng et al. (1993).

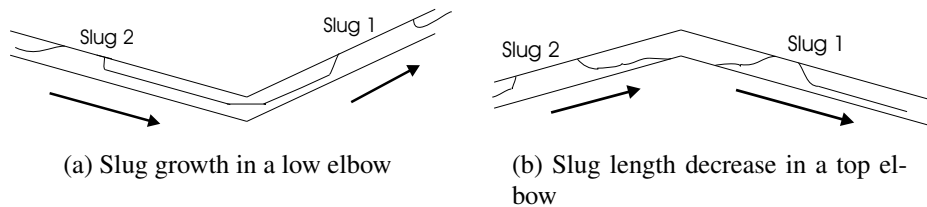


Figure 2.7: *Slug length development in a low and a top elbow. In (a) slug 1 is longer than 2, in (b) it is vice versa.*

2.4 Different mechanisms for slug length increase

Slugs can grow in different ways, as shown in the previous paragraph. The growth rate is related to several quantities, which are also inter-related.

2.4.1 Slug growth due to merging of small slugs

Slugs can change when flowing through a tube, as shown for the topology effect in figure 2.7. There is another mechanism by which the length of the slugs can increase, the merging of several separate slugs into a larger one. From the instabilities induced by a passing slug, new slugs can be formed in the neighborhood of the initial slug. Since not all slugs have the same length, and the bubble length between the slugs differs, the slugs can travel at different velocities. A fast moving slug can merge with a slower moving one in front, giving rise to a larger slug, as described by Moïssis and Griffith (1962); Zheng et al. (1993). When two slugs merge as a result of overtaking, a single slug is created, whose length is approximately the sum of the two (Dukler et al. (1984)).

2.4.2 Hold-up up- and downstream of the slug : local environment

At the front or nose of the slug, liquid from the stratified environment enters into the slug body. Similar, liquid leaves the slug at its back or tail. The amount of liquid that enters (or leaves), is related to the local hold-up upstream (or downstream) of the slug. For slugs with stable length, the hold-up on both sides are the same. When the upstream hold-up in front is larger (smaller) than downstream, the slug will grow (shrink).

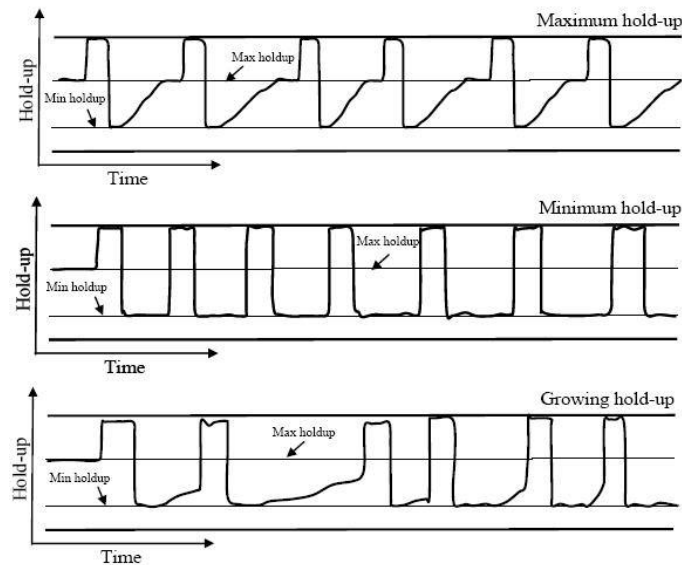


Figure 2.8: Three situations of slug flow with different hold-ups. In the upper image, the hold-up is at maximum in front of the slug, in the middle image the hold-up at the front of the slug is at minimum value. After the slug, the hold-up is always at minimum. The hold-up in the third image is between its minimum and maximum value at the slug front, i.e. the hold-up is still growing in this case. From Kadri et al. (2007b).

In the situations shown in figure 2.8, the minimum and maximum value of the hold-up are indicated. In the middle image, the hold-up before and after the slugs is the same, so the slug is stable. In the other two situations, the hold-up in front is larger than at the tail, so slugs will tend to grow, taking up the difference between front and tail liquid level.

2.4.3 Difference in front and tail velocity

When the velocities at the front and the tail of the slug are not equal, the slugs will change length. The reference point of a slug is defined at the tail of the slug. Experiments, as shown in chapter 5, have shown that the tail of the slugs move in the same way for all slugs present in the system. For ratios of front over tail velocity $v_f/v_t > 1$, the slugs will grow, with a growth rate related to the velocity ratio by

$$\frac{dL}{dx} = \frac{v_f}{v_t} - 1. \quad (2.12)$$

2.4.4 Time interval between successive slugs

The time interval between slugs is also of influence on the growth behavior. In the growing hold-up regime, liquid accumulates forming a higher liquid layer. After a slug has passed, the hold-up drops to its initial value (minimum hold-up). When the time between slugs is large, the liquid layer has time to rebuild to a higher level. As explained before, this extra liquid can be taken up by the next passing slug, which can grow considerably. When the slugs are closer together, the time for liquid level rebuild is much shorter. The available amount of liquid is limited, such that the slug can not grow fast.

2.5 Slug frequency

The rate at which slugs occur is an important design parameter for the separation devices, but also the rest of the system should be able to stand up against the intermittent nature of slug flow. The proper sizing of separation devices is not only depending on the length of the slugs, but also on the number of slugs it has to process per unit of time. In situations where separation and processing facilities are not designed for the large variations in gas and liquid flow rates, this may lead to considerable, undesirable, process upsets.

Slug initiation is considered as an entrance phenomenon where short (high frequency) slugs are formed. Further downstream, longer (low frequency) slugs will be present due to rapid merging of the short slugs. When the slugs are long enough to be stable, this results in the developed frequency for stable slugs further downstream (Zabaras (2000)).

In several studies, the frequency of the slugging process has been monitored. Woods et al. (2006) investigated air-water flows in 0.0763 m and 0.095 m tubes for high liquid rates ($U_{sl} \geq 0.5$ m/s). In that situation, slugs are initiated close to the entrance, and the time between slugs is stochastic. The hold-up was measured at several locations along the 20 m long set-up. For superficial gas velocities below 3 m/s, the slugs are initiated from disturbances reaching the top of the tube in the beginning of the set-up. For higher gas rates, wave coalescence further downstream is the most important mechanism for slug formation. When the stratified flow in front of the slugs is higher than the stable-slug height h_0 , the slug will grow by picking up liquid at the front as long as $h_{strat,front} \geq h_0$. This h_0 liquid level is the same as the minimum hold-up environment as discussed in the previous section. When the liquid level in front of the slug equals h_0 , the slugs will move further downstream with fixed length, or decay into large amplitude roll waves in case the slug has not reached a stable length yet. Other slugs can overtake these roll waves, since slugs move faster than these waves, increasing the length of these slugs.

The slug frequency can be related to the length of the slugs. According to Woods et al. (2006), the frequency of slugging for a fully developed flow can be derived from the intermittancy of the flow. For a stationary observer, the time that slugs are present is denoted by the intermittancy I as

$$I = \frac{f_s L_s}{C} \quad (2.13)$$

with f_s the slug frequency, L_s the slug length, and C the velocity with which the whole structure moves. This intermittancy can also be estimated based on the superficial velocities

$$I \approx \frac{U_{sl}}{U_{sl} + U_{sg}}. \quad (2.14)$$

The velocity C equals

$$C = 1.2(U_{sg} + U_{sl}), \quad (2.15)$$

as shown by Bendiksen (1984); Woods and Hanratty (1996). Combining these expressions, the slug frequency f_s for stable, fully developed slugs equals

$$\frac{f_s D}{U_{sl}} = 1.2 \left(\frac{L_s}{D} \right)^{-1}, \quad (2.16)$$

with D the diameter of the tube, L_s the length of the slug and U_{sl} the superficial liquid velocity. This simple relation ignores the transport of liquid in the stratified flow and of the the gas inside the liquid slugs. These effects are studied in more detail by Woods and Hanratty (1999). Since the terms D on both sides cancel, the relation becomes $f_s = 1.2 U_{sl} / L_s$, which is quite easy to check with experimental data. For slugs with constant length, the slug frequency will also be constant. The fact that $f_s L_s = \text{constant}$ represents conservation of the amount of liquid in the system. Many short slugs develop into fewer longer slugs. For higher liquid flow rates, more liquid is available, so more or longer slugs can be formed.

A similar relation can be derived with a more physical background, as shown in Oliemans (2001). The length of a unit-cell L_u , consisting of a liquid slug together with the gas bubble, equals

$$L_u = \frac{U_t}{f_s} \quad (2.17)$$

with U_t the translational velocity and f_s the slugging frequency. The translational velocity equals $U_t = 1.2 U_{mix}$, with U_{mix} the mixture velocity defined as the sum of the superficial gas and liquid velocities. The length of the unit equals $L_u = L_s + L_b$ with s and b indicating the liquid slug and the gas bubble. The slug length can be expressed as (Heywood and Richardson (1979))

$$\frac{L_s}{L_u} = \lambda_l - 0.10, \quad (2.18)$$

with λ_l the liquid volume fraction defined as

$$\lambda_l = \frac{U_{sl}}{U_{sl} + U_{sg}} = \frac{U_{sl}}{U_{mix}}. \quad (2.19)$$

The slug length thus equals

$$L_s = (\lambda_l - 0.10) L_u = (\lambda_l - 0.10) \frac{U_t}{f_s} = (\lambda_l - 0.10) \frac{1.2 U_{mix}}{f_s}, \quad (2.20)$$

which for high liquid volume fractions $\lambda_l \gg 0.10$ can be approximated by

$$L_s = (\lambda_l - 0.10) \frac{1.2 U_{mix}}{f_s} \approx \frac{1.2 \lambda_l U_{mix}}{f_s} = \frac{1.2 U_{sl}}{f_s}, \quad (2.21)$$

as derived by Woods et al. (2006) in (2.16). Because the liquid volume fraction is assumed to be high, $\lambda_l \gg 0.10$, the relation only holds for large liquid flows.

The dependence on gas and liquid flow rates is illustrated by figure 2.9. For all constant liquid velocities, the frequency shows similar relations to the gas velocity, a local minimum for gas velocities around 4 m/s and the frequency is no longer affected by the gas flow rate for $U_{sg} > 10$ m/s.

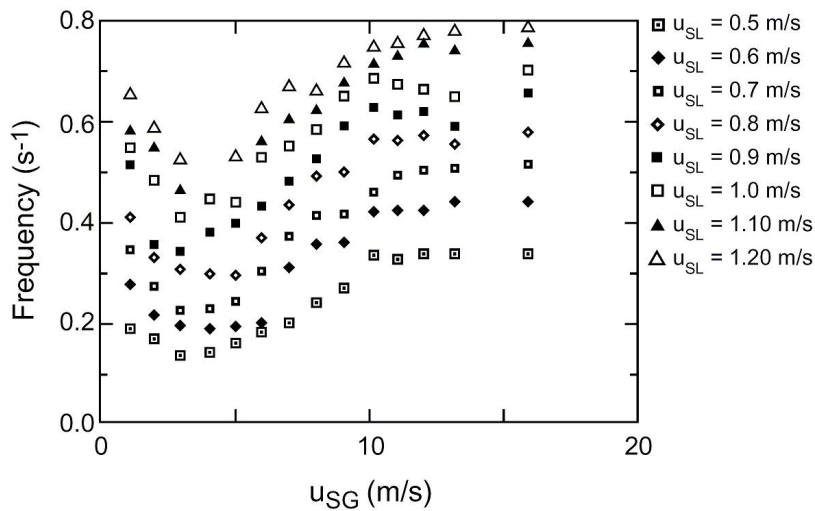


Figure 2.9: Slug frequency for different combinations of gas and liquid velocities in a $D = 0.095$ m pipe. The frequency increases linearly with the liquid velocity and has a minimum around 4 m/s gas velocity. For high gas velocities, the frequency becomes independent of the gas rate. From Woods et al. (2006).

The dip which is present at $U_{sg} \approx 4$ m/s is, according to Andritsos and Hanratty (1987), due to the presence of KH-waves which start to occur around 4 m/s superficial gas velocity. For lower gas velocities, the slugs are formed by waves touching the top of the tube. For larger velocities, the formation is dictated by the coalescence of rollwaves.

For high gas velocities, $U_{sg} \geq 10$ m/s, the frequency has become independent of the gas velocity, and only changes for different liquid velocities. In this regime, there is a linear relation between the slugging frequency and the liquid velocity. When increasing the liquid velocity, in the picture the range from $U_{sl} = 0.5$ m/s upto $U_{sl} = 1.2$ m/s is shown, the frequency of slugging will also increase, as already indicated by (2.16). When looking in the graph at constant gas velocity, a doubling of the liquid velocity will also give a double slug frequency.

In the lower gas velocity part of the figure, a double liquid velocity also gives an increase in slug frequency, but is now more than a factor two. From experiments, it is observed that also the slug length will decrease for higher liquid flow rates (see chapter 5), which according to (2.16) also influences the slug frequency. For the high gas velocity part this effect of the slug length does not play any role, because in the hydrodynamic slug region, all slugs have approximately the same length, independent of the gas velocity.

The frequency at which slugs occur has also been studied by Ujang et al. (2006). In a 0.078 m tube of 37 m length, the passing liquid slugs were measured in an air-water system. Most of the slugs were initiated in the first 3 m of the tube, so similar to the observations by Woods et al. (2006) close to the inlet. The value of the slug frequency decreased towards the end of the tube, where it has reached its fully developed value. The pressure in the system does not strongly influence the rate of slugging. As a result of the increased pressure (up to 9 bar(a)), the onset of slug initiation was delayed, with slug precursors being formed at locations further downstream. During the initiation phase, close to the entrance, the slug arrival times can be approximated with an uncorrelated Poisson process. For the fully developed situation downstream, both the slug length and the slug arrival time fit a log-normal distribution.

A model for predicting the slug frequency under various conditions was proposed by Taitel and Dukler (1977). In this model for predicting the slug flow regime, the conditions for which slug flow is likely to occur (by Taitel and Dukler (1976)) and the pressure drop are dependent on the slug frequency, which is usually set as an input parameter. Since the pressure drop is almost directly proportional to the slug frequency, it is necessary to have a good estimate of this frequency before something can be said about the pressure drop.

Since the slug frequency depends on numerous factors, most of the experimentalists report their data as a function of liquid and gas flow rates for fixed tube diameters. Gregory and Scott (1969) attempted a more general correlation, which turned out to be unsuccessful. The correlations are unreliable for situations other than were used in the derivation. Taitel and Dukler (1977) modeled the complicated entrance phenomenon using open channel flow equations for predicting the slug frequency analytically as well as to improve the understanding of slug initiation problems. The basic assumption was that the frequency equals the inverse of the time needed to rebuild the film equilibrium, the sequence shown in figure 2.10.

The slug frequency can be calculated based on the different stages of the slug formation mechanism. From experiments, it is known that slugs start from unsteady waves on a growing stratified layer. The time the liquid layer needs to rebuild from the lower, stability level (h_s) after the slug till the upper equilibrium level (h_e) from which the new slugs are formed, is the characteristic timescale in the process. The frequency is the inverse of this timescale. From momentum and continuity equations on the liquid phase, the time dependent liquid level profile $h(x, t)$ can be calculated. When the values h_s and h_e are known, the time required for the growth $h_s \rightarrow e$ can be calculated, which gives a value for the time interval and thus the fre-

quency. For details on the equations and the schemes used for the calculations, see Taitel and Dukler (1977) where the different steps are described, but no general analytical expression for the slug frequency is given.

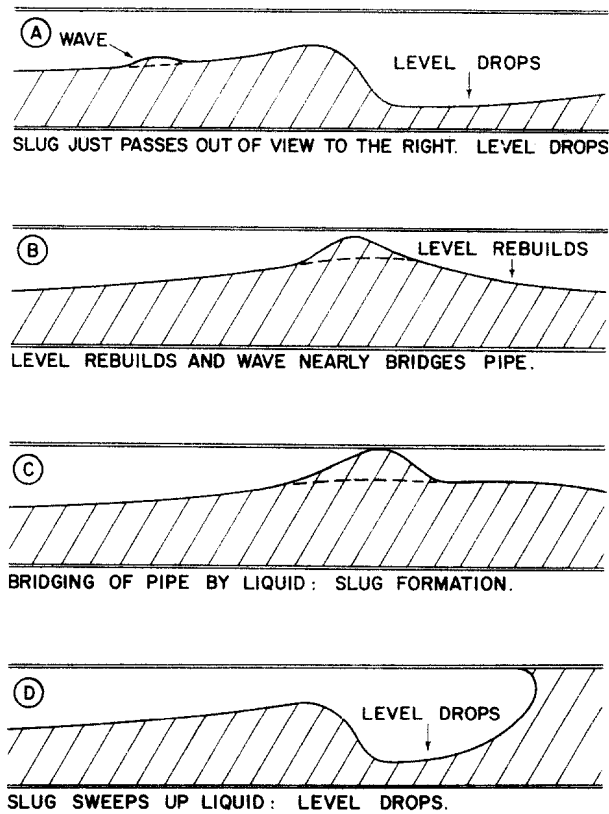
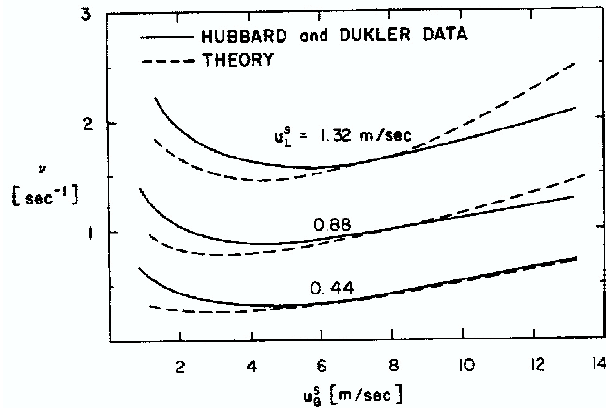


Figure 2.10: Different stages of a slug initiation from a stratified layer. The first image is just after the previous slug has gone. In B waves start to grow, which block the pipe cross section in C. The fluid is accelerated, sweeps the liquid in front, creating a liquid slug (D). After the slug has moved to the right, the mechanism starts at A again. From Taitel and Dukler (1977).

Figure 2.11 shows the comparison between experimental data and the theory derived by Taitel and Dukler (1977). The theory behind slug frequency is based on the different stages of slug formation as illustrated in figure 2.10



(a) Air-water flow in a 3.81 cm pipe.

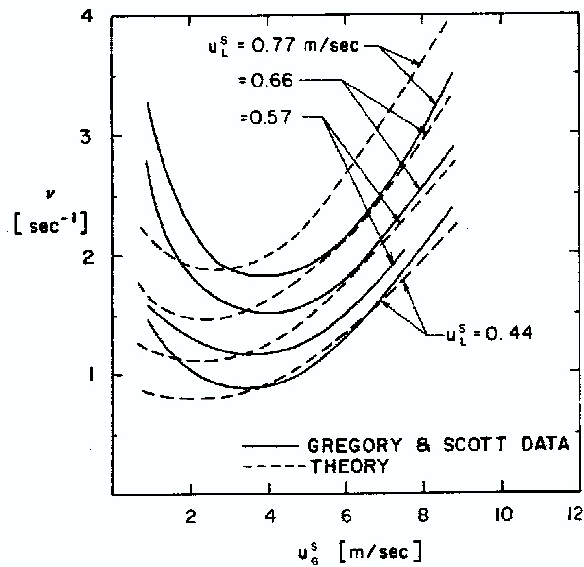
(b) CO₂-water flow in a 1.9 cm pipe.

Figure 2.11: Comparison between the theoretical and experimental slug frequency ν [s^{-1}] (vertical axis) for a range of superficial gas velocities U_{SG} [m/s] (horizontal axis). The different sets of lines show the superficial liquid velocities investigated. The upper graph shows air-water flow in a $D = 3.81$ cm tube, in the lower graph the experiments with water-CO₂ in a $D = 1.9$ cm tube is shown. From Taitel and Dukler (1977).

Tronconi (1990) collected several sets of experimental data from other investigators. The datasets were compared to the theoretical slug frequency calculated as

$$f_s = 0.61 \frac{\rho_g}{\rho_l} \frac{u_g}{D - h_l}, \quad (2.22)$$

which only depends on the two densities, the gas actual velocity u_g and the equilibrium level of the stratified layer h_l in the entrance region. The slug frequency prediction is now reduced to the problem of determining the configuration of the stratified flow at the inlet. The theoretical relation is based on the assumption that the slug frequency is one half of the frequency of the unstable wave precursors of the slug. The relation for f_s was derived by adapting the wave instability analysis by Kordyban and Ranov (1970) and Mishima and Ishii (1980). The method by Taitel and Dukler (1977) is used to estimate the equilibrium liquid level. The value of h_l can be related to the Lockhart-Martinelli parameter

$$X = \left[\frac{(-dp/dx)_l}{(-dp/dx)_g} \right]^{0.5}. \quad (2.23)$$

When the interfacial friction factor equals the gas wall friction factor, $f_i/f_g = 1$, all terms in (2.24) only depend on the dimensionless liquid height h_l/D .

$$X^2 = \frac{\left[\frac{S_g}{A_g} + \left(\frac{S_l}{A_l} + \frac{S_i}{A_g} \right) \frac{f_i}{f_g} \right] (u_g D_g)^{-m} A_l \left(\frac{u_g}{u_l} \right)^2}{(u_l D_l)^{-n} S_l}, \quad (2.24)$$

with n, m the constants from the Blasius-type expressions

$$f_g = C_g Re_g^{-m}, \quad f_l = C_l Re_l^{-n}. \quad (2.25)$$

Since the value of the slug frequency is affected by numerous factors, it is difficult to design a general expression for the slugging rate. Usually, the data are presented for fixed tube diameter and fluid properties, and an expression as function of the flow rates is derived. In these empirical relations, usually for small diameter pipes (smaller than 2 inch), only a few parameters are involved. Besides the Froude number and the flowing liquid fraction, also the diameter, length and topography of the tube, gas and liquid flow rates, densities and viscosities should be taken into account.

Several slug frequency relations for hydrodynamic slugs have been proposed by different authors, most of them resulting in a similar expression. One of the first correlations for the slug frequency f_s by Gregory and Scott (1969) reads as

$$f_s = 0.0226 \left[\frac{U_{sl}}{gD} \left(\frac{19.75}{U_m} + U_m \right) \right]^{1.2}, \quad (2.26)$$

with U_{sl} and U_m the superficial liquid and mixture velocities respectively, D the tube diameter and g the gravitational acceleration. Crowley et al. used another set of experiments (other fluids), and came to a similar relation, but the factor in front is twice as large.

Greskovich and Shrier (1972) tested the Gregory and Scott relation, and observed a deviation. Based on several sets of data, they changed the correlation into

$$f_s = 0.0226 \left[\lambda \left(\frac{79.5276}{D} + \frac{U_m^2}{gD} \right) \right]^{1.2}, \quad (2.27)$$

with

$$\lambda = \frac{U_{sl}}{U_{sl} + U_{sg}} \quad (2.28)$$

defining the flowing liquid fraction.

Heywood and Richardson (1979) used air-water experiments to make a fit for the slug frequency. The results are similar to that of Greskovich and Shrier, only differing in the constant and the exponent

$$f_s = 0.0434 \left[\lambda \left(\frac{79.5276}{D} + \frac{U_m^2}{gD} \right) \right]^{1.02}. \quad (2.29)$$

A set of available experimental and field data is compared with various models by Zabaras (2000). Both empirical and mechanistic models were examined, and put side by side with laboratory and published data. In total 399 data points were collected from hydrodynamic slug experiments, ranging in diameter from 1 up to 8 inch, and inclinations from horizontal to 11 degrees upward. In total, 8 of the tested models did not give satisfactory agreement with the experimental data sets.

From the complete 399-points data set, it was observed that the slug frequency increases with the inclination angle from horizontal. Based on the angle effect and the correlation by Gregory and Scott (2.26), the expression

$$\frac{f_s}{f_{sh}} = a + b [\sin(\beta)]^c \quad (2.30)$$

was fitted, with f_s the experimental slug frequency, f_{sh} the value given by (2.26) and β the inclination from horizontal.

The parameter a , b and c were optimized for the set of 399 data points, making the average error equal to zero and the average absolute error to be minimal. The final expression is

$$f_s = 0.0226 \left[\frac{U_{sl}}{gD} \left(\frac{19.75}{U_m} + U_m \right) \right]^{1.2} \left[0.836 + 2.75 \sin^{0.25}(\beta) \right], \quad (2.31)$$

in which an angle dependent term is introduced. For pure horizontal flow, only the constant in front changes.

For exact calculation of the slug frequency, the model by Taitel and Dukler is CPU-time expensive, but gives accurate results. For a fast calculation the expression in (2.31) gives good results for most of the standard situations (diameters up to 8 inch, liquid viscosity below 10 cp, etc.). The new model is significantly more accurate than the models available so far.

In table 2.1, the various expressions for the slug frequency f_s are summarized.

| Study | Slug frequency expression |
|--------------------------|--|
| Woods et al. (2006) | $\frac{f_s D}{U_{sl}} = 1.2 \left(\frac{L_s}{D} \right)^{-1}$, so $f_s = 1.2 U_{sl} / L_s$ |
| Tronconi (1990) | $f_s = 0.61 \frac{\rho_g}{\rho_l} \frac{U_g}{D - h_l}$ |
| Gregory and Scott (1969) | $f_s = 0.0226 \left[\frac{U_{sl}}{gD} \left(\frac{19.75}{U_m} + U_m \right) \right]^{1.2}$ |
| Greskovich and Shrier | $f_s = 0.0226 \left[\lambda \left(\frac{79.5276}{D} + \frac{U_m^2}{gD} \right) \right]^{1.2}$ with $\lambda = \frac{U_{sl}}{U_{sl} + U_{sg}}$ |
| Heywood and Richardson | $f_s = 0.0434 \left[\lambda \left(\frac{79.5276}{D} + \frac{U_m^2}{gD} \right) \right]^{1.02}$ with $\lambda = \frac{U_{sl}}{U_{sl} + U_{sg}}$ |
| Zabaras (2000) | $f_s = 0.0226 \left[\frac{U_{sl}}{gD} \left(\frac{19.75}{U_m} + U_m \right) \right]^{1.2} \left[0.836 + 2.75 \sin^{0.25}(\beta) \right]$ |

Table 2.1: Overview of the slug frequency expressions.

It is clear that the second group of expressions have a similar form, based on the liquid and mixture velocities.

2.6 Literature review on experimental work

In several other groups around the world, related research is done. Hanratty and coworkers did a lot of nice work on slug flow. The initiation of slug flow is described in Fan et al. (1993); Hurlburt and Hanratty (2002); Lin and Hanratty (1986); Woods et al. (2000) and several other slug related studies by Andritsos and Hanratty (1987); Al-Sarkhi and Hanratty (2001); Lin and Hanratty (1987); Soleimani et al. (2002); Soleimani and Hanratty (2003); Woods and Hanratty (1996, 1999).

Another group which has been working on slug flow for many years is Barnea and Taitel (1993); Taitel and Barnea (1997) who focused on the modeling of the slug transitions. Most of these studies focus on the short, hydrodynamic type of slugs.

The current research is on the long slugs, which were also investigated before by Nydal and Andreussi (1991); Nydal et al. (1992); Nydal and Banerjee (1996) and Kristiansen (2004). These studies cover a large range of flow conditions, which also include the hydrodynamic slugging region. The current study only investigates the slug region, where growth behavior is studied in greater detail compared to other researchers.

2.6.1 Multiphase flow experiments with different inlet conditions

Experimental work was recently done by Kristiansen (2004), who did series of measurements under various conditions. His work gives a nice overview of the possible flow pattern that may occur when working in different regimes. Besides the air-water experiments, also experiments with SF₆ were done to study density effects. In the high pressure facility at SINTEF, gas densities up to $\rho_g = 52 \text{ kg/m}^3$ were used at a pressure of $p = 8 \text{ bar}$. Also the inlet conditions were taken into account. The flow pattern at the inlet was set to slug-flow by inclining the first part of the flow line. Stratified flow at the inlet was obtained with a declined inlet section.

In the study different experimental techniques were used. In the short NTNU flowloop, a conductance based technique was used to detect the passing slug. Two metal rings in the inner wall of the tube, 1.9 cm apart, give a signals when the slug passes the rings. The limited length of the set-up does not allow to measure the whole growth process of the slugs.

In the much longer SINTEF set-up, a γ -ray technique was applied for densitometric measurements on the slugs. The detector on top of the tube measures the radiation from the Cs¹³⁷ source positioned below the tube. Based on the signal measured by the detector, the liquid height can be calculated. For the liquid hold-up measurements, a set of 5 capacitance probes was used.

In table 2.2 below, the properties of the set-ups in the different studies are summarized. The two set-ups used by Kristiansen (2004) were also operated with 3-phase air-oil-water mixtures, but here only the 2-phase experiments are mentioned.

| Properties \ Set-up | Kristiansen NTNU | Kristiansen SINTEF | Ujang Imp Coll | Zoeteweyj TU Delft |
|-----------------------------------|--------------------------|-----------------------|--------------------------|---------------------------|
| L [m] | 16 | 217* | 37 | 137 |
| D [m] | 0.06 | 0.069 | 0.078 | 0.052 |
| L/D [-] | 267 | 3145 | 474 | 2740 |
| Gas | Air | Air / SF ₆ | Air | Air |
| Gas density [kg/m ³] | 1.2 | 1.2 / 8-52 | 1.2 | 1.2 |
| Gas pressure [bara] | 1 | 1-8 | 1 / 4 / 9 | 1 |
| Gas velocity [m/s] | 0.25-6.0 | 0.2-8.0 | 2.2-8.0 | 0.5-3.0 |
| Liquid | Water | Water | Water | Water |
| Liq. density [kg/m ³] | 998 | 998 | 998 | 998 |
| Liq. velocity [m/s] | 0.03-1.0 | 0.05-1.0 | 0.2-1.0 | 0.04-0.3 |
| Inclination [deg] | 0/-0.5/-1.0 | 0-±1.0 | 0 | 0 |
| Measurement technique | Conductance (ringprobes) | γ-ray Capacitance | Conductance (lineprobes) | Conductance (line + mesh) |
| Number of measurement locations | 4 | 6 + 5 | 14 | 8+4 |
| Samplefreq [Hz] | 100 | 200 | 500 | 1000 |

* The test section measures 103 m, which corresponds to a $L/D=1492$.
This 103 m test section starts just after the 180° turn in the tube.

Table 2.2: Overview of the experimental facilities used by different researchers.

2.6.2 Two phase experiments in the hydrodynamic slugging region

Another interesting study was performed in the group of Hewitt by Ujang et al. (2006). The evolution of hydrodynamic slugs is studied for air-water flow in a horizontal pipeline at different pressures, atmospheric, 4.0 bar(a) and 9.0 bar(a). In the 37 m long set-up with 7.8 cm inner diameter ($L/D = 474$), the liquid level was measured using conductance probes at 14 locations. A set of two parallel wires in each probe measures the local liquid height in the center of the tube. Other designs contain multiple pairs of wires, positioned at ± 0.0128 m and ± 0.0256 m from the center of the tube. In all situations, the distance between the wires in a single pair measures 0.002 m. The intrusive measurement technique used in this study is similar to the one used in the current study.

Slugs are initiated in the first meters of the set-up and develop further downstream. Before the end of the pipe, the slug frequency had decreased to its fully developed value. The slug frequency strongly depends on the gas- and liquid velocities, and is hardly effected by the pressure in the system. The main difference due to increased pressures is the delayed onset of slug initiation.

Most of the experiments were done in the natural slug area, which showed nice agreements with literature and the current research. In the current research, the regime is extended to other flow areas, such as the stratified wavy flow and the growing slugs. Since most slugs were observed to be initiated in the first 3 m of the set-up, Ujang et al. (2006) installed several sensors in that particular part of the system. The other sensors were distributed over the rest of the set-up. The tube used in the current study is much longer (see table 2.2), and sensors are distributed over larger distances. Initiation of slugs is not observed in great detail, but development can be measured over a much longer distance, which is of interest outside the region of hydrodynamic slugging. Together with the broader range of flow conditions, these are the main improvements in the current research compared to the work of Ujang et al. (2006). This is also nicely illustrated in figure 2.12, where the long and the hydrodynamic slug regions are indicated. In table 2.3, the flow ranges are summarized for the different experimental set-ups. The dimensionless velocities are calculated as

$$\tilde{U} = \frac{U}{\sqrt{gD}}, \quad (2.32)$$

which is derived from the Froude number $Fr = U^2/(gD)$.

| Properties \ Set-up | | Kristiansen NTNU | Kristiansen SINTEF | Ujang Imp Coll | Zoetewij TU Delft |
|-----------------------|-------|---------------------|-----------------------|-------------------|----------------------|
| D | [m] | 0.06 | 0.069 | 0.078 | 0.052 |
| Gas velocity range | [m/s] | 0.25-6.0 | 0.2-8.0 | 2.2-8.0 | 0.5-3.0 |
| Liquid velocity range | [m/s] | 0.03-1.0 | 0.05-1.0 | 0.2-1.0 | 0.04-0.3 |
| Gas range* | [-] | 0.33-7.8 | 0.24-9.7 | 2.5-9.1 | 0.71-4.3 |
| Liquid range* | [-] | 0.04-1.3 | 0.06-1.2 | 0.23-1.1 | 0.06-0.43 |

* Non-dimensional velocities

Table 2.3: Overview of the flow ranges investigated by different researchers. For easy comparison, the ranges are also indicated in non-dimensional quantities $\tilde{U} = U/\sqrt{gD}$, so scaled for the difference in tube diameter.

In figure 2.12, the regimes investigated by the different groups are indicated.

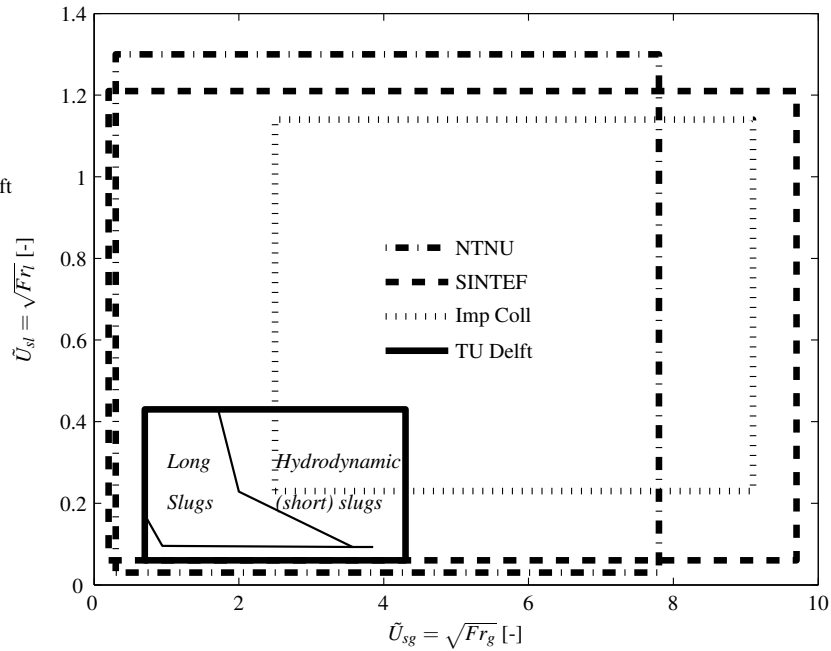


Figure 2.12: Overview of the non-dimensional velocity ranges investigated in the studies by Kristiansen (2004) (dashed and dash-dotted lines), Ujang et al. (2006) (dotted line) and the current study (solid line).

In the flowmap as shown in figures 1.4 and 2.2, different regimes can be defined. For low liquid velocities, stratified flow is present. When increasing the liquid flowrate for low gas velocities, long slugs will be formed, which can be large compared to the diameter of the tube ($L/D > 40$). Increasing the liquid flow even more, the slugs will become shorter ($L/D \leq 40$). For higher gas velocities, the transition goes directly from stratified(-wavy) flow to the short or hydrodynamic slugging regime. These different slug regimes are indicated in the flowmap with the thin lines, which are the transition lines as measured in 2" air-water flow study at TU Delft.

The work by Ujang et al. (2006) covers only the hydrodynamic slugging region, while in the current study the lower velocity ranges were investigated where the long and growing slugs are present. Since these long slugs are the major concern in industrial applications, it is necessary to have a detailed analysis in this regime.

CHAPTER 3

Experimental Set-up

The experiments presented in this thesis are performed in a 137 meter long horizontal set-up with perspex tubes of 52 mm (2") inner diameter. The tubes are mounted on opposing sides of a 68 m long steel beam for stability (see figure 3.1(a)). The tubes are straight for 68 m on one side of the supporting beam, make a wide turn, and another 68 m of straight tubes lead to the end of the flowline, which is close to the inlet. Figure 3.1(b) shows the supporting beam with the tubes mounted at both sides. The water from the outlet flows into a large vessel, which also supplies the water for the pump at the inlet.

At $x = 40$ m, a flexible tube is installed which allows the set-up to be partially inclined or declined. The first 40 m are horizontal, the next part till the turn is inclined (declined). After the turn, the tube is declined (inclined) and the last 40 m towards the outlet are horizontal.

Besides the 2" tube, also a 1" tube is installed, also having the possibility to measure in inclined and declined situations. In the current study, only the 2" tube is investigated for pure horizontal flow. The inclined geometry and scaling to the 1" tube is recommended for future research.

In section 3.1 the different parts of the set-up are shown, with special attention to the used inlets in section 3.2. The effect of the bend in the set-up is discussed in section 3.3. The alignment to the horizontal and the effect of the outlet geometry are shown in section 3.4. The instrumentation used for the experiments is discussed in chapter 4.



(a) Part of the set-up. The tubes are mounted on a steel beam for stability.



(b) Bottom view of the set-up. Left and right of the supporting steel beam, the tubes are mounted.

Figure 3.1: Pictures of the set-up. In (a) the 2" and 1" tube mounted on the supporting beam. In (b) a view from below, showing the tubes mounted on both sides of the supporting beam.

3.1 Overview of the different parts of the used set-up

The test fluids used for this study are water and compressed air, which are regulated by valves at the inlet. The volumetric flow rates [m^3/s] of both phases are measured using rotameters with different ranges, as indicated in figure 3.2. For the gas-phase, an additional electronic flow meter is installed. The superficial velocities that can be obtained are 0.1 m/s to 5 m/s for the gas phase and 0.01 m/s to 0.4 m/s for the liquid phase. At the Y-shaped inlet section, the two phases are combined.

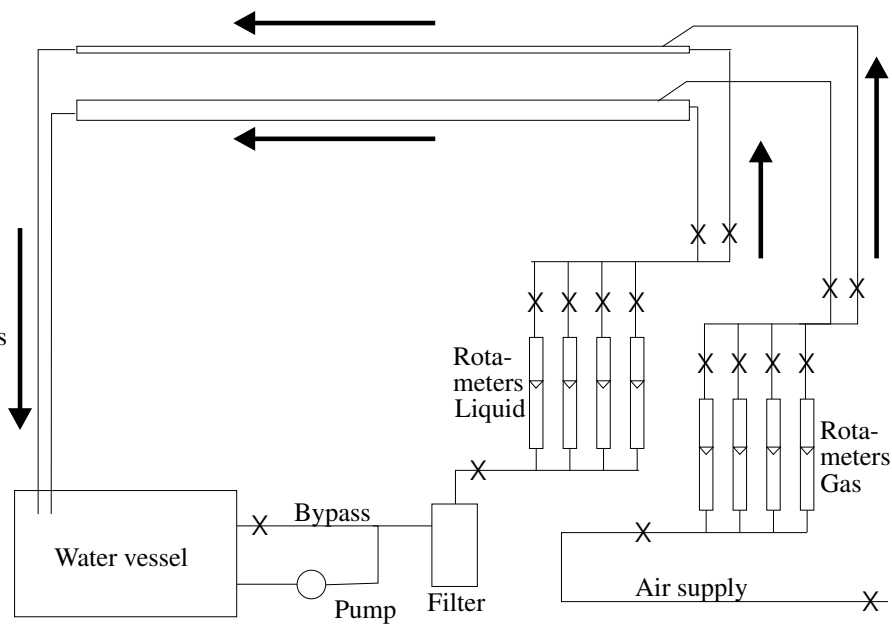


Figure 3.2: Schematic drawing of the two-phase flow set-up used in this study. On top, the 1" and 2" flowlines, both 137 m long. The turn halfway at 68 m is omitted in this schematic drawing. The valves are indicated by X. At the right, air comes from the central air supply. The flow is regulated by a valve and measured using a set of rotameters. The water is pumped from a storage vessel through a filter to the set-up. With valves and a bypass circuit, the liquid flow can be set. The water is filtered before entering the set-up and rotameters measure the actual liquid flow. At the end, water returns to the open storage vessel, allowing the gas phase to escape. The arrows indicate the flow direction.

There are two flowlines available. The top one measures 1 inch, the lower one is 2 inch diameter. In this study, only the 2 inch was used for the experiments. With a set of valves, one of the two flowlines can be selected. At 68 m from the inlet, halfway the flowline, there is a wide turn (see figure 3.3(a)), with a radius of $R = 0.30$ m, giving a ratio of $R/D = 6$ for the 2" tube. At the outlet, a 450 liter storage vessel is installed, collecting the liquid from the flowline. The vessel is large compared to the 270 liter total volume of the flowline. The water is used in a closed system, so the pump takes water from the same vessel. To prevent the pump from overheating at low flowrates, a bypass is installed. In that case, most of the flow from the pump goes back into the vessel, and only a small amount enters the set-up. For large flow rates, the bypass is closed, and all the water is pumped into the set-up.



(a) Image of the turning point halfway the set-up. The radius of the turn is large compared to the diameter of the pipe ($R/D = 6$), so the effect on the flow is limited. Within 2-5 m after the turn, the effect has completely vanished.



(b) Image of the set of rotameters which are used to measure the flow rates of both the gas (upper row) and liquid phase (lower row). The overlapping ranges allow accurate measurements in all regimes.

Figure 3.3: Photographs of the turn halfway the set-up (a) and the set of rotameters at the beginning of the set-up (b).

The array of rotameters (see figure 3.3(b)), for both phases, have overlapping ranges so all flow rates can be measured with accuracies in the order of 1% full-scale for the liquid phase and 3% full-scale for the gas phase. For the gas phase, an additional electronic flow meter is installed, which is connected to the data acquisition system. For an experiment, the average gas flow rate can be determined with an accuracy of 1%, including the calibration uncertainty. The data acquisition system also registers the measured pressures in the set-up at various locations. Near the inlet the pressure is measured, and assuming ambient pressure at the outlet (open end), the inlet pressure gives the total pressure drop in the system.

3.2 Different inlet geometries

At the inlet, the gas and liquid flows are combined using an Y-shaped inlet section. The liquid enters horizontal or from below. The gas phase always enters above the liquid phase, as indicated in figure 3.4.

A horizontal separator plate can be installed inside the inlet section to suppress wave formation at the inlet. Three inlets were available, which are shown in figure 3.4. The first geometry (a) is without separator plate, (b) and (c) have separator plates at different levels of $D/2$ and $D/3$ respectively. In order to prevent the impact of the gas-jet coming from above, the inlet section can be turned such that the liquid enters from below and the gas flows in horizontal direction (d).

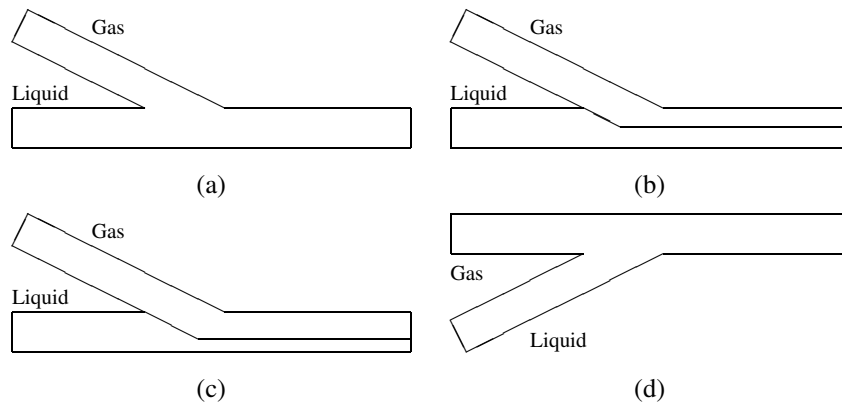


Figure 3.4: Geometries of the different inlet sections used. The standard Y-shaped inlet is shown in (a). In (b) and (c) separator plates are installed to suppress wave formation. In (d), the inlet is turned upside down to suppress wave formation.

All inlet types were tested, and type (a) showed the most waves at the interface. Since in (d) the air flows in horizontally, very little wave formation was observed, even without a separate plate installed. For most of the experiments, inlet type (b) was used, which is shown in figure 3.5.



Figure 3.5: Image of the inlet type 'b' installed in the set-up. The liquid comes in horizontally, the gas from above. After the inlet, which is 1 m in length, both phases flow parallel because of the separator plate that is installed inside the tube.

Bendiksen and Malnes (1987) performed a study to the effect of inlet and outlet geometry in a $D = 2.42$ cm horizontal tube. In figure 3.6, the transition between stratified and slug flow is indicated for different inlet and outlet configurations. The solid line compares with the present study since neither inlet nor outlet was inclined.

For high gas velocities, the geometry of the inlet and outlet is of less importance, because all lines in figure 3.6 combine for superficial gas velocities larger than $U_{sg} > 5$ m/s. The transition for lower gas velocities largely depends on the chosen inlet and outlet geometry. In the intermediate region, the upward inlet encourages the formation of slugs, such that the critical liquid velocity drops from $U_{sl} \approx 0.05$ m/s to $U_{sl} \approx 0.025$ m/s for the $U_{sg} = 3$ m/s situation. For even lower gas velocities, the effect of the outlet plays the most important role. With an upward inclined outlet, the slugs can be formed easily due to liquid accumulation. The other two lines, corresponding to downward inclined outlet, go up for lower gas velocities, making it harder for slugs to be formed. In the present study, both inlet and outlet were horizontal, which is most comparable to the situation indicated by the solid line.

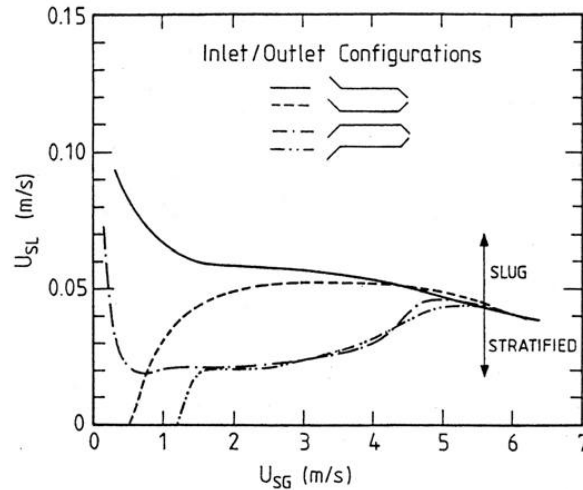


Figure 3.6: Stratified to slug flow transition for air-water using different inlet and outlet configurations in a $D = 2.42$ cm tube. From Bendiksen and Malnes (1987).

3.3 The effect of the bend halfway the pipeline

As shown in figure 3.3(a), there is a wide turn in the tube halfway the experimental set-up. After a straight part of 68 m, a wide turn with $R/D = 6$ is installed, and another 68 m of straight tube leads to the outlet. The effect of the bend is visible in the stratified flow, which starts to rotate around the central axis of the tube due to centrifugal forces. The shape of the stratified flow remains constant, only the orientation of the interface changes, as shown in figure 3.7.

This motion has vanished within several meters, depending of the fluid velocities. For high velocity situations, this length can be upto 10 m ($L/D = 200$), which is still small compared to the total length of the set-up which equals $L/D = 2740$. Due to extra friction in the bend, the velocity might drop by 10 – 15% at maximum (shown in figure 4.3 of the next chapter). Since the slug only slows down, the slug length is not effected by the bend.

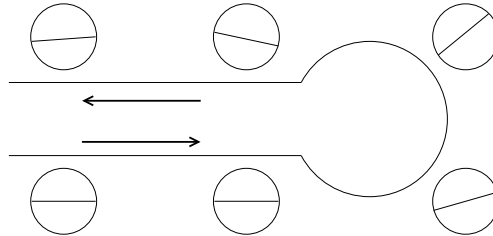


Figure 3.7: *Effect of the bend on the liquid flow in the tube. The circles next to the flow-line show the orientation of the gas-liquid interface when looking in streamwise direction (indicated by the arrows).*

3.4 The effect of the alignment of the pipeline

The tube is aligned to the horizontal. With a laser beam as a reference, the height of the tube was adjusted to horizontal, as shown in figure 3.8.

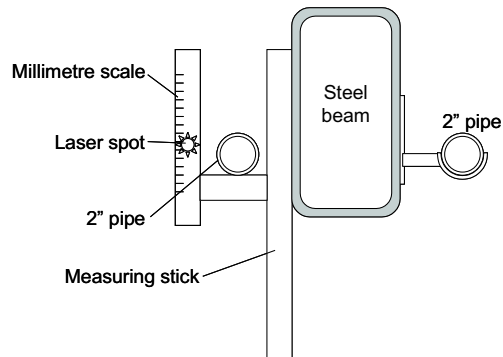


Figure 3.8: *The pipeline was aligned to a horizontal laser beam which was used as a reference.*

For determining the reference points over the total length of the 68 m long set-up, a long hose filled with water was used. The stagnant liquid levels to the same equilibrium height at both the beginning and the other end (turn halfway) of the set-up.

The deviation in tube height from the horizontal reference is

$$|h_{tube} - h_{ref}| \leq 3 \text{ mm}, \quad (3.1)$$

which is small compared to the diameter of the tube ($\Delta h \leq 0.06D$).

Initially, the error in alignment was at some locations more than the tube diameter ($D = 0.052 \text{ m}$), having large effect on the slug behavior, as illustrated in section 2.3 with the high and low elbow effect. The outlet was inclined with a total height difference of 7 cm over the last 30 m, which enhanced slug formation near the outlet.

The last element of the tube was connected to a long hose, through which the air-water mixture returned to the storage tank positioned 5 m below. When a slug leaves the tube, and moves down through the hose, gravity will give a suctioning effect of the flow inside the tube. To prevent this unwanted suction effect on the flow, the vertical hose was replaced by short near-horizontal hose, which enters a large diameter tube through which the water can return to the storage tank. Both the old and new configuration are shown in figure 3.9.

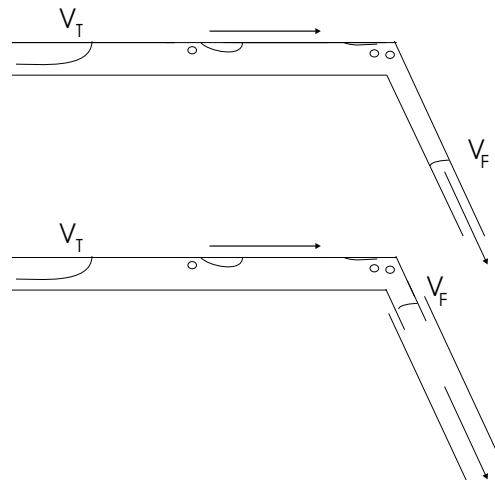


Figure 3.9: The outlet in the old (upper) and new configuration (lower image). After changing the outlet, the suction effect was gone.

The effect of the outlet was observed for long slug when measuring the tail velocity of the slug near the outlet (see chapter 4 for details on the velocity measurements). For these slugs, the tail velocity (V_T) suddenly increased at the moment the front (V_F) of the slug left the set-up and started moving downwards, being accelerated due to gravity.

3.5 Conclusions

The set-up used in the current study gives good opportunities to study the slug flow. Because of its large length of 137 m, which equals $L/D = 2740$, the development of the slugs can be measured over large distances. The waterpump and the compressed air supply provide constant inlet conditions at the Y-shaped inlet, where the gas and liquid phases are combined. A horizontal plate in the inlet section prevents the formation of slugs near the inlet. A set of rotameters measure the gas and liquid flow that enter the pipe.

The wide turn ($R/D = 6$) halfway the set-up only has some local effect on the flow, but does not influence the development of the liquid slugs. The alignment to the horizontal has much more effect on the behavior of the flow. With a laser reference, the tube was aligned to the horizontal within 3 mm from the reference.

The inlet was adapted with a horizontal plate to prevent wave formation, from which slugs might be initiated. At the outlet, the liquid flows into a large diameter pipe while the gas can escape. This was done to prevent the suction effect due to the gravity working on the liquid slug when flowing vertically back to the storage tank.

CHAPTER 4

Experimental techniques; possibilities and limitations

In this chapter, the experimental techniques used during the experiments are discussed. Two types of sensors, both based on the conductive properties of the fluids are presented. Section 4.1 deals with the point detector system, which measures only slug passages. The more advanced wire-mesh technique, discussed in section 4.2 also allows measurements in the stratified region and gives more information on the details of the slugs compared to the point detector system. Also the interior structure of the liquid slug can now be investigated in more detail. As an extension of the wire-mesh system, additional level indicators are installed in the system, which is what section 4.3 is about. With some examples from real experiments, the possibilities of the system are illustrated.

The methods used are based on the conductive properties of the water, which changes with temperature. The effect on the measurements and the correction applied is discussed in section 4.4. Finally, section 4.5 shows the data handling of the different measurement systems.

4.1 Different types of instrumentation

In the set-up, two different measurement techniques are installed, both based on the conductivity of the liquid phase. As indicated in figure 4.1, measurement sections are distributed over the whole pipeline. The first set of sensors, as indicated by the vertical lines, measures the presence of passing slugs. The bullets in the figure represent the wire-mesh sensors which

measure the structure of the stratified flow and the slugs in more detail. These sensors will be discussed in the next section.

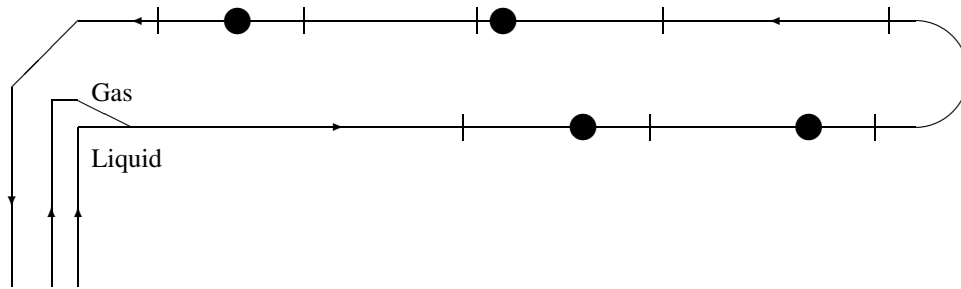


Figure 4.1: Experimental set-up with a total length of 137 m. On the left, gas and liquid flows are combined in a Y-shaped inlet section. The vertical lines indicate the positions of the point probe sensors. The more sophisticated wire-mesh sensors are located at the positions indicated by the black circles. For some measurements, the sensors were re-arranged to other locations.

4.1.1 Slug detectors for slug development measurements

The point detector sections, as shown in figure 4.2 are positioned at 8 locations in the tube. With these detectors the length and velocity of the passing slugs can be determined. Each measurement section contains 2 sensors separated by 70 cm.

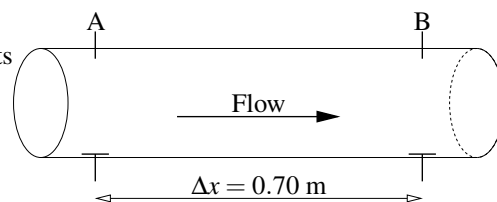


Figure 4.2: Schematic drawing of a measurement section with two point probes installed. Each probe consists of a metal contact at the bottom of the tube and one at the top of the tube. Electrical conductance between the upper and lower contact indicates the passing liquid slugs.

The sensors consist of an electrode at the bottom of the tube and one on top. Since the contacts at the bottom of the tube are circular plates of 1 cm diameter, there is always good electrical

conductance between the liquid and the contact. The top electrodes consist of a small metal pin, 1 mm in diameter which points only 1 – 2 mm into the tube interior. Because of its small size, this results in a very sharp change in conductance when a slug passes. The conductance measurements result in a 2-level signal, as shown in figure 4.4. If a slug is present, there is conductance (fixed value), without a slug there is no conductance, so zero signal. Small bubbles in the top region of the slug can influence the signal. Then the value drops to zero when the upper probe is inside the bubble, and recovers completely when the tip touches liquid again. The slug detection sensors can only determine whether a slug is present or not. The slug length and velocity can be measured at 8 location (see table 4.1), also giving the opportunity to calculate the development of the slugs when passing through the set-up, as illustrated by figure 4.3. From the time lag between the signals at probes A and B, the slug velocity can be calculated (see figure 4.4).

| Sensor | 1 | 2 | 3 | 4 | 5 | 6 | 7 | 8 |
|--------------|----|----|----|----|----|-----|-----|-----|
| Position [m] | 29 | 43 | 62 | 74 | 93 | 107 | 120 | 132 |

Table 4.1: Positions of the point probes in the set-up, as used during most of the experiments.

The length and velocity development of several slugs is shown in figure 4.3. The velocity in (a) is relatively constant and ranges between 4 m/s and 5 m/s for all slugs at all positions. The local dip, which is present for all slugs at $x = 80$ m is due to the effect of the turn half-way the set-up. This slows down the slugs a little, but initial velocity is recovered before the next sensor is reached.

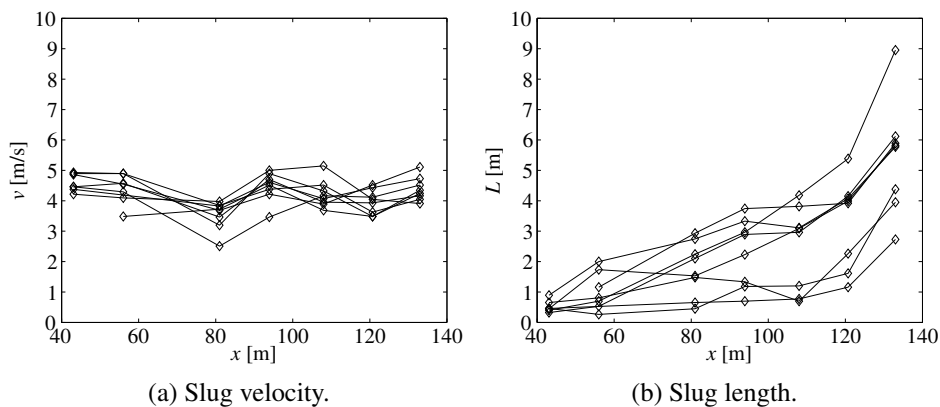


Figure 4.3: Slug development along the length of the tube, measured with the point probe sensors. The dip in velocity (a) at 80 m is due to the turn halfway. In (b) the increase in slug length is shown.

For the slug length in figure 4.3(b), two regimes can be defined. The short slugs, which remain shorter than $L \approx 2$ m ($L/D \approx 40$) till they reach the $x = 120$ point. Near the end of the set-up, they start growing, which is related to the suction effect of the outlet, as illustrated in figure 3.9. Other slugs, which start growing from the beginning of the set-up, leave the set-up as long slugs with lengths upto $L \approx 9$ m ($L/D \approx 180$), partially due to the suction effect.

4.1.2 Data processing for the slug detector signals

From the time difference between the slugs passing the first (A) and second sensor (B) of the same section (see figure 4.2), the slug velocity can be calculated. Because also the length of the slug-pulse is known, the slug length can be calculated using the velocity as calculated before. The calculation of velocity and length is illustrated in figure 4.4. Since the sampling frequency is 1 kHz and the upper probe is very small, errors in time and space may be neglected compared to slug lengths of several meters and velocities in the order of 0.5 – 5 m/s.

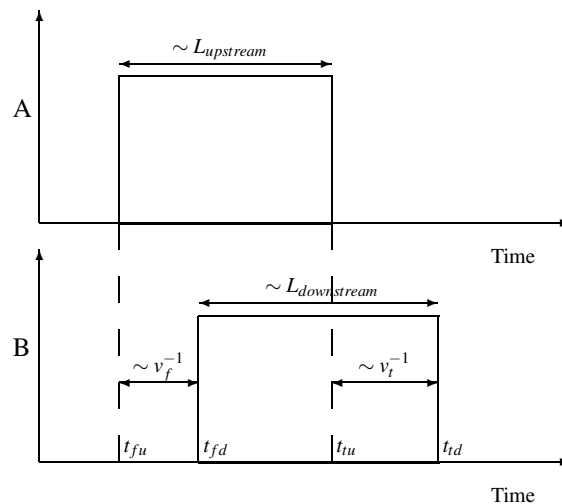


Figure 4.4: Timing signals from the two slug detectors. The upper graph represents (simplified) the signal of sensor A (upstream) and the lower graph corresponds to sensor B (downstream).

The velocity of the slug front can be calculated from the difference in arrival time of the slug at positions A and B. The same can be done at the tail of the slug, giving the tail velocity. The distance between the 2 measurement points A and B equals $\Delta x = 70$ cm.

$$v_{front} = \frac{\Delta x}{t_{fd} - t_{fu}}, \quad (4.1)$$

$$v_{tail} = \frac{\Delta x}{t_{td} - t_{tu}}, \quad (4.2)$$

$$L_{slug} = \Delta t \times v_{tail}, \quad (4.3)$$

with Δt being equal to $t_{tu} - t_{fu}$ or $t_{td} - t_{fd}$ for the upstream or downstream slug length respectively. In (4.3), the tail velocity v_{tail} is chosen for the slug length calculation, because this value is more representative for the slug propagation velocity than the front velocity. The slug tail velocity is constant during the whole travel of the slug, while the front velocity starts high(er) and decreases towards the tail velocity further downstream, as indicated in figure 4.5. Assuming a homogeneous liquid slug, the center of mass moves with a velocity $v_{cm} = \frac{1}{2}(v_{front} + v_{tail})$.

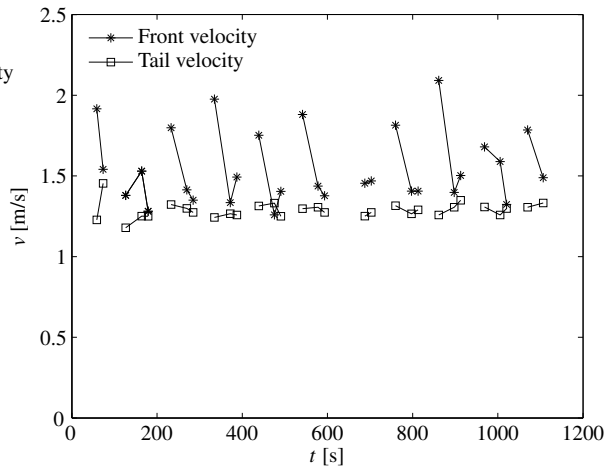


Figure 4.5: Front and tail velocity for different slugs in a single experiment (constant gas and liquid flow). The connected points correspond to the same slugs, measured when passing the different measurement locations.

The tail velocity of the slugs defines the propagation velocity of the whole slug, which is equal to the velocity of the gas bubble behind the slug. When the velocity of the slug front differs from the tail velocity, the slug length will change. From figure 4.5, it is clear that the front velocity of the slugs is larger than its tail velocity, indicating a growing slug. The growth rate, the ratio of front and tail velocity is not the same for all slugs. The tail velocity, equal to

the velocity of the bubble behind the slug, can be calculated from the mixture velocity, and equals for the flow parameters in the example 1.36 m/s, which is in good agreement with the data points shown in figure 4.5.

4.1.3 Slug development length

The growthrate can be expressed per unit of time, or per unit of length the slug has moved. Since in the set-up, the sensors are at fixed positions, slugs with different velocities will be captured at different times, so also in different stages of the growth process. Fast slugs might have left the set-up before the growth process was measured accurately. Appendix A explains that for slugs with similar growthrate, defined as

$$\frac{dL}{dx} = \frac{v_f}{v_t} - 1, \quad (4.4)$$

there is no difference in fast slugs or slow slug. For both situations, the same part of the growth process is measured.

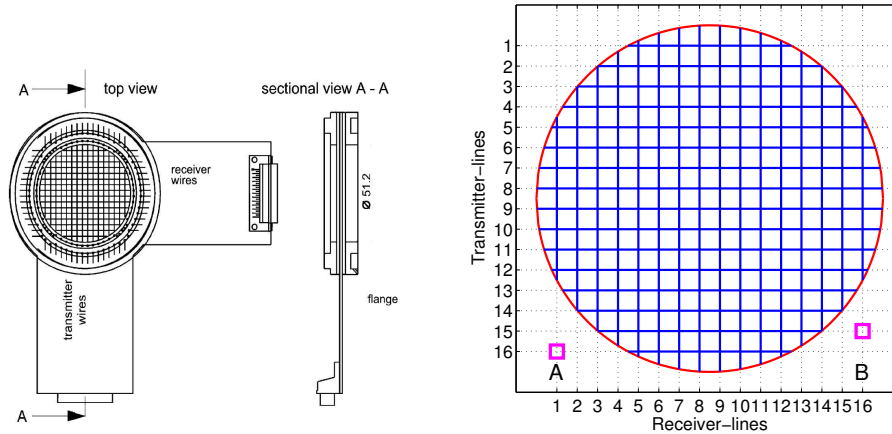
4.2 Wire-mesh sensors for detailed flow imaging in stratified and slug flow

The point probe sensors as discussed in the previous paragraphs give nice results on the length and velocity of the slugs, as shown in figures 4.3, but nothing can be said about the structure of the slugs. Also the local void fraction and the shape of the slugs are interesting parameters, which can be measured with an additional set of sensors. A set of 4 wire-mesh sensors is installed (indicated with the circles in figure 4.1) which are able to measure the structure. The locations of these sensors are given in table 4.2.

| | | | | |
|--------------|----|----|-----|-----|
| Sensor | 1 | 2 | 3 | 4 |
| Position [m] | 38 | 56 | 105 | 125 |

Table 4.2: Positions of the wire-mesh sensors in the set-up, as used during most of the experiments.

The measurement technique used to visualize the structure of the flow is the wire-mesh, which is based on the difference in electrical conductivity of both phases. The sensor used in this study is shown in figure 4.6. The sensor, originally designed by Prasser et al. (1998); Prasser (2000); Prasser et al. (2001), is used for the first time in horizontal flow in this study.



(a) Wire mesh sensor. The wires form a 16x16 grid, of which only a circular part is used. From Prasser et al. (2001).

(b) Measure grid with 3 mm wire distance. From the 256 points in the mesh, only 216 are within the radius of the tube.

Figure 4.6: Side view of the wire-mesh sensor (a). In (b) the grid with the transmitter and receiver lines is shown in detail.

The sensor consists of two planes with 16 parallel 0.12 mm wires each. The spacing between the two planes equals 1.5 mm, between two parallel wires 3 mm. Since the square sensor is installed in a circular tube, only 216 of the total 256 wire crossing points are within the radius of the tube, as indicated in figure 4.6(b). In total, 4 of these sensors are installed in the set-up (figure 4.1). During the measurements, the horizontal transmitter lines are pulsed one after another. By measuring the signal of all crossing vertical receiver wires, the local conductivity around the crossing points in the mesh is known. This conductivity signal is a measure for the amount of water, and thus indicates the local phase composition in the grid cell.

4.2.1 Data acquisition with the wire-mesh

The wire-mesh system is used to measure the structure of the interior to the liquid slug and the surrounding stratified layer. The measurement system can handle sampling frequencies up to $f = 5$ kHz (the measurement time is limited to 17 s at $f = 5$ kHz). Since the measurements usually are much longer, the system is used in a continuous mode, for which the frequency is limited to $f = 1$ kHz. The frequency of the measurements was for most of the experiments $f = 500$ Hz or $f = 1000$ Hz, allowing for long measurements up to several hours.

A single frame contains 32x32 datapoints (4 sensors with 16x16 points each). For each of the 1024 points, a 12 bits long signal is recorded, resulting in 1536 bytes per frame (8 bits per byte). At a framerate of $f = 1$ kHz, the datarate equals 1.5 Mbytes per second, filling up a 1 Gbyte datafile in less than 12 minutes. For continuous measurements, a new file is created automatically after reaching the 1 Gbyte filesize. During post-processing, these separate files can be combined. A more detailed description on the components and the structure of the wire-mesh measurements is given in appendix E.

4.2.2 What is actually measured. Different approaches to the measurement volume

The grid, 16x16 points in each wire-mesh sensor (see figure 4.6), divides the area of the tube into small volumes. In total, 4 of these sensors are installed distributed over the length of the tube (see figure 4.1). When a bubble is present inside one of these volumes, the signal in that specific point will drop. The total liquid hold-up can be calculated by adding the contributions of all individual local hold-up values obtained by the measurement points in the grid. The total gas volume fraction is defined as 1 minus the liquid hold-up.

The size and shape of the active volume around the grid cells can be defined in different ways. According to Richter et al. (2002), the measuring volume should be taken equal to a mesh cell around the crossing point, since the potential is set to zero outside this cell. This cubic cell, with sizes of 3 mm \times 3 mm in the plane of the mesh and a thickness of 1.5 mm, is indicated in figure 4.7. This approach results in volumes that are symmetric for both transmitting wires and receiving wires. The total volume of the cell equals 13.5 mm³. The whole area is covered by the cells, and there is no overlap between the cells.

Detailed measurements on the bubble sensitivity showed that also other grid cells, neighboring cells and even further away, were influenced by a passing bubble. From a linear approximation, the volume can reach up to 2 wires on each side of the grid point, which is far beyond the cubic range as proposed in figure 4.7.

Within a measurement cycle, as described in detail in appendix E, the transmitter wires are pulsed one after another. All other (non-pulsed) wires are connected to zero potential with a low impedance, according to Prasser et al. (1998). Within the pulse on a transmitter wire, current measurements are evaluated simultaneously for all receiving wires and converted into voltages and stored in 16 separate sample and hold circuits.

When looking to a single transmitter wire at a certain non-zero potential, it crosses several identical receiving wires, all with low impedance connected to zero potential. The electric field is the same and symmetrical around each of the receiving wires, as indicated in figure 4.8(a). When defining the unit cell on the crossing transmitting wire, this results in a unit

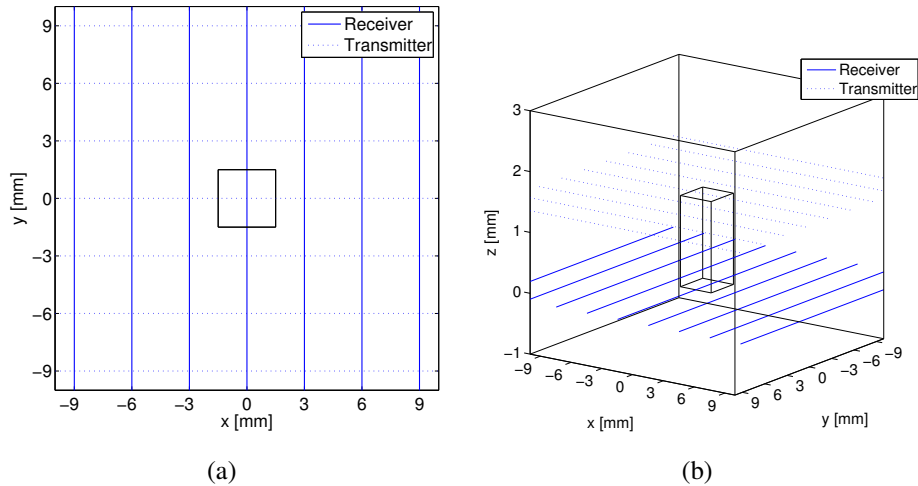


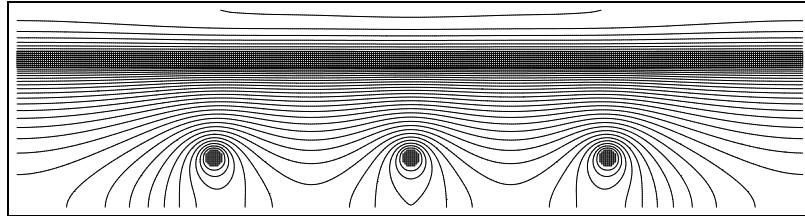
Figure 4.7: *Effective volume defined as a cubic. Note that the vertical axis in (b) is stretched for clarity.*

of one wire-wire distance centered around the receiver wire.

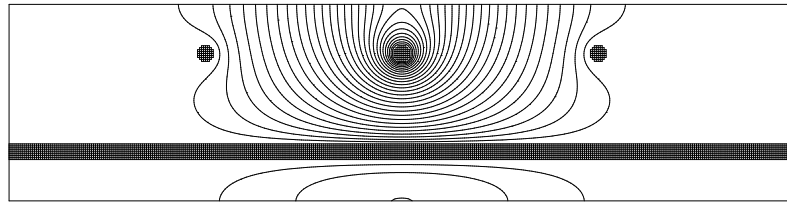
On the other hand, a single receiver wire (zero potential) crosses several transmitter wires. One of these transmitter wires, the pulsed one is at a certain potential, while the other ones (non-pulsed) are set to zero potential, which is different for the central wire in figure 4.8(b) compared to the neighboring wires.

In figure 4.8, the iso-potential lines are plot for the two different situations. For simplicity, the calculations by Smeets (2007) are based on a 3×3 rod geometry instead of the actual 16×16 .

From the potential images, the electric field lines can be calculated, which are perpendicular to the iso-potential lines. Using these field lines, the size and shape of the cell can be approximated. The volume around a grid point (crossing wires) is 3 mm wide on the transmitting wire (1.5 mm on both sides of the center) and 12 mm on the receiving wire (6 mm on each side). The total thickness equals the plane-plane distance of 1.5 mm. A schematic drawing of the volume is shown in figure 4.9, which clearly shows that the symmetry between the two planes is broken, The volume of the cell now equals 9 mm^3 , which is smaller than the 13.5 mm^3 calculated for the cubic cell. The total cell volume of all cells together is not equal to the total volume of the whole mesh. Some points in space are counted double, because of the overlapping cell volumes. Other points are in "dead zones", which are in none of the cell volumes.



(a) Iso-potential plot of a pulsed transmitting wire (top) and multiple receiving wires.



(b) Iso-potential plot of a receiving wire (bottom) and multiple transmitting wires (middle one is pulsed).

Figure 4.8: Iso-potential plot for transmitting wire crossing multiple receiving wires (a) and a receiving wire crossing several transmitter wires (b) of which one is pulsed and the other transmitter wires are at zero potential. From Smeets (2007)

Based on the potential plots, the pyramid-structure is more realistic than more simple cubic approximation. The major drawback of the pyramids is that there will be a certain overlap between adjacent volumes, so a single bubble will influence multiple cells. Since the number of bubbles is larger than the number of grid points, a unique bubble reconstruction is not possible. Because the main parameter in this study is the average hold-up (void fraction), the more simple cubic volumes will be used.

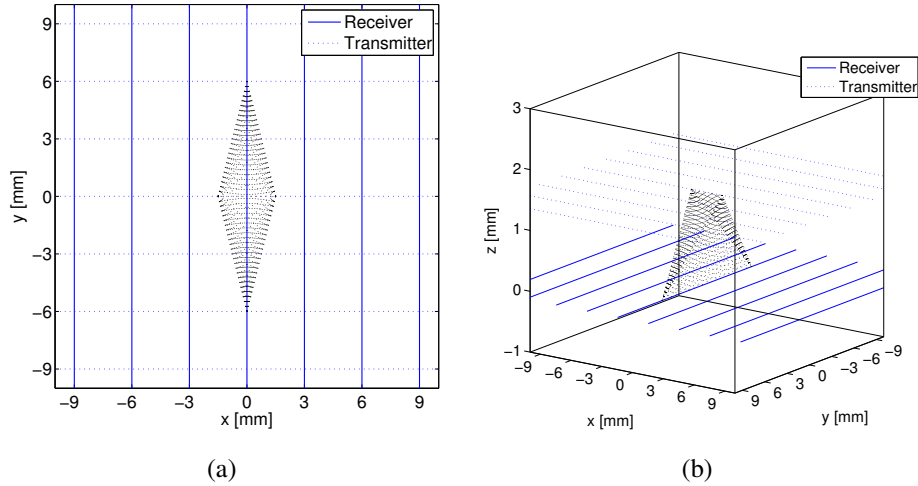


Figure 4.9: Effective volume defined as a pyramid structure. Note that the vertical axis in (b) is stretched for clarity.

4.2.3 The amount and distribution of gas bubbles in the liquid slug

Liquid slugs may contain small gas bubbles, defined as the void fraction of the slug, also defined as the gas hold-up α_g . Since the gas and liquid hold-up sum up to one, $\alpha_g + \alpha_l = 1$, and $\alpha_l = H$, the void fraction can be calculated as $1 - H$ from the hold-up experiments, as shown in figure 4.10.

Assuming cubic cell volumes, each grid point corresponds to a $3 \times 3 \times 1.5 \text{ mm}^3$ volume centered around the crossing of the wires. For the total hold-up in the plane, the local hold-up of all individual cell volumes is summed and normalized by the number of grid points. All cells in the interior of the cell have a weight of $w_{i,j} = 1$, while the points near the wall have a weight equal to the ratio of the volume of the cell which is inside the tube and the volume of an interior cell. Figure 4.11 shows two different masks. In the left figure (a), only cells for which the grid point is inside the tube are counted. Therefore, some cells are used with $w_{i,j} = 1$ while part of the cell is outside the tube, and other cells are neglected $w_{i,j} = 0$ while part of the cell is inside the tube. In the second figure (b) the weight of each cell is related to the part of the cell volume which is inside the tube.

The local hold-up in a single grid point is calculated as

$$h_{i,j} = \frac{S_{i,j}}{C_{i,j}}, \quad (4.5)$$

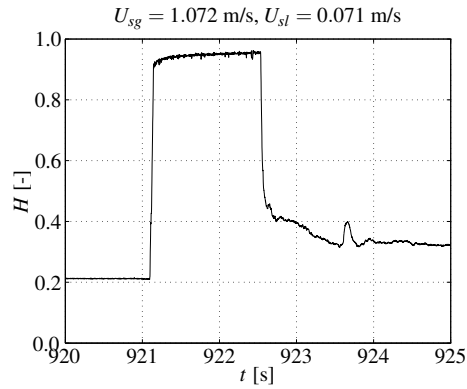
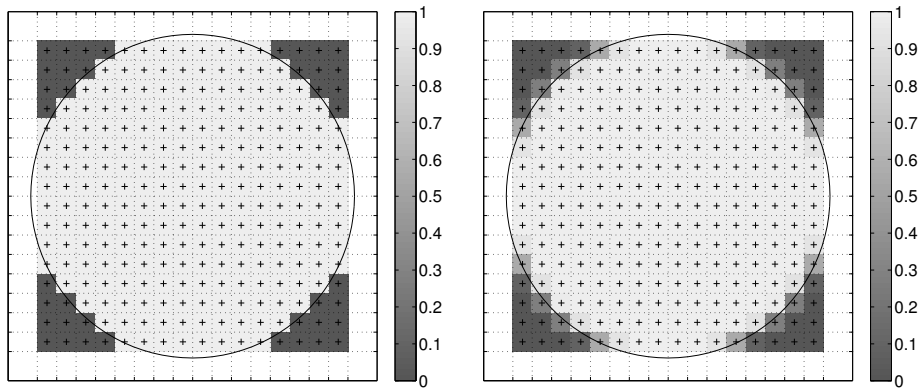


Figure 4.10: Hold-up in the slug body. The hold-up in the stratified flow before the slug is 0.22. The slug body starts with a hold-up of $H = 0.94$ in the front ($\epsilon = 6\%$) and increased to $H = 0.98$ in the tail of the slug ($\epsilon = 2\%$).



(a) Binary mask, only using the cells of which the center is within the radius of the tube.

(b) Mask with weight factors $w_{i,j}$ indicating the active volume of the cells.

Figure 4.11: Two different masks used for the total hold-up calculations. In (a), the position of the cell center (=grid point) determines the mask, while in (b) the actual cell volume fraction is used. The lines indicate the boundaries of the cells, while the plus-signs denote the centers of the cells, which is equal to the point where the wires cross.

with $S_{i,j}$ the signal measured in point (i,j) and $C_{i,j}$ the corresponding time dependent calibration value. The total hold-up H is calculated as a weighted sum of the local hold-up

values

$$H = \frac{\sum_{i,j} w_{i,j} h_{i,j}}{\sum_{i,j} w_{i,j}}, \quad (4.6)$$

which is shown in figure 4.10 for the whole slug.

Most of the entrained bubbles are present in the front of the slug, and the slug body becomes more solid towards the tail, as shown in figure 4.10. The structure and distribution of the bubbles can be seen in the cross-sectional planes. In figure 4.12, the phase distribution in a plane in the front part of the slug (a) and in the tail of the slug (b) are shown. From the images, it is clear that most of the bubbles are present in the front of the slug, which agrees with the hold-up measured in figure 4.10.

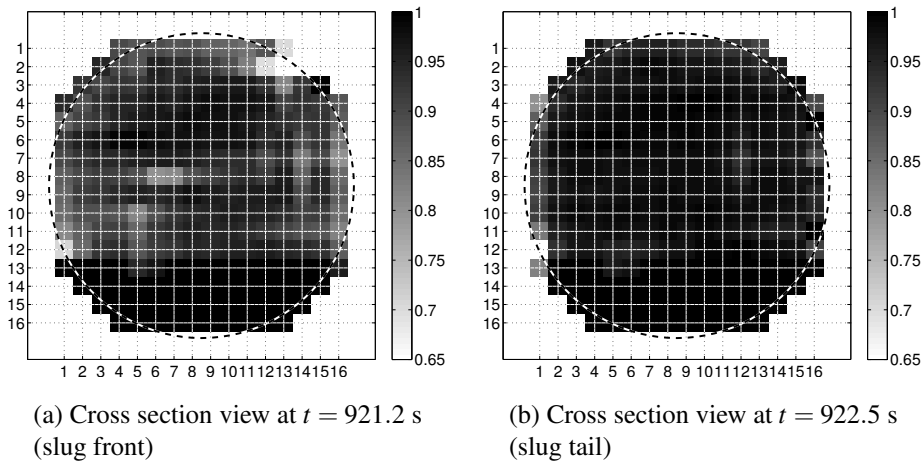


Figure 4.12: Void fraction distribution in the front (a) and tail (b) of the slug. The lines inside the mesh correspond to the wires of the sensor. Each measurement cell is positioned around a wire-crossing-point.

4.3 Measuring the liquid level

The wire-mesh sensors installed in the set-up are used for different types of measurements. The structure of the slug body is measured with the meshes, while additional level indicators installed before and after the mesh (see figure 4.13) are used for slug velocity and slug length measurements. Combining the structure information with the calculated slug velocities, a moving 3D representation of the slug can be obtained.

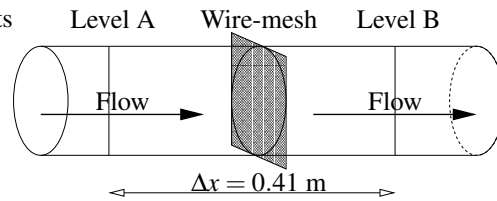


Figure 4.13: Tube element with the wire-mesh sensor and the additional level indicators A and B. The distance between the indicators A and B equals $\Delta x = 41 \text{ cm}$.

Because only a circular part of the square 16×16 mesh is used, the points outside the radius of the tube do not measure any flow. The level indicators A and B are connected electronically to the wires corresponding to the points A and B in figure 4.6(b). In that way, the data of the level sensors is recorded simultaneously with the data from the wire-mesh

The level sensors before and after the wire-mesh sensor (see figure 4.13) are used for the length and velocity calculations. These sensors consist of a set of parallel wires in vertical direction in the center of the tube, measuring the conductance through the liquid layer. The thicker the liquid layer, the higher the conductance and so the signal.

4.3.1 Design of the level sensors

At 20 cm before and after the wire-mesh sensors, additional level sensors are installed, of which one is shown in figure 4.14. Since the wire-mesh has a thickness of 1 cm, the distance between the two level sensors A and B equals $\Delta x = 41 \text{ cm}$. The level sensors consists of 9 wires in a 3×3 matrix geometry. One of the wires is pulsed, another one is connected to the data acquisition system of the wire-mesh for capturing the signal. The other 7 wires are connected to ground potential to shield most of the electric field from the transmitting (pulsed) wire. In the wire-mesh itself the wires cross perpendicular, while in the level indicators the wires are parallel for the whole tube diameter of $D = 5.2 \text{ cm}$. This gives a much larger electric field, and also a larger signal. In order to get both signals in the same order, the

shielding was applied. The lower middle wire in figure 4.14 is pulsed. Without the shielding in the middle (grounded wires), the electric current towards the upper receiving wire would be much too large. With the grounded wires in the middle, most of the current goes directly to ground potential, while only a part is measured in the upper receiving wire. By using this shielding geometry, the current between the pulsed and measured wires is in the same order as the current measured in the crossing points in the wire-mesh. In this way, all signals (mesh and levels) are in the same range and can easily be processed by the wire-mesh data acquisition system.

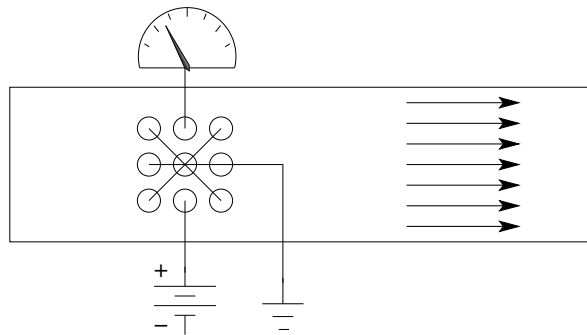


Figure 4.14: Position of the metal wires in the tube. The image is a top-view, so the wires are positioned in vertical direction in a 3×3 -matrix structure. The distance between the wires is 2.5 mm in x and y direction. The diameter of the wires is 0.25 mm.

When looking in the streamwise direction, the left and right wires in the middle row were chosen for the liquid level measurements, and not the first and last one in streamwise direction. This was done to have maximum spatial resolution for the wave measurements in streamwise direction. The drawback is that the spatial resolution in spanwise direction is limited, because the signal is averaged over a distance of 5 mm between the transmitting and receiving wire.

4.3.2 From sensor data to slug properties

The data of the level indicators A and B obtained in the wire-mesh measurements is processed similar as described in section 4.1.2. The distance between the two level indicators now equals $\Delta x = 41$ cm. Because these signals are not as square as in figure 4.4, a cross correlation is used to determine the velocities of the front and tail of the slug more accurately. If the slug front and tail are very steep, a threshold value of *e.g.* 0.75 on the liquid level can be used to obtain a binary signal similar to the one shown in figure 4.4. The design of the level sensors

is such that when the tube is completely filled with liquid, the signal is about 80% of the full scale. The 12-bit ADC-conversion results in $2^{12} * 0.80 = 3276$ steps, which makes it possible to measure the liquid level with an accuracy of $52/3276 \ll 0.05$ mm, which allows to measure waveheights with a sub-millimeter accuracy.

From the level sensor data, the velocity of the slug can be calculated, as explained in section 4.1.2. Figure 4.15 shows the signals of the two level sensors and the wire-mesh, which are installed in the third section at 105 m from the inlet.

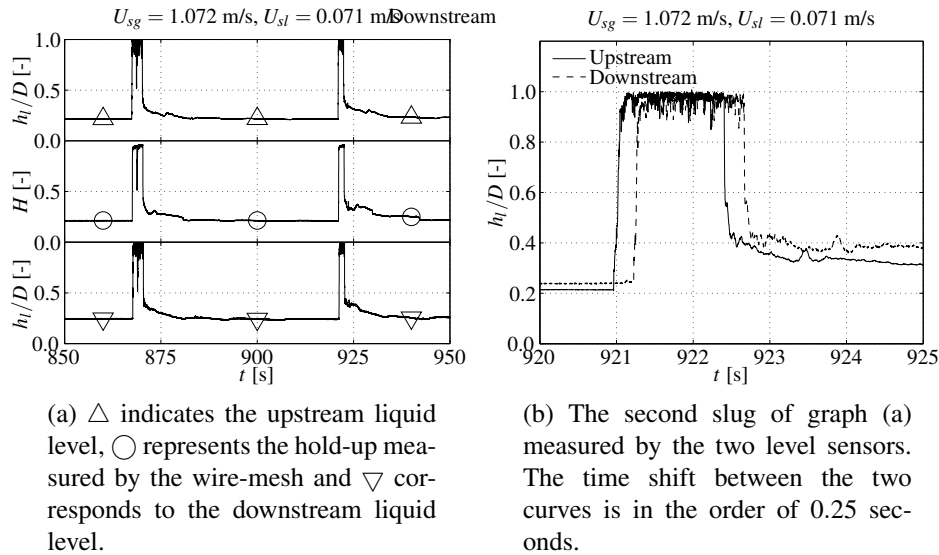


Figure 4.15: Liquid levels and hold-up, measured at 105 m from the inlet.

The liquid level is calculated from the total conductance of the line probes which are installed vertically in the center of the tube. The sensors were calibrated in a tube completely filled with water. Calibration was done several times during the measurement cycle to obtain a time dependent correction for the changing water temperature (see section 4.4 on temperature effects).

The values of the liquid levels shown in the graph are not exactly equal to one because of the air bubbles present inside the slug. This effect is smaller in the calculation of the hold-up, because this value is averaged over the whole cross-section, while the level is a more local measure over a single column of fluid in the middle of the tube.

Using an unbiased correlation function on the signals given by the up- and downstream level sensors A and B, the velocity of the passing structure can be calculated. The correlation

function calculates

$$C(m) = \frac{1}{N-m} \sum_{n=0}^{N-|m|-1} B(n)A(n+m), \quad (4.7)$$

which is maximum when the curves A and B overlap when shifted $\tau = m\delta t$. Here δt indicates the time between two frames ($\delta t = f_{sample}^{-1}$). The values of N and m are the number of samples and the shift respectively. Because the stratified flow between the slugs also contributes to the correlation, the average height of the stratified flow is subtracted from the signal before the correlation is calculated. This does not change the position of the peaks, it only gives a more clear picture.

Because the front and tail velocity differ, the correlations are calculated for a small time interval around the front and tail of the slug separately.

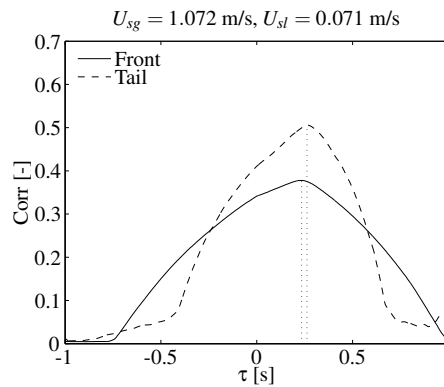


Figure 4.16: Correlation function for the front and tail of the slug shown in figure 4.15(b) The correlation shows two different peaks for the front ($\tau = 0.234$ s) and tail ($\tau = 0.262$ s).

The $\tau = 0.262$ s for the slug tail corresponds to a slug velocity of

$$v_{tail} = \frac{\Delta x}{\tau} = \frac{0.41}{0.262} = 1.56 \text{ m/s}. \quad (4.8)$$

With a framerate of $f_{sample} = 500$ Hz, the value of τ can be estimated with an accuracy of $\delta t = 0.002$ s. The error in τ and thus in the slug tail velocity is in the order of 1%. For the front of the slug, the velocity is slightly higher, $v_{front} = 0.41/0.234 = 1.75$ m/s. Since the peak for the tail velocity is sharper, this will result in a more reliable estimate for the slug velocity. The tail velocity equals the velocity of the gas bubble behind the slug, which is the driving force of the liquid slug. The slug front moves, in this example, faster than the tail of the slug. The slug is growing by taking up more liquid at the front than is shed at the tail.

The slug tail velocity can also be calculated using the relation by Bendiksen (1984), in which the slug tail velocity equals the velocity of the nose of the bubble behind the slug

$$v_{tail} = C_0 U_m + v_{b,0}, \quad (4.9)$$

with U_m the mixture velocity $v_{b,0}$ the bubble rise velocity in stagnant liquid. The constant C_0 equals $C_0 = 1.05$ for Froude numbers $Fr < 3.5$ and $C_0 = 1.20$ for $Fr > 3.5$.

The bubble rise velocity for $Fr < 3.5$ is given by

$$v_{b,0} = (0.54 \cos \theta + 0.35 \sin \theta) \sqrt{\frac{gD(\rho_l - \rho_g)}{\rho_l}}, \quad (4.10)$$

with θ the angle to the horizontal. For air-water flow, the last term simplifies to \sqrt{gD} since the density of air is negligible to the density of water. In the experiment shown in figure 4.15, the mixture velocity equals $U_m = U_{sg} + U_{sl} = 1.072 + 0.071 = 1.143$ m/s, resulting in a Froude number of $Fr = 1.6$. Using (4.9) with $C_0 = 1.05$, this results in a slug tail velocity of $v_{tail} = 1.05 \times 1.143 + 0.37 = 1.57$ m/s which corresponds to the value obtained from the correlation peak shown in figure 4.16.

The tail velocity of $v_{tail} = 1.57$ m/s is constant for all slugs in the experiment. The front velocity can differ considerably from slug to slug, as shown in figure 4.17, indicating the dynamic behavior of the slugs. Most of the slugs are growing since $v_f > v_t$. The tail velocity, as calculated from the time lag in the upstream and downstream signal, is constant for all slugs passing the sensor during the measurement.

With the known slug velocity, the length of the slug can be calculated from the peak-width in the time-signal, $L_{slug} = v_t \times \Delta t$, as shown in (4.3). This exercise is repeated for all other measurement locations in the set-up. In such a way, the development of slug length $L(x)$ as function of position x can be determined.

For the slugs shown in figure 4.15, the slug length can be calculated for the upstream and downstream level measurement as well as for the peak from the wire-mesh. Since the velocity of the front is larger than of the tail, as shown in figure 4.16, the slug is growing with distance. This effect can also be seen when calculating the length based on the three different peaks of the two level sensors and the wire-mesh. Using the tail velocity of $v_t = 1.56$ m/s on the $t = 921$ s slug, this results in

$$L_{3-} = 1.56 \times \Delta t_{3-} = 1.56 \times 1.376 = 2.146 \text{ m}, \quad (4.11a)$$

$$L_3 = 1.56 \times \Delta t_3 = 1.56 \times 1.392 = 2.171 \text{ m}, \quad (4.11b)$$

$$L_{3+} = 1.56 \times \Delta t_{3+} = 1.56 \times 1.402 = 2.187 \text{ m}, \quad (4.11c)$$

with the subscript 3 indicating the third measurement section at $x = 105$ m and the $-$ and $+$ representing the upstream and downstream level sensor respectively. The value of L_3

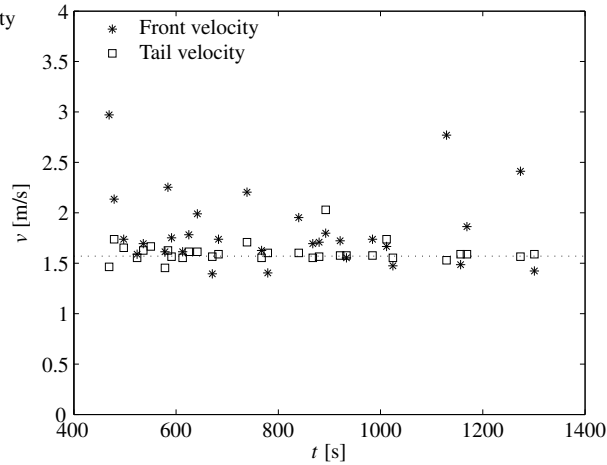


Figure 4.17: Front and tail velocity for different slugs in a single experiment (constant gas and liquid flow)

is calculated from the width Δt_3 of the wire-mesh peak. The three sensors, separated by $\Delta x = 20.5$ cm each, show an increasing length, with a growthrate equal to

$$\frac{dL}{dx} = 0.10 \text{ m/m.} \quad (4.12)$$

These lengths were calculated by applying a threshold of $h_l/D > 0.75$ on the level detector signals. For the wire-mesh, $H > 0.90$ was used. When using these same threshold points on the level sensors, this results in front and tail velocities of $v_f = 1.75$ m/s and $v_t = 1.58$ m/s. From the velocities, the growthrate can be calculated as

$$\frac{dL}{dx} = \frac{v_f}{v_t} - 1 = \frac{1.75}{1.58} - 1 = 0.11 \text{ m/m,} \quad (4.13)$$

which is close to the value obtained from the length measurements.

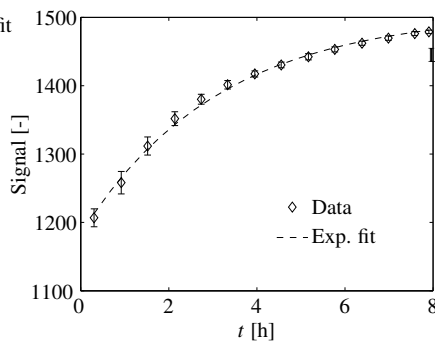
In a similar way, the growthrate can be calculated from the velocities obtained in the correlation calculations, giving

$$\frac{dL}{dx} = \frac{v_f}{v_t} - 1 = \frac{1.75}{1.56} - 1 = 0.12 \text{ m/m.} \quad (4.14)$$

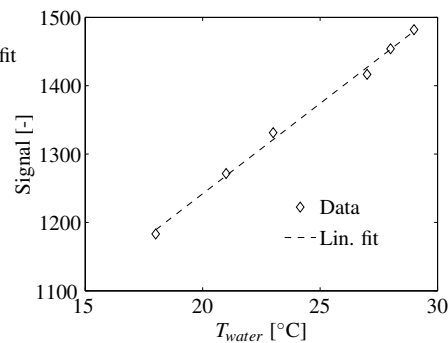
Although this value is larger, it is still close to the other values obtained. Since the maximum distance is only $\Delta x = 0.41$ m, the increase in length is only in the order of centimeters, which is captured quite well.

4.4 Stability of the signal and drift effects

The measurements of the liquid level at locations A and B, as well as the phase distribution measurements by the wire-mesh are based on the electrical conductivity of the liquid phase, in this situation the water. Due to friction in set-up, the effect of solar heating of the set-up, and heat production in the water pump, the temperature of the water can change during the experiments. Since the conductivity of water is temperature dependent, this will cause a drift in the measured signals. In figure 4.18(a), the time evolution of a single point of the wire-mesh is shown for a single-phase water experiment. The drift in the signal shows an exponential time dependence, which was also observed in the increase of the water temperature. In figure 4.18(b), the direct relation between the drift and the temperature is shown.



(a) The measured signal shows an exponential time dependence.



(b) The drift in the measured signal is linear with the temperature of the water.

Figure 4.18: Drift in the measured signal (a), which is linear related to the change in water temperature (b). The errorbars in (a) indicate the noise level (σ) in the steady state signal.

The temperature, which is linearly related to the conductivity and thus to the signal, shows an exponential behavior in time. The wire-mesh calibration is therefore also taken as an exponential function in time. The signal can change with 25% over a whole day, but after correction for time (and thus temperature variations) the difference between data and exponential fit is less than 0.65% of the signal. This deviation is small compared to the noise in the signal for a fully loaded pipe which equals $\sigma/\mu \leq 1.2\%$.

By using an exponential time dependence, it is assumed that also the water temperature changes exponentially in time. Assuming a constant power production in the pump, the temperature of the water will change as $dT_w/dt \sim (T_{pump} - T_w)$, which results in an exponent in time, which is also observed for the measurements where temperature was recorded separately. Since the signal is related to the conductivity, which depends linearly on the water temperature, also the signal will change exponentially in time.

4.4.1 Electronic drift in the wire-mesh data acquisition equipment

Besides the effect of the temperature of the water, there is also a small influence of the temperature of the electronic circuits. In figure 4.19, the small effect is shown for two long measurements. A single resistor was inserted between the transmitting and receiving electronics. The effect on the signal is less than 1% during start-up, and even less than 0.2% during the rest of the measurement. The left and right picture were taken for different gridpoints, therefore the signals in (a) and (b) are not the same. The drift during measurement (neglecting the start-up effect in (a)), is less than the noise in the signals with a standard deviation $\sigma \leq 10$ which is in the order of 0.5%. Compared to the water temperature effect, which changes the signal by 25% over a whole day, the effect of electronic drift and noise are negligible.

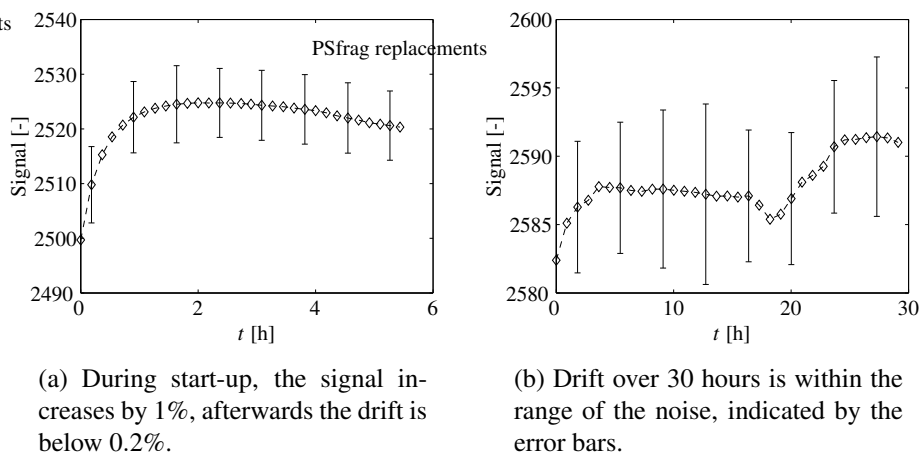


Figure 4.19: *Electronic drift, measured with a single resistor for several hours.*

4.5 Data acquisition systems

The wire-mesh uses its own software to control the sensors and to save the data into files on disk, as discussed in section 4.2. For more information, see Manual for Wire-Mesh-System 32x32 V 1.0.5 (2004) and appendix E. All analog signals from the pressure sensors and the gas flow meter are recorded via a ADC-box which is connected to the computer by USB. Also a trigger signal from the wire-mesh is recorded by the ADC-box for synchronization of the different signals. In this section, the measurement equipment is discussed in detail.

4.5.1 Measuring analogue signals from the flowloop

Several signals are recorded during the experiments. The analogue signals are recored via an analogue-digital-converter (ADC), which is connected via USB to the computer. The used sample frequency is 500 Hz. The gasflow rate is measured near the inlet with rota meters and also with a electronic flow meter. The DC-voltage from the flow meter can be converted to the superficial gas velocity using the calibration curve. For all sensors used, the calibrations are in appendix D. The pressure sensors measure the absolute pressure at different locations, or the pressuredrop over a pipe segment. The signal of a single point probe near the pressure measurements were also recorded to have a better comparison between the slugs and the patterns in the pressure signals. A pulse signal from the wire-mesh, which is only high during measurement, was recorded for synchronization.

| Channel | Signal |
|---------|------------------------------|
| 0 | Gas flow rate |
| 1 | Pressure difference I |
| 2 | Pressure difference II |
| 3 | Absolute pressure A |
| 4 | Absolute pressure B |
| 5 | Absolute pressure inlet |
| 6 | Point probe slug detector 6a |
| 7 | Wire mesh trigger signal |

Table 4.3: Analogue signals from various sensors measured with a computer and ADC-module.

4.5.2 Slug detector units, data storage and reconstruction

The slug detectors, as discussed in section 4.1.1, produce a pulse when a slug is measured, and zero in other situations. This signal, 0 or 1, is recorded for 8 sets with 2 detectors each, resulting in an array of 16 digits. For data compression, this 16 bits array is converted to a decimal number and stored in a file. The binary number is treated as a 16 two's complement number, which gives decimal values ranging from $-32768 \dots 32767$. In fact, the last 15 bits represent the decimal number for positive numbers. When the first bit equals 1, the value is negative, calculated as the positive 15 bit value minus 32768. Some examples are given in table 4.4.

| Binary | Decimal |
|---------------------|---------|
| 1000 0000 0000 0000 | -32768 |
| 1000 0000 0000 0001 | -32767 |
| 1000 0000 0000 0010 | -32766 |
| 1111 1111 1111 1110 | -2 |
| 1111 1111 1111 1111 | -1 |
| 0000 0000 0000 0000 | 0 |
| 0000 0000 0000 0001 | 1 |
| 0000 0000 0000 0010 | 2 |
| 0111 1111 1111 1101 | 32765 |
| 0111 1111 1111 1110 | 32766 |
| 0111 1111 1111 1111 | 32767 |

Table 4.4: Binary to decimal conversion based on the two's complement relation.

The data can be saved in two different file formats. The first option is to sample the 16 detector signals each 1 ms ($f_{sample} = 1$ kHz) and store for each sample the corresponding decimal value in a file. The second, more advanced mode, only writes data to the file when one or more detector signals changed, so when the decimal number is different compared to the previous sample. In that case, the timestamp (in milliseconds) and the new decimal value are stored in file. This last mode is used during the experiments.

4.6 Conclusions

Two types of instrumentation are used, both based on the conductive properties of the liquid phase. The point probe system measures slug passage, and slug velocity and length can be calculated afterwards.

The more advanced wire-mesh technique also measures the interior of the liquid slug and the level of the stratified layer between the slugs. From this information. From the wire-mesh, which measures the local conductivity in the flow at 216 equally spaced points in the cross-section of the tube, the phase distribution can be reconstructed. In the current study a simple linear reconstruction technique was used. For detailed information on the bubble sizes of the gas inside the liquid slugs, a more advanced reconstruction technique should be implemented. For the average quantities as used here, the simple technique is sufficient.

For determining the velocity of the slugs, additional sensors are installed, which are recorded simultaneously with the wire-mesh data. Using a cross correlation on the signal of two sensors separated by a distance Δx , the velocity can be calculated.

The techniques are based on the conductive properties of the liquid, in the current experiments the water. Since temperature changes during the day, also the conductivity and the signal will change. This effect can be corrected for using a time dependent correction (temperature changes exponentially in time) on the measured signal. After error in this correction is of the same order as the noise in the signal for a stationary situation, with $\sigma/\mu \leq 1.2\%$.

CHAPTER 5

Slug development in different regimes

This chapter describes the experiments carried out in the 2" flow facility. For different combinations of superficial gas and liquid velocities, a variety of the flow patterns was observed. In section 5.1, an overview is given on the different types of slug behavior while traveling along the pipeline. The flowmap with the different regimes indicated in section 5.2 shows the relation between the different flow patterns and the inlet velocities.

In section 5.3, the focus is on the slug length, and how it can change during the travel through the system. Different types of growth behavior are observed and discussed. Also for situations where the slug is not fully developed at the end of the set-up, *i.e.* the slugs have not obtained their final maximum length, an estimate can be made of the stable slug length by extrapolation of the measured data. A special case is the slugs that are formed just after a change in the inlet conditions. These first slugs show a different behavior compared to the rest of the slugs.

The slug frequency, the pattern of slugs in time, is treated in section 5.4. Different patterns are discussed from regular slugging with a fixed characteristic frequency to situations with different modes.

The results of section 5.3 (length) and section 5.4 (frequency) are combined in section 5.5 where the relation between the length and frequency is discussed.

5.1 Different flowtypes investigated

Depending on the flowrates at the inlet, different flow patterns can be formed. Without any slugs present, the flow is stratified when the interface is smooth, and stratified-wavy when small waves are present on the gas-liquid interface. The occurrence of slugs can have different causes. By optimizing the alignment of the set-up, the effect of topology-induced slugs was minimized, so all slugs evolve from instabilities in the flow. No artificial slugs were injected into the system. Both inlet and outlet are horizontal, as discussed in section 3.2, so slug formation is not enhanced by the geometry of the system.

The slugs are categorized based on their length, and growth behavior, as indicated schematically in figure 5.1. For the growing slugs, the length will increase in downstream direction. In most of the situations, the slugs are growing when passing the first measurement locations (increasing length with position), and are at fixed length (horizontal line) when passing the last section. This is illustrated by the cases B and C in figure 5.1. In some cases, the final length is not reached before the end of the 137 m long set-up (last measurement location is at $x/D = 2500$), and the slugs are still growing when leaving the tube (case A).

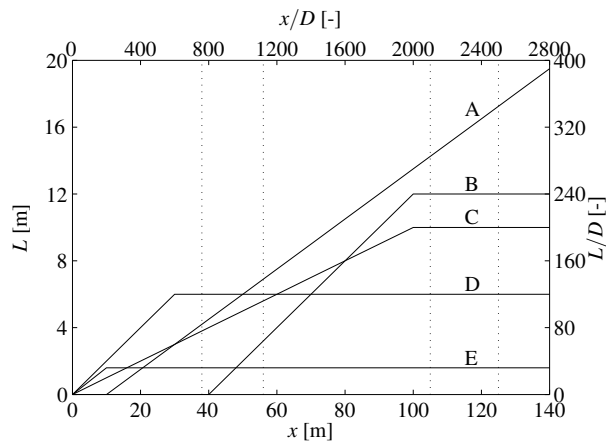


Figure 5.1: Schematic representation of the different slugs that might occur in the pipeline. The graph shows 5 possible scenarios of the development of slug length L as function of the distance x from the inlet. The measurement locations are indicated by the vertical dotted lines.

Another set of slugs was observed with the same length in all measurement locations (cases D and E). When the final slug length is already obtained when reaching the first measurement point, the whole growth process from $L = 0$ m to $L = L_{max}$ is completed in the first 38 m of the tube. The difference between case D and case E is only the length of the slugs. Short slugs are slugs below 2 m ($= 40D$) length (E), everything longer is called long slugs (D).

In the experiments, basically two sets of slugs are observed, the short hydrodynamic slugs (type E) and the long slugs (types A-D). The difference in the types A-D is only determined by which part of the growth process that is recorded by the measurements. Because the first sensor is located at $x = 38$ m ($x/D = 760$), no information on the initiation or the first part of the growth is known. By putting more sensors upstream of $x = 38$ m, the growing part of a D-type slug can be captured, which shows the similarity with types B and C. The slugs indicated by A are still growing when passing the last sensor at $x = 125$ m ($x/D = 2500$). When using a longer set-up, with more sensors downstream, also the stage of constant slug length will be reached, similar to the B, C and D types slugs.

5.2 Which flow type for which inlet conditions : the flow map

The flowmap can be divided into 3 separate regions. The first one is the stratified or stratified wavy flow, for which conditions no slugs are present. The other two are the long slugs region and the hydrodynamic slugging regime. The only difference between the two slug types is the slug length, which is smaller than $40D$ for the hydrodynamic slugs and larger than $40D$ for the long slugs. The fact whether the slugs are growing or not only depends on the position where the measurements were done, and says nothing on the physics. An interesting parameter in the long slug region is the maximum slug length that can be reached, which can be different for different inlet conditions (gas and liquid velocities).

For a large range of gas- and liquid superficial velocities, the flow properties were determined. In graph 5.2, the different flow regimes are indicated. For low liquid velocities, the two phases flow separately as stratified (+) or stratified wavy flow (x). The middle region is the most interesting part, indicated by the stars (*), where the slugs are growing with position. In most of the cases, at some moment a maximum length is reached, but also slugs which continue growing till the end were observed. Since length changes, it is difficult to predict the development of the flow, and hence difficult to control these kind of flows. The aim of the current study is to gain more knowledge on slug flow, and growing slugs in particular. For large liquid velocities, indicated by the triangles in the flowmap, the slugs flow with a fixed length trough the system. Since the length is known and fixed, it is easier to control this type of flows.

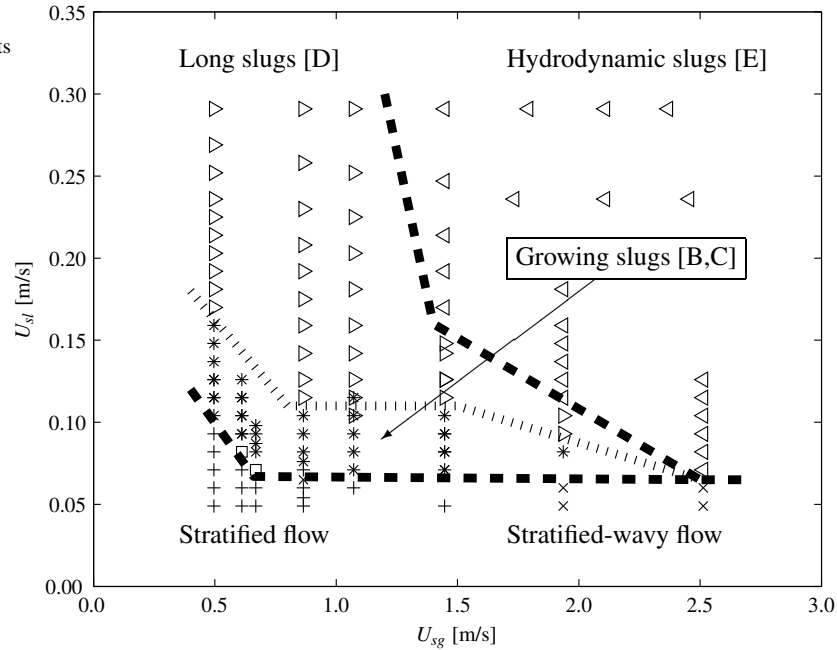


Figure 5.2: Flow map indicating the flow regimes for different combinations of the superficial liquid velocity (U_{sl}) and superficial gas velocity (U_{sg}). For low liquid velocities, stratified or stratified-wavy flow is observed, indicated by the plus signs and crosses respectively. For higher liquid velocities, two different types of slugs can be present. The growing slugs, indicated by stars (type B and C), and the slugs with constant length (triangles). The two different triangles indicate long slugs (\triangleright) for lower gas rates (type D) and short slugs (\triangleleft) for higher gas rates (type E). The lines indicate the transition area between the different regimes. A special group of the growing slugs are the points indicated by the squares, which slugs continue growing at the way to the end of the set-up, which corresponds to type A in figure 5.1.

From the flow map shown in figure 5.2, it is clear that the growing slugs are present only in the region of low gas velocities. Towards the right (increasing gas rate), the region of the growing slugs (*) between the two lines vanishes at a gas velocity of $U_{sg} = 2.5$ m/s. For higher velocities, the transition goes directly from stratified wavy to the regime with short hydrodynamic slugs (\triangleleft). The transition directly to hydrodynamic slug flow could be related to the waves which are already present on the interface of the stratified-wavy flow, although the boundary between stratified and stratified-wavy flow does not coincide with the $U_{sg} = 2.5$ m/s point.

In the lower left corner, so for low gas and liquid velocities, there are even some slugs present (indicated with squares) which keep on growing during the whole travel trough the flow line. The other growing slugs, indicated by the stars reach a final length within the length of the set-up.

For the triangles, indicating slugs with fixed length, the growing stage was completed before reaching the first measurement location at 38 m from the inlet. The development of the flow was completed before reaching the first measurement point, so all locations measured a fully developed flow, as indicated by the cases D and E in figure 5.1.

The difference between the D-type slugs (\triangleright) and the E-type slugs (\triangleleft) is the slug length that is reached. For the hydrodynamic slugs (E), the length is (on average) below $40D$, which corresponds to $L = 2$ m in the current set-up.

The D-type slugs are (much) longer, at least $L \geq 40D$ but can reach lengths upto several hundred tube diameters, similar to the B and C type slugs. The difference between the B,C and D type slugs is only based on the way they are measured, but physically they are all similar; all slugs reach a stable slug length that is larger than $40D$. The same holds for the situation of the squares in the figure, indicating another type of long slugs. These A-type slugs continue growing till the end of the setup, and have not reached their maximum length when passing the last measurement location, as indicated in figure 5.1. The slug development length is thus large for the A-type slugs (longer than the setup), and short (less than the $x = 760D$ of the first sensor) for the D-type slugs. For the B and C type slugs, the development is observed at different measurement locations, such that the growth rate can be calculated.

In general, the slug lengths observed are largest for the A-type of slugs, than the B and C types, and relatively short (still much larger than $40D$) for the D-type slugs. When moving through the D-type region with increasing liquid flowrate, the slugs become shorter and finally changes into the shorter type E hydrodynamic slugs, as shown in figure 5.2 at $U_{sg} \approx 1.5$ m/s and $U_{sl} \approx 0.15$ m/s. A similar transition will also occur for lower gas flow rated, but than for higher liquid flow rated than studied in the current research.

The transition lines shown in figure 5.2 are only indicative. In reality, the transition regimes are not that straight or kinked.

5.3 Slug development, changes in slug length

The most important characteristic number of a slug is its length. All slugs travel with the same propagation velocity through the pipe, the slug arrival time is linearly related to the positions of the subsequent sensors, as will be discussed later in this section. Since the inlet conditions are fixed, the conditions for all slugs will be the same, and thus also the velocities of the subsequent slugs. The slug velocity is thus a fixed number, which can be related to the inlet velocities via the mixture velocity. The only property that can change during travel through the line is the slug length.

Measurements have been performed at 4 locations along the pipe (see figure 5.1). At $x = 38$ m and $x = 56$ m upstream of the bend, and at $x = 105$ m and $x = 125$ m downstream of the bend. Due to this coarse grid geometry, only the development of the slugs can be indicated. The initiation process of the liquid slugs can not be studied in detail, unless the instrumentation is relocated.

When having a closer look at the length of the slugs presented in figure 5.2, there are several regimes. In the lowest region, the stratified wavy flow, no slugs are present. The next regime is that of the growing slugs, so length increases as function of the position of the slug. Some slugs continue growing all the way through the flowline, while others will reach their final length before the end of the set-up. For these regimes, the average maximum slug length was calculated from the slug passage-time (see section 4.1.2) and plotted in figure 5.3. The average maximum length was calculated based on a large sequence of similar slugs. Usually the last measurement location was used, since there the slugs were at maximum length, as indicated in figure 5.1 for the cases A, B and C.

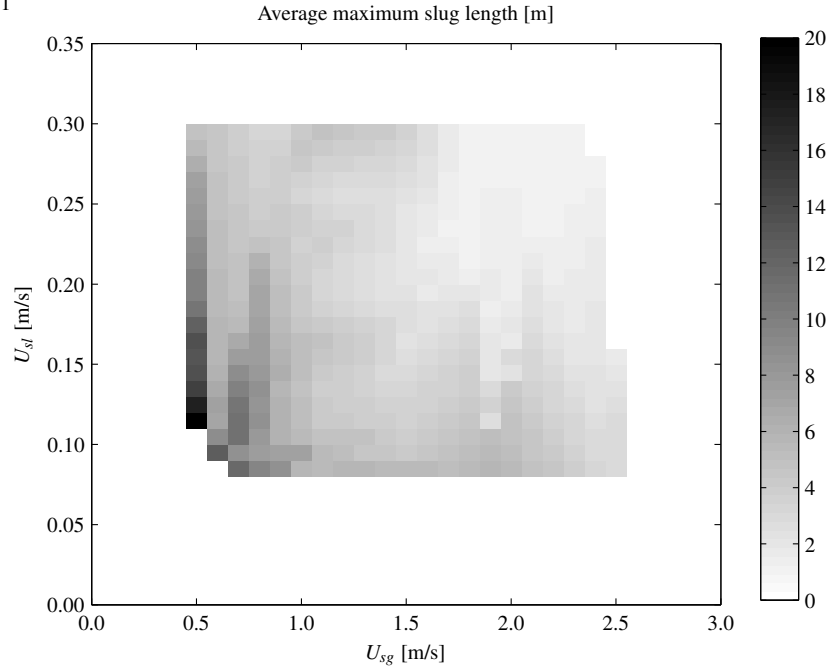


Figure 5.3: Average length of the slugs measured at different locations. Near the transition at low U_{sl} , the slugs are quite long, and in some cases still growing when leaving the set-up. For increasing flow rates, both for the gas and the liquid, the slugs become smaller.

For other regimes, cases D and E in figure 5.1, the slugs have a constant length while passing the different measurement locations. The average slug length was calculated over large series of equivalent slugs (same flow conditions). The averaging was done for multiple slugs and over multiple locations.

The slug length observed depends both on the gas and liquid flow rates. In figure 5.4, the slug length behavior is shown for different series of constant liquid velocity. The relation between the slug length L and the superficial gas velocity U_{sg} shows to be a power law relation with a slope of -1.5 , so $L_{slug} \propto U_{sg}^{-1.5}$ for fixed U_{sl} .

Since the lines for different liquid velocities are parallel, the slope of -1.5 is independent of the liquid velocity. Because the lines are shifted, there will be a constant which is a function of U_{sl} , so the relation becomes

$$L = C_1(U_{sl})U_{sg}^{-1.5}. \quad (5.1)$$

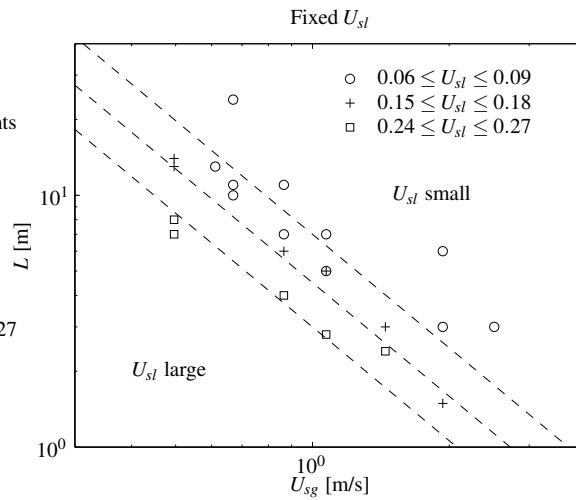


Figure 5.4: Relation between average slug length and U_{sg} . The different symbols represent different liquid velocities U_{sl} . For each fixed liquid velocity, there is a log-log relation with -1.5 slope.

A similar plot is made in figure 5.5 for series of constant superficial gas velocity U_{sg} . Again, a power law behavior is observed in the log-log plot, now with a slope of -1 , which fits quite well for each branch.

Slug length decreases with liquid velocity with a power of -1 , so the relation for the slug length now becomes

$$L = C_2(U_{sg})U_{sl}^{-1}. \quad (5.2)$$

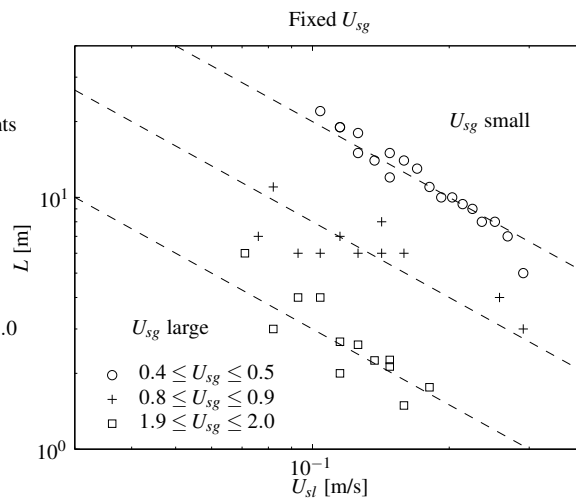


Figure 5.5: Relation between average slug length and U_{sl} . The different symbols represent different gas velocities U_{sg} . For each fixed gas velocity, there is a log-log relation with -1 slope.

Since both powers calculated are negative, the slug length L decreases for increasing gas and liquid velocities. The maximum slug length L_{max} is thus expected for the lowest gas and liquid velocities. This relation holds for all experiments shown in the figure. The upper branch with circles in figure 5.5 indicates the series of lowest gas velocity measured. The line shows a constant slope, and reached a maximum length for the lowest liquid velocity in the top left of the graph. The maximum slug length in figures 5.2 and 5.3 is observed in the lower left corner, so again for small gas and liquid velocities.

When combining the expressions in (5.1) and (5.2), this results in

$$L = \frac{C}{U_{sg}^{1.5}U_{sl}}. \quad (5.3)$$

5.3.1 Slugs with increasing length, the behavior

Figure 5.6 shows the length development of growing slugs. In (a), the slugs are still growing when passing the last measurement location at 125 m downstream. When extrapolating the slug length upstream, it is clear that the sensors positioned at 56 m did not observe any slugs. The long slugs were initiated earlier in the set-up (probably in the neighborhood of the bend at 68 m) than the shorter ones (initiated close to 100 m). All slugs have similar growth-rates of $dL/dx \approx 0.35$ m/m independent of the length or position. In (b), the slugs are growing in the first part of the set-up, and have reached a final length of 10 m ($L/D \approx 200$) after approximately 100 m. In the growing part, all slugs have similar growth rates. Since it is not known where the slugs have obtained their constant final length of 10 m, the growth rate based on the derivative in the graph is a low estimate. In case the slugs have reached their final length already at 80 m, the average growth rate would be twice as large as indicated in the figure. Since no additional data points from other locations are available for this measurement, the growth rate can only be estimated based on the slope which gives $dL/dx \geq 0.14$ m/m. All slugs shown in this graph were initiated before the bend at 68 m, and no slugs were added by the disturbing effect of the bend.

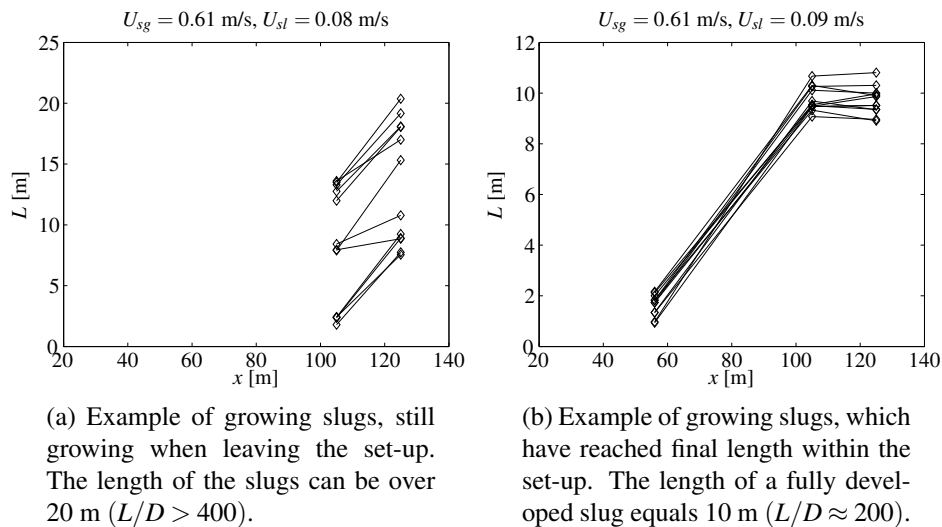
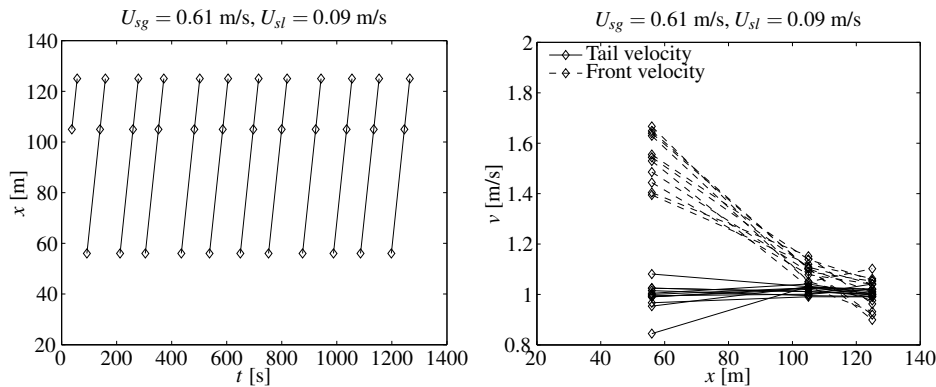


Figure 5.6: Different types of growing slugs for a constant gas flow of $U_{sg} = 0.611$ m/s. In situation (a) the slugs are still growing (type A). After increasing the liquid load from $U_{sl} = 0.082$ to $U_{sl} = 0.093$ m/s, as shown in (b), the slugs have reached final length before leaving the set-up (type B).

The slugs shown in figure 5.6(b) can also be represented in a different way. When plotting the positions of the different slugs as function of time, the movement of the slug is clearly visible.



(a) Position of the different slugs in time. From the straight line, it is clear that the slug propagation velocity is constant.

(b) Front and tail velocity develop similarly for all slugs along the tube.

Figure 5.7: Several slugs moving through the set-up. Since the vertical lines in (a) are straight and parallel over all positions, the velocities at which the slugs travel is constant for all slugs at all positions. It is also shown that the time interval between the slugs is approximately constant, and equal to 110 seconds. In (b) the front and tail velocities of the slugs are shown. Towards the end of the set-up, the two velocities become equal.

All slugs move with the same velocity. The slope of the lines shown in figure 5.7(a) corresponds to the tail velocity obtained from the measurements. In figure 5.7(b), the velocities of the slugs are shown at different locations along the set-up. It is clear that the tail of the slug moves at constant velocity, and that the velocity of the slug front changes with position. Again, all slugs have a similar development in the front velocity.

All slugs are initiated between $x = 38$ m (no slugs observed) and $x = 56$ m (all slugs present), as can also be derived from figure 5.6(b) by extrapolation of the lines towards $L = 0$ m on the horizontal axis. The slugs, all initiated in the same part of the tube, experience similar circumstances (fixed inlet conditions). Since the time between slugs is constant, the hold-up is assumed to have rebuilt to the same level after all slugs, before new slugs were formed. For these reasons, the development of all the slugs is also expected to be similar. This is shown in figure 5.7(b) for the velocity of the front and tail of each slug.

The fresh slugs, measured at $x = 56$ m in figure 5.6(b) are growing, which can also be explained by the difference in front and tail velocities as shown in figure 5.7(b). Further downstream, the front and tail velocities become nearly equal, and the length of the slugs remains constant (figure 5.6(b)).

In figure 5.7(a), the interval between consecutive slugs approximates 110 seconds. When using the simple relation proposed by Woods et al. (2006) $f_s = 1.2U_{sl}/L_s$, the slug frequency equals $f_s \approx 0.011$ when using a developed slug length of 10 m as indicated in figure 5.6(b). The 90 seconds slug spacing is quite a good estimate considering the quite coarse assumptions that were made in deriving the slug frequency expression. A more detailed analysis of the slug frequency will be given in section 5.4.

In figure 5.8, both length and velocity are plotted for the slugs that seemed to be infinitely growing. The velocities of front and tail are getting closer towards the end of the tube, so the growth rate decreases downstream. Since the velocities are not equal at the end of the set-up, slugs are still growing and the fully developed length of the slugs is not reached within the length of the set-up. There is a certain spread in the front velocities, which is also observed in the distributions of the lengths. The length can be related to the growth rate, which is related to the difference in front and tail velocity. Since the tail velocity of the slugs is constant for all slugs at all positions, the front velocity determines the growth and the length of the slug.

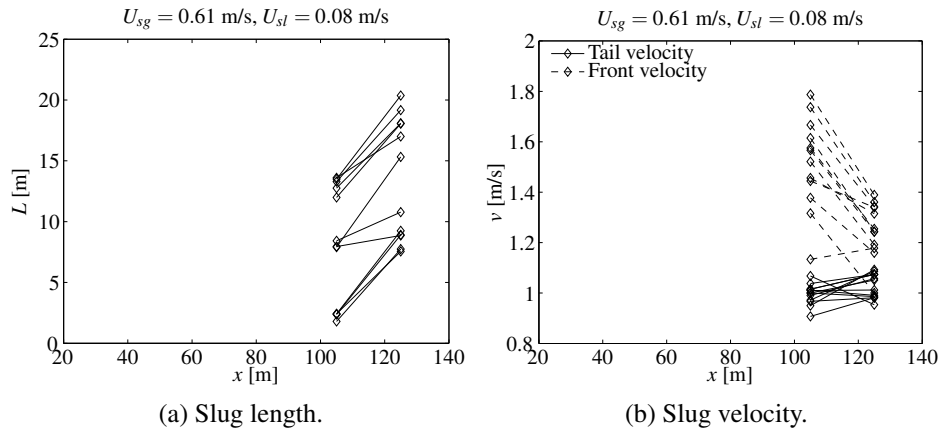


Figure 5.8: In (a) the growing slugs as in figure 5.6(a). Now in (b) the velocities on front and tail are plotted. Slugs are still growing, since the front velocity is larger than for the slug tail. However, the difference decreases with position, so finally, these slugs will also reach a fully developed length, which in this case can be (far) over 400 tube diameters.

The length of fully developed slugs is reached when it stops growing, *i.e.* when the front velocity equals the tail velocity. As shown in figure 5.9, short slugs grow faster, and long slugs which are close to their final length grow less fast. The slope of the lines is approximately the same for all slugs, so extrapolation can be applied to obtain the final length. The slugs as shown above tend to grow up to lengths in the range of 12 m to 23 m, which results in a maximum slug length of $L/D \approx 450$.

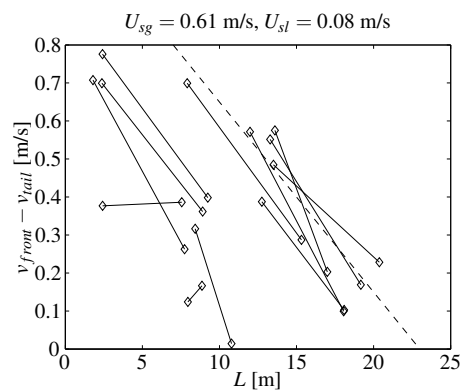


Figure 5.9: The slug length can be related to the growth rate, in this graph indicated by the difference between front and tail velocity. The lines can be extrapolated towards a velocity difference equal to zero, giving the fully developed slug length of $L_{max} \approx 23$ m.

5.3.2 A special case, the first slug

In the previous section, all slugs showed a similar behavior, because the conditions were constant during the measurements. In a stationary situation, the flows are constant, so also the patterns arising will be similar. The slugs move through a similar environment, which is in agreement with the flow conditions.

In general, there is a difference between the first slug after a change in the flow conditions and the rest of the slugs. Since the environment (*i.e.* local hold-up before the slug) is related to the flow conditions (gas and liquid velocities), a change in flowrate will also change the environment. The slugs created just after the change will experience an environment which is left from the old situation just before the change. This first slug has the old environment at the front, but leaves a new environment, corresponding to the actual flow conditions, at the back. The difference in these environments, usually a change in the hold-up of the stratified layer, is taken up by the first slug, which may result in a different (growth) behavior. All subsequent slugs will experience the same, new, environment, so they will all behave similarly.

Figure 5.10 shows the hold-up for the four measurement locations in the set-up. At the first location ($x = 38$ m), several disturbances are visible, but only one real slug was observed at $t = 1000$ s. Further downstream, at $x = 56$ m, all slugs are present, which move further towards the end of the tube. The disturbance in the beginning of $x = 56$ m is the start of the first slug, which is visible as a real slug in the locations downstream. This first slug differs from the rest, based on the jump in hold-up before and after the slug. The hold-up changes from $H = 0.4$ to $H = 0.22$, which is quite different compared to the other slugs which have a $H = 0.22$ on both sides of the slug. This difference in liquid level before and after the slug is taken up by the first slug, which results in a fast growth for this particular slug.

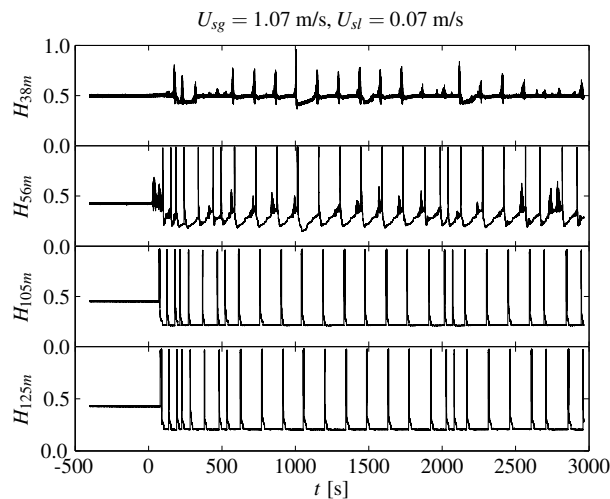
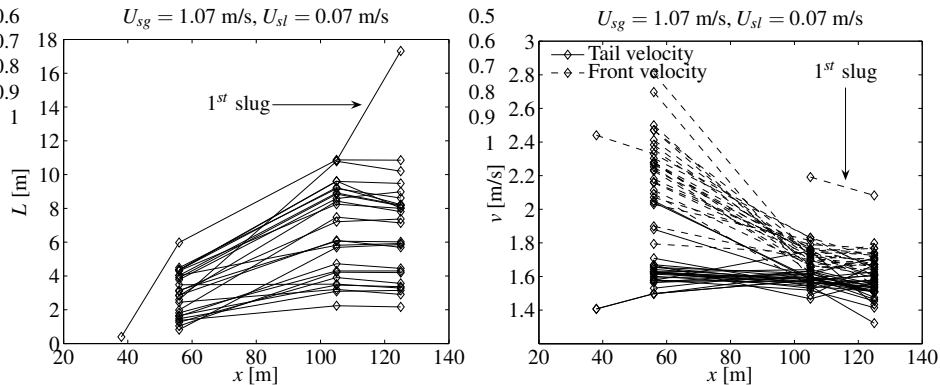


Figure 5.10: Hold-up at the four locations along the tube.

The first slug occurred after a slight increase in the liquid flow rate at $t = 0$ s. The experiment was running with a gas flow of $U_{sg} = 1.072$ m/s and a liquid flow of $U_{sl} = 0.060$ m/s for almost one hour. At $t = 0$, the liquid flow rate was suddenly increased to $U_{sl} = 0.071$ m/s at constant gas flow rate. The next slugs arrive in a $H = 0.22$ hold-up environment, and less liquid is available for growth. These slugs will be stable (constant length) or grow less fast compared to the first one.

The development of the slug length along the length of the set-up is shown in figure 5.11(a). Most of the slugs are initiated between $x = 40$ m and $x = 50$ m, although large disturbances were already observed at the $x = 38$ m location, as shown in the upper graph of figure 5.10. The slugs grow and reach lengths up to a maximum final slug length between 2 and 10 meters at the end of the set-up.

Only one slug, the first one, reaches a much larger length, up to $L_s = 17$ m at $x = 125$ m, and is still growing because of the high front velocity of $v_f = 2.1$ m/s as indicated in figure 5.11(b).



(a) Slug length development of growing slugs. The maximum is about 10 m.

(b) Towards the end of the set-up, front and tail velocity become equal.

Figure 5.11: *The first shows a different behavior compared tot the rest of the slugs.*

The slug that is already observed at $x = 38$ m is also a special one, since it grows larger than the rest, reaching more than 10 m near the outlet. Having a closer look at figure 5.10, there is a dip in the hold-up visible for the $t = 1000$ s slug at $x = 38$ m, while for the other slugs the hold-up before and after is approximately the same. Compared to the other slugs, the $t = 1000$ s slug already took some liquid further downstream, and could in that way grow to a larger length. Since the lines in figure 5.11(a) are parallel, the growth rate between $x = 56$ m and $x = 105$ m is similar to the value observed for other slugs, as can also be seen in the velocity plot of figure 5.11(b).

The first slug grows up to 17 m, which is much larger than the rest of the slugs reaching lengths of about 10 m at maximum. The longer slug is the first slug that occurred after a slight increase in the liquid flow rate. Since the hold-up in front of the slug is higher than the equilibrium value corresponding to the inlet flow, the slug will take up a large amount of liquid. The difference between the hold-up in front and at the back of the slug sets the growth rate. After the first slug has passed, the hold-up has dropped and later slugs will experience a lower hold-up, and will also have a lower growth rate.

The first slug takes the excess amount of liquid, and grows. After that, the hold-up is the normal equilibrium value corresponding to the flow conditions. After the first slug (or several), the pattern becomes quite regular, as shown in figure 5.10.

In figure 5.12, the length and velocity of the slug are plotted in the order of their initiation. Again the first one is larger, moving with higher velocity, while the rest of the slugs have more constant properties. Note that for the velocity in (b) only the data of the last two measurement locations at 105 m and 125 m is plotted for all slugs.

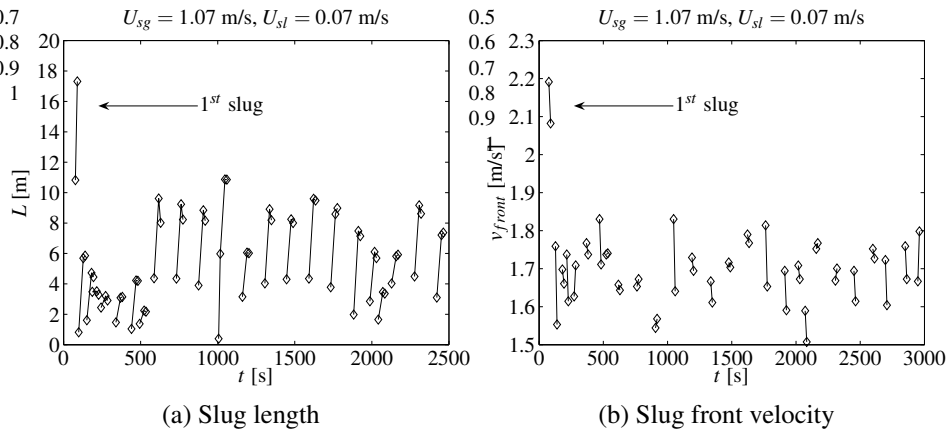


Figure 5.12: Sequence of growing slugs. The first slug is longest and fastest one.

A similar behavior is observed in another experiment, at a lower gas flow rate. The transition from $U_{sl} = 0.093$ m/s to $U_{sl} = 0.104$ m/s was done at a fixed gas flow rate of $U_{sg} = 0.496$ m/s at $t = 100$ s. At $t = 125$ s, the first disturbance is visible in the $x = 38$ m sensor.

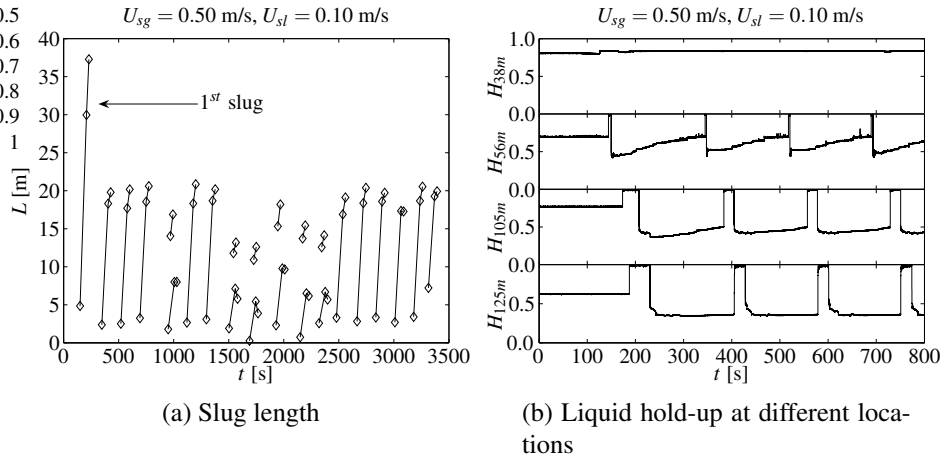


Figure 5.13: Growing slug situation. The first slug which is formed is the longest one.

The first four slugs are single slugs. Later on, slugs are also occurring in pairs as indicated in figure 5.13(a) with the separate lines for the same moment in time. First a small slug is created which starts growing. Later on, a new slug appears in front, which will grow by taking up all the available liquid. The old slug will not grow any further.

As indicated in figure 5.13, the first slug grows up to more than 35 m, while the other slugs reach at maximum 20 m. The difference in hold-up before and after the first slug is quite large, the liquid level drops from $H = 0.72$ to $H = 0.35$. This extra amount of liquid is used for the slug to grow.

This length can be estimated based on the difference in hold-up before and after the slug. The volume of the slug, assuming a pure liquid slug without bubbles, equals LA with L the length and A the area. This volume can change due to inflow at the front and outflow at the tail. In a reference frame moving with the slug velocity, this yields

$$\frac{d}{dt}LA = u_{front}^*A_{front} - u_{tail}^*A_{tail}, \quad (5.4)$$

with the velocities u_{front}^* and u_{tail}^* defined as

$$u_{front}^* = v_{slug} - u_{initial}, \quad (5.5a)$$

$$u_{tail}^* = v_{slug} - u_{final}. \quad (5.5b)$$

The liquid velocities $u_{initial}$ and u_{final} before and after the slug are related to the flow rates before (initial) and after the change in liquid flow rate (final) as

$$u_{initial} = \frac{\Phi_{initial}}{A_{initial}}, \quad (5.6a)$$

$$u_{final} = \frac{\Phi_{final}}{A_{final}}. \quad (5.6b)$$

The slug is assumed to be on the border between the initial flow situation (present in front of the slug) and the new flow situation (final) behind the tail.

Combining these expressions in (5.4), this results in (with s =slug, i =initial, and f =final)

$$\begin{aligned} \frac{d}{dt}LA &= (v_{slug} - u_{initial})A_{initial} - (v_{slug} - u_{final})A_{final} \\ &= \left(v_s - \frac{\Phi_i}{A_i}\right)A_i - \left(v_s - \frac{\Phi_f}{A_f}\right)A_f \\ \frac{dL}{dt} &= \frac{1}{A}[\Phi_f - \Phi_i + v_s(A_i - A_f)] \\ &= \frac{\Phi_f}{A} - \frac{\Phi_i}{A} + v_s \frac{A_i - A_f}{A} \\ \frac{dL}{dt} &= (U_{sl,f} - U_{sl,i}) + v_s(H_i - H_f), \end{aligned} \quad (5.7)$$

which shows two contributions to the slug length increase dL/dt . The first is the change in local liquid flow rates, which equals $U_{sl,f} - U_{sl,i} = 0.104 - 0.093 = 0.011$ m/s in the current experiment. When comparing this to the second contribution of the length increase, which equals $v_s(H_i - H_f) = 0.87(0.72 - 0.35) = 0.32$, the first term can be neglected.

Assuming constant growth rate, the final length can be calculated when the slug existence time is known

$$T = \frac{\Delta x}{v_{slug}}. \quad (5.8)$$

The length at Δx m after slug initiation now equals

$$\begin{aligned} L_x &= \frac{dL}{dt}T \approx v_s(H_i - H_f) \frac{\Delta x}{v_s}, \\ &= (x - x_{initiation})(H_i - H_f), \end{aligned} \quad (5.9)$$

which is now independent of the actual slug velocity (when neglecting the first term in (5.7)). The volume of the slug, the length L multiplied by the slug hold-up $H = 1$ equals the volume of the water package $\Delta x \times \Delta H$ which is taken up from the stratified flow.

Assuming that the slug was initiated at $x = 40$ m (a small wrinkle is visible at $x = 38$ m and at $x = 56$ m the slug is already formed), the length at $x = 125$ m can be calculated as

$$L_{125m} = (125 - 40)(0.72 - 0.35) = 31.5 \text{ m.} \quad (5.10)$$

The slug length is the difference between the hold-ups in front and behind the slug, multiplied by the length of the path over which this liquid is collected by the liquid slug.

When also the other term in (5.7) is taken into account, the length is slightly larger

$$L_{125m} = \frac{dL}{dt}T = [0.011 + 0.87(0.72 - 0.35)] \frac{125 - 40}{0.87} = 32.5 \text{ m,} \quad (5.11)$$

which is relatively close to the $L = 37$ m obtained in the experiment.

For the first slug, it is clear that the slug enters an environment with a high holdup at the front, and leaves a low hold-up at its tail. The difference is used for the slug to grow. This situation is constant over the whole path of the slug, and the slug can grow to infinite length. This is really a nightmare for the operators in the field, since for long flowlines these slugs can continue growing. For the slugs that are formed later in time, it is not exactly known how the hold-up evolves with time and position. For that reason, it is not possible to calculate the amount of available liquid between the initiation point and the end of the set-up like in the case of the first slug.

5.4 Slug behavior in time : slug frequency

The slug frequency is based on the number of slugs passing during a fixed period in time. In figure 5.14, the average time between two slugs is shown for various combinations of the gas and liquid superficial velocities. In the lower left part of the graph, for low gas and liquid velocities, the time between the slugs is quite large, upto a few hundred seconds. For increasing gas and liquid flow rates, the slugs pass more often, resulting in a interval of only several seconds for the highest gas and liquid flow rates.

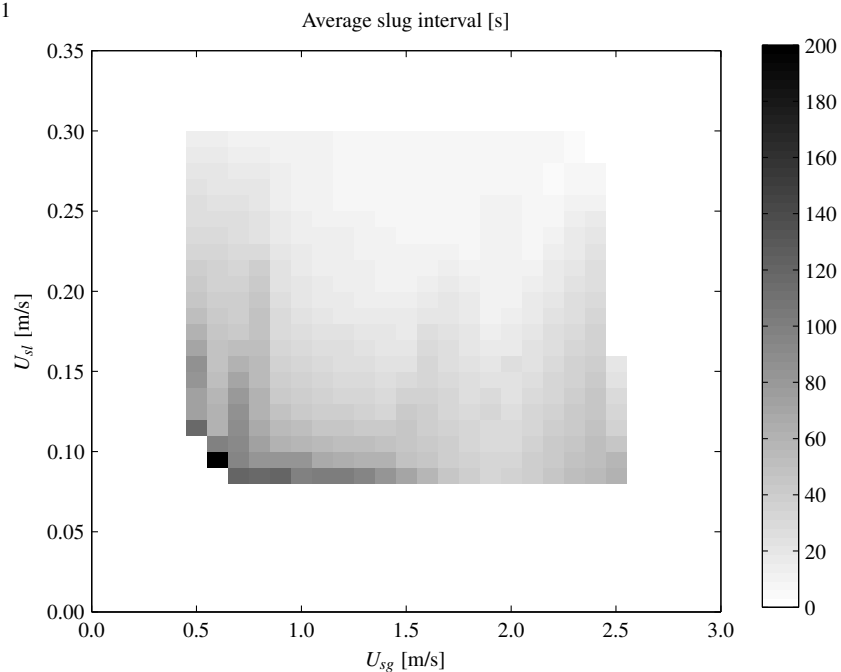


Figure 5.14: Near the transition, at low liquid velocities, slugs are far apart from each other, while for larger flow-rates, the frequency increases.

Several series of measurements at constant liquid flow rate U_{sl} were investigated separately, which resulted in a power law relation between the time interval Δt and the superficial gas flow rate U_{sg} .

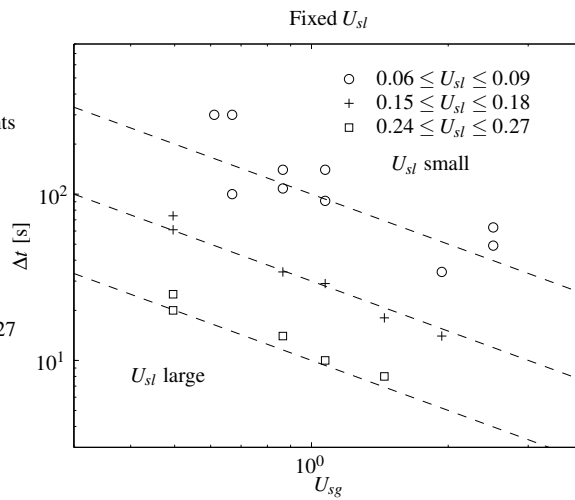


Figure 5.15: Relation between average slug interval and U_{sg} . The different symbols represent different liquid velocities U_{sl} . For each fixed liquid velocity, there is a log-log relation with -1 slope.

The slope of -1 in the log-log plot of figure 5.15 shows that the time interval between two successive slugs is inversely proportional to the gas velocity U_{sg} . This means that

$$f_s = \frac{1}{\Delta t} \propto U_{sg}, \quad (5.12)$$

which is qualitatively easy to understand because the whole slug formation process is driven by the gas flow for the situation of constant liquid flow. When the gas velocity increases, the whole process of slugging will go faster, such that the slug frequency f_s is increased with the same factor. Apparently, the pattern of liquid slugs can be treated as a fixed structure which moves with the mixture velocity. Since the liquid velocity is small compared to the gas velocity, the mixture velocity can be approximated by the gas velocity.

For the whole range of gas and liquid velocities investigated, the points are in good agreement with the fitted lines. All points, independent whether it concerns long or hydrodynamic slugs, show similar relations. The $f_s \propto U_{sg}$ thus holds in all slug regimes.

The slugging frequency is proportional to the gas velocity, as shown in figure 5.15. This linear relation is shown again in figure 5.16, where all lines start at the origin of the graph.

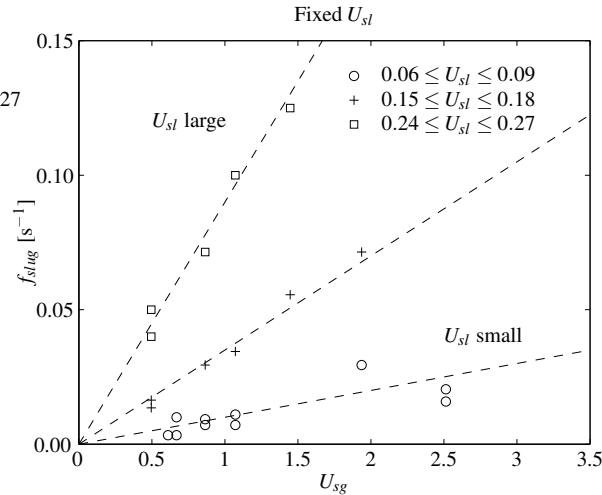


Figure 5.16: The frequency increases linearly with gas velocity. The slope is larger for higher liquid velocities. The experiments are performed in a $D = 0.052$ m tube.

The slug frequency increase as observed in the current study differs from the trends shown in figure 5.17, where the frequency decreases for gas velocities below $U_{sg} \leq 4$ m/s as observed by Fan in a $D = 0.095$ m tube (see Woods et al. (2006)). In both studies, the gas flowrate was varied with constant liquid flow rate. The situation where the frequency becomes independent of the gas velocity only occurs for gas velocities much larger than the range investigated in the current study.

In the experiments by Fan, the shape of the lines is similar for all liquid velocities, while in the current study an increased slope for higher liquid velocities is observed. Since at higher flowrates more liquid is present, more slugs can be formed, assuming that more slugs are formed instead of longer slugs. In section 5.3, it is shown that $L \propto U_{sl}^{-1}$, so slugs will not grow longer for increasing liquid flowrates. The extra liquid should thus produce more slugs.

The values for the slug frequency obtained in both the current study and the work by Fan are of the same order of magnitude. Since the liquid velocities used in the current study are lower than used by Fan, the values in figure 5.16 are lower than in figure 5.17 for the same range of gas velocities. Another difference is the tube diameter which differs almost a factor 2.

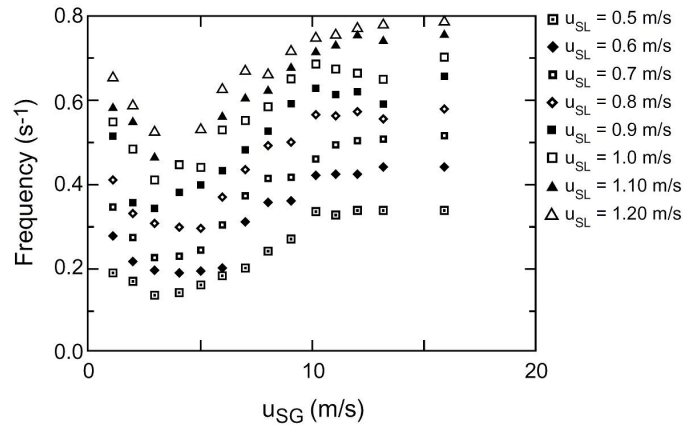


Figure 5.17: Slug flow experiments by Fan in a $D = 0.095$ m tube. The trend is similar for all U_{sl} , with the highest frequencies for the largest liquid velocity. From Woods et al. (2006)

When having a closer look at the time interval Δt for constant gas velocity U_{sg} , so as a function of the liquid flow rate U_{sl} , the power derived from figure 5.18 is equal to -2 , which is again valid for all combinations of gas and liquid velocities, so both for the short and the long slugs.

Since $f_s = \Delta t^{-1}$, this results in

$$f_s = \frac{1}{\Delta t} \propto U_{sl}^2. \quad (5.13)$$

Woods et al. (2006) derived for the slug frequency for hydrodynamic slugging

$$f_s = 1.2 \frac{U_{sl}}{L_s}. \quad (5.14)$$

The length L_s also depends on the liquid velocity. As derived in figure 5.5, the length depends on the velocity as

$$L \propto U_{sl}^{-1} \quad (5.15)$$

Combining (5.14) and (5.15), the relation becomes

$$f_s = 1.2 \frac{U_{sl}}{L_s} \propto \frac{U_{sl}}{U_{sl}^{-1}} = U_{sl}^2 \quad (5.16)$$

which is in agreement with relation (5.13) obtained in the current research. In figure 5.18, the results for the hydrodynamic as well as the long slugs are presented. The frequencies of

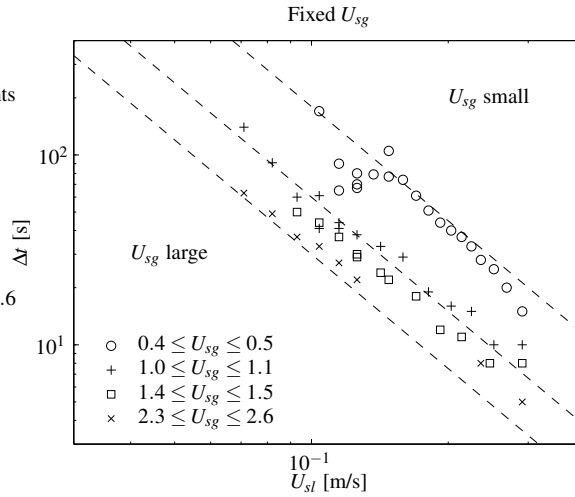


Figure 5.18: Relation between average slug interval and U_{sl} . The different symbols represent different gas velocities U_{sg} . For each fixed gas velocity, there is a log-log relation with -2 slope.

both slug types can be fitted with the same expression. Apparently, the relation (5.14) is also valid for the situations with long slugs. The validity of the Woods et al. (2006) relation will be discussed in more detail in section 5.5.

The expressions obtained for constant gas and constant liquid velocities can be combined to obtain a general expression for the slug frequency

$$f_s = C_1 U_{sg} U_{sl}^2, \quad (5.17)$$

or for the time interval between the slugs

$$\Delta t = \frac{C_2}{U_{sg} U_{sl}^2}, \quad (5.18)$$

which are valid for the hydrodynamic slugs as well as for the situation of long slugs.

5.4.1 Regular occurring long slugs; a constant slug frequency

In figure 5.19, a situation for low flowrates, both gas and liquid, is shown. This results in B-type slugs, which grow and reach a final length within the length of the set-up. The slugs are initiated between $x = 40$ m and $x = 50$ m from the inlet, so before the bend in the tube. The initial time interval, is approximately 175 s, which remains the major peak toward the end of the line. At $x = 105$ m, some of the slugs move in pairs, which can also be seen in the histograms where peaks at lower time intervals, about 15 s to 40 s, occur. The initial peak in the slugs time interval at $x = 56$ m, around 175 s with its tail to higher time differences, remains at 175 s, but its tail tends more to the lower values because of the extra slugs being formed. The characteristic time scale in this situation is the 145 s interval. When comparing this value with (2.31) by Zabaras (2000), this results in an interval time of only 13 s, which is completely different from the 145 s observed in the experiments. The Zabaras (2000) theory is only valid for the short hydrodynamic slugs, and not for the long slugs in the current experiment.

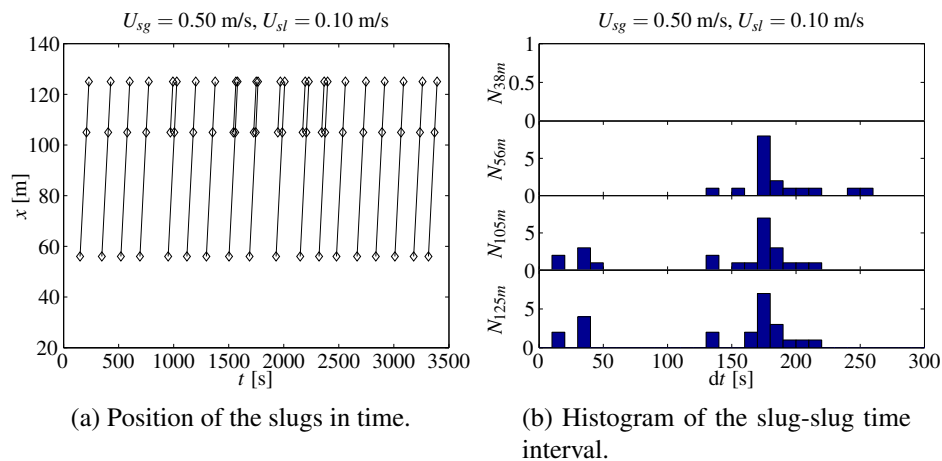


Figure 5.19: Slug interval time for low gas and liquid flowrates, just above slug transition. In (a), the slugs are shown, which initiate at regular time intervals. In (b), this histogram is shown for the different positions.

At position $x = 56$ m, slugs start at regular time intervals, also indicated by the sharp peak in figure 5.19(b), and move downstream. At $x = 105$ m, some slugs appear in pairs. The second slug within each of these pairs corresponds to the slug formed upstream, indicated by the straight lines of constant slug propagation velocity. The first one within the pairs is formed separately further downstream, and moves in front of the old slug. This is also clear from figure 5.20, where the slugs are shown for each individual location. Since the first slug in the pairs at $x = 105$ m sometimes occurs almost at the same moment as the slugs at $x = 56$ m, this can not be the same slug.

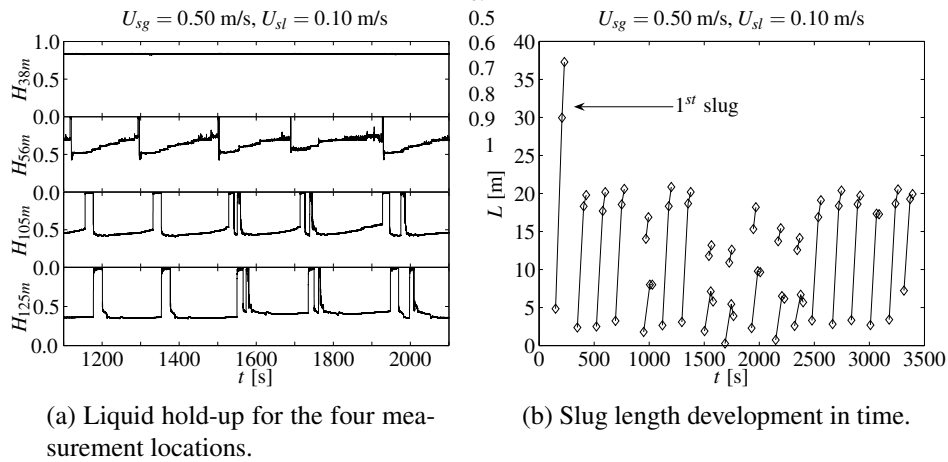
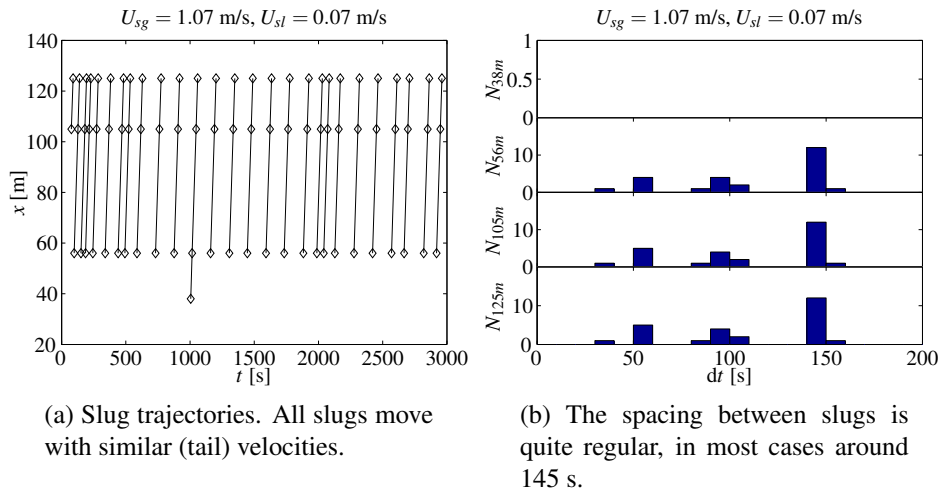


Figure 5.20: The hold-up (a) and slug length (b) for the slugs in the time interval between 1100 and 2100 seconds. Based on the average slug propagation velocity, a match can be made on which peaks correspond to the same slugs, as shown in figure 5.19(b). Since for several slugs, the peak in sensor 2 is almost at the same moment as in sensor 3, it is obvious that the first peak of the slug pairs is from a fresh slug, and the second peak corresponds to the old slug. This is also observed in the length plots.

From figure 5.20, it is observed that there are regions with long single slugs, alternated by regions with double slugs. For the slug pairs, the front one is observed only in the last part of the set-up, and grows to longer lengths compared to the second slug in the pair. Because the liquid is already taken by the first slug, there is hardly any liquid left for the second, old slug to grow.

Another example of B-type growing slugs occurring in a regular pattern is shown in figure 5.21, which is the same experiment as already discussed in figure 5.10. Most slugs have a 145 seconds spacing, in the beginning this time interval is less.



(a) Slug trajectories. All slugs move with similar (tail) velocities.

(b) The spacing between slugs is quite regular, in most cases around 145 s.

Figure 5.21: Growing slugs, which occur in a regular time interval.

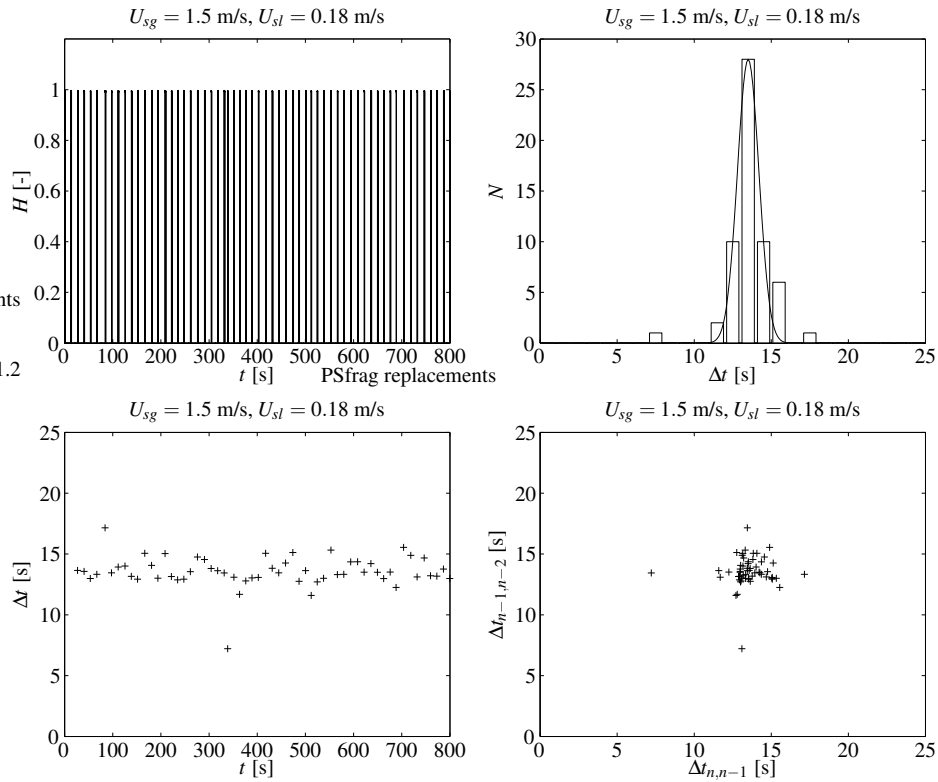


Figure 5.22: Slug-slug interval for the situation with $U_{sg} = 1.5$ m/s, $U_{sl} = 0.18$ m/s. The slug pattern is quite regular with a constant interval of $\Delta t = 13.5 \pm 2$ seconds.

For the hydrodynamic slugging situations (type E) as shown in figures 5.22 and 5.23, the frequency of slugging is much higher, with interval times in the order of 10 to 15 s. As shown in the lower graphs of figures 5.22, the time interval is constant. This is also shown in the histogram, which is very narrow. This experiment was done for velocities close to the transition line in figure 5.2. Most of the slugs observed are of the hydrodynamics type (E), with also some slug growing to longer lengths (type D).

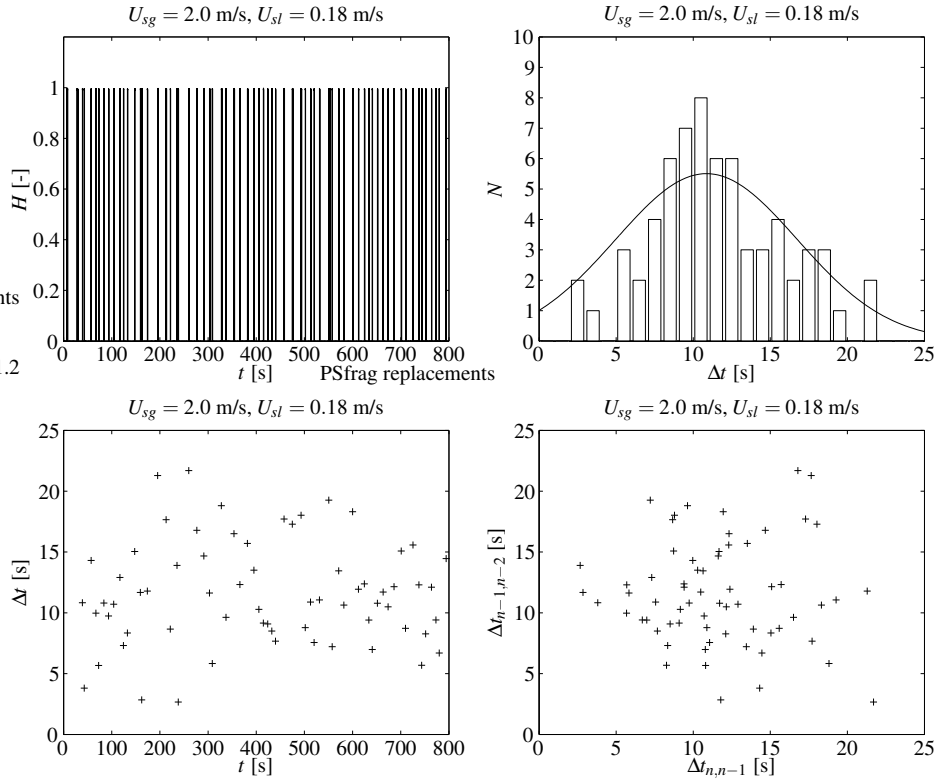


Figure 5.23: Slug-slug interval, similar to figure 5.22, but now for $U_{sg} = 2.0$ m/s and $U_{sl} = 0.18$ m/s. The peak is shifted to a lower value of $\Delta t \approx 10$ s and the spread in interval time is much larger.

A small increase in the gas flowrate, from $U_{sg} = 1.5$ m/s in figure 5.22 to $U_{sg} = 2.0$ m/s in figure 5.23, gives a smaller time between the slugs, as can be expected because the flow as a whole moves faster. This experiment showed only the short hydrodynamic slugs, which corresponds to flowtype E in figure 5.1. The ratio of the peak positions in the histogram $\approx 13.5/10 = 1.35$, is directly related to the the velocity ratio as

$$\frac{\Delta t_{1.5}}{\Delta t_{2.0}} \sim \left(\frac{U_{mix,1.5}}{U_{mix,2.0}} \right)^{-1} \approx \left(\frac{U_{sg,2.0}}{U_{sg,1.5}} \right) = \frac{2.0}{1.5} = 1.33, \quad (5.19)$$

which confirms the relation shown in (5.12) that $f_s \propto U_{sg}$. Another interesting difference is the spread in the histograms, which is much broader for the high gas velocity situation.

5.4.2 Slug patterns with two characteristic frequencies

The second group of slugs is the alternating slugging, which occurred for the growing slug situation (B,C-type). There is a regular, pattern (over more than 1 slug), which is repeated in time. There is no constant time interval between two successive slugs, so there is not a unique value for Δt . In figure 5.24(a), the histogram for the time interval Δt_n is plotted, which shows two peaks at 70 s and 115 s. In (b) the time interval is plotted vs the previous time interval, resulting in 2 groups of points. After a slug with $\Delta t_1 = 70$ s, the next slug will arrive after $\Delta t_2 = 115$ s, and then after $\Delta t_1 = 70$ s again, as indicated with the large circles in figure 5.24(b). The small circle shows the sequences of slugs with only $\Delta t = 70$ s intervals.

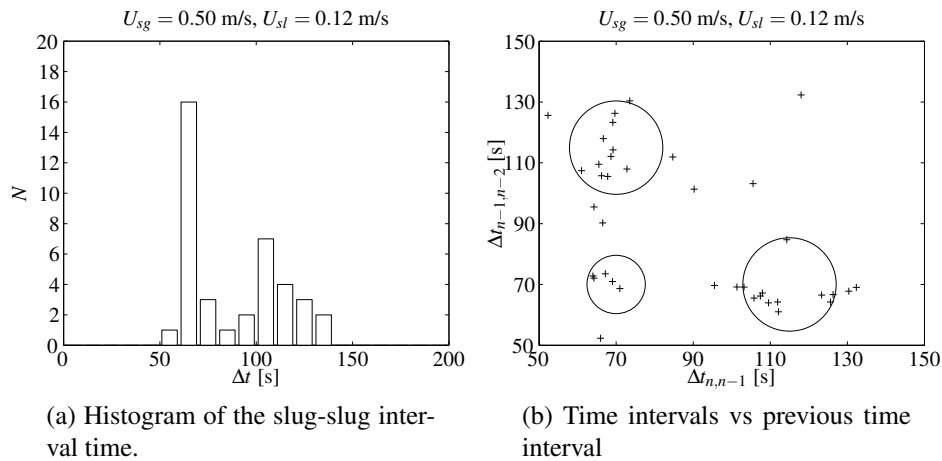


Figure 5.24: In (a), two peaks are visible in the histogram of the time intervals. In (b), the alternating behavior is illustrated.

5.4.3 Slugs with an irregular pattern in time

The last regime is the slugs that occur at irregular time intervals. In figure 5.25, the slugs are shown for the situation of $U_{sg} = 2.5$ m/s and $U_{sl} = 0.07$ m/s. Several differences with the low gas velocity situations are observed. Besides the higher slug frequency, also the pattern becomes more irregular. The slugs observed are a mixture of short hydrodynamic slugs, and other slugs that can grow upto $L \approx 7$ m. The hydrodynamic slugs correspond to the lowest time intervals, the slugs that are formed after a longer Δt are usually much longer. This can easily be understood, because after a longer time, the liquid level has rebuild to a higher level which can be taken up by the passing growing slug.

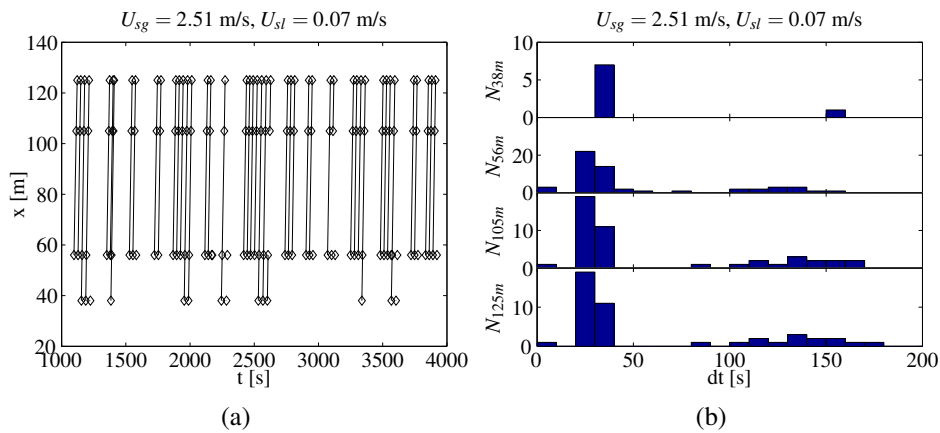


Figure 5.25: Slug interval time for low liquid and high gas flowrates, just above slug transition. In (a), the slugs are shown, which are initiated in groups. Within those groups, the slugs are equally spread. In (b), this histogram is shown for the different positions.

The main peak is around 30 s, but there are also periods longer than 100 s when no slugs are present. After these longer times, the long slugs are formed. The slugs are created in sequences of hydrodynamic slugs, with a fixed time interval of about 30 s as shown in figure 5.25(a). This value is in agreement with the predicted time interval by Zabaras (2000), which results in a 28 s slug spacing for the hydrodynamic slugs. The time between the several sequences is larger, and each new sequence starts with a longer slug. Since this interval is not related to hydrodynamic slugging, the Zabaras (2000) theory can not predict the longer timescale.

Since the combination of gas and liquid velocity is close to the point where the transition lines shown in figure 5.2 join, different types of slugs can be present. All regimes B, C, D and E come together at $U_{sg} = 2.5$ m/s and $U_{sl} = 0.07$ m/s.

5.4.4 Initiation of slugs for slightly upward flow

In the experiment shown in figure 5.26, slugs are plotted for three different locations at $x = 108$ m, $x = 121$ m and $x = 133$ m for the flow conditions of $U_{sg} = 2.00$ m/s and $U_{sl} = 0.04$ m/s. According to the flowmap presented in figure 5.2, no slugs can be present under these flow conditions. Since the tube has a small upward inclination of 0.1° , slugs are formed already at lower liquid velocities. Because only the last part of the set-up ($x > 100$ m) has this upward inclination, the absolute distance from the inlet has no meaning in this experiment. Only the development on the 25 m segment between $x = 108$ m and $x = 133$ m is of interest.

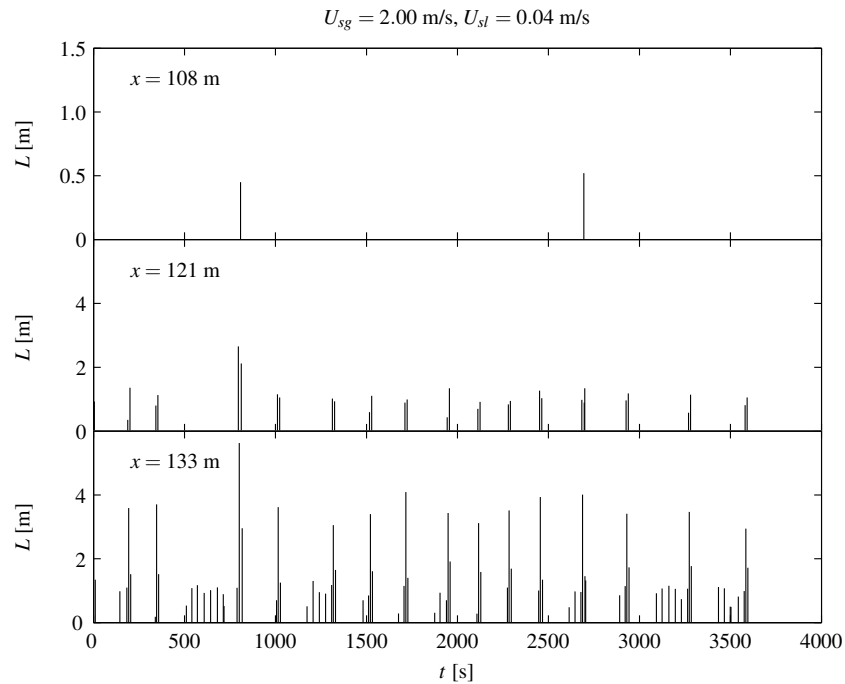


Figure 5.26: Slugs are being initiated at regular time intervals in front of the slugs already present. In the graph, the length of the passing slugs at different locations. At $x = 108$ m, only two small slugs are observed (note different vertical scale), while further downstream more and larger slugs were measured. At $x = 121$ m, slugs are formed in pairs, while at $x = 133$ m sequences of slugs with regular time intervals were observed. The new slugs are, for both the locations $x = 121$ m and $x = 133$ m, formed in regular patterns before the older slugs.

At $x = 108$ m, two slugs were observed, both half a meter long (note the different vertical scale). In the next position, at $x = 121$ m, more slugs were observed, in a regular pattern. Most of the slugs have lengths in the order of $L \approx 1 - 2$ m. The slugs were observed in pairs, with a $\Delta t \approx 12$ s average spacing, and a large time interval of about $\Delta t \approx 200$ s, as shown in graph 5.27. It is clear that this alternating pattern between $\Delta t \approx 12$ s and $\Delta t \approx 200$ s is repeating in time.

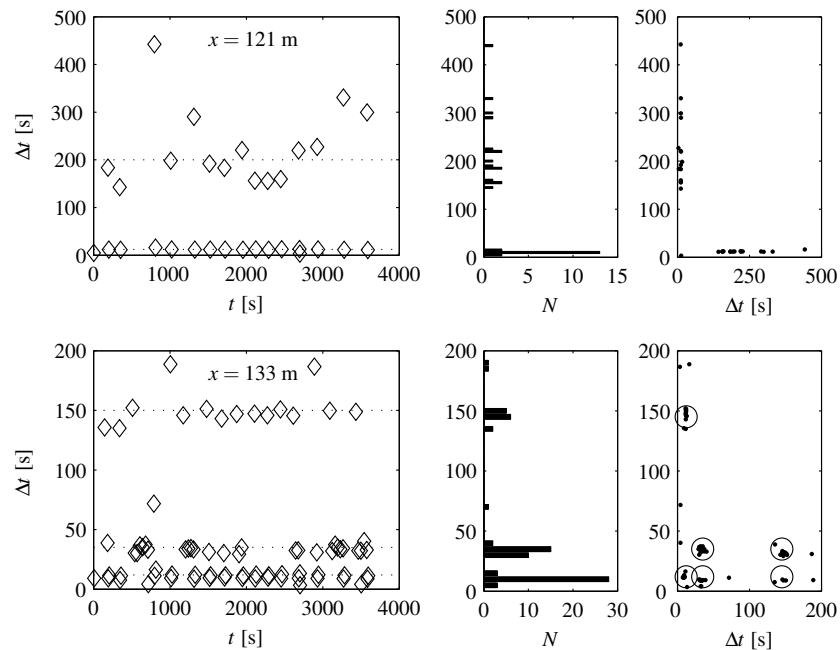


Figure 5.27: Time between slugs for the last two locations in the set-up. The time interval Δt between slugs has the highest provability for the discrete values of 12 s, 35 s and 145 s at $x = 133$ m from the inlet. Note that the inclined part started around $x = 100$ m, so the actual development length of the flow is in the order of 30 m.

In the last location at $x = 133$ m, even more slugs were detected, with the new slugs moving in front of the old ones formed earlier. Again several characteristic time scales were found of $\Delta t \approx 12$ s, $\Delta t \approx 35$ s and $\Delta t \approx 150$ s. In this case, not all groups of slugs are equal in the number of slugs and the inter-slug time interval, but there are several discrete situations. Since this experiment was done with a small upward inclination, the terrain influence allows slugs to be present for the flow conditions which normally would result in stratified flow. The maximum slug length observed at the last measurement location $x = 133$ m is between

$L \approx 3 - 4$ m for most of the slugs. The old slugs are growing, and new slugs are initiated, which remain small (based on the limited measurement length of $\Delta x = 25$ m).

From the diagrams on the right in figure 5.27 it is clear that there is a certain regularity in the slug interval times. On the horizontal axis is the Δt of the current slug, versus the Δt of the next slug on the vertical axis. For the $x = 121$ m position, there is an alternating pattern between the short 12 s interval and a long interval between 150 s and 450 s.

Further downstream, at $x = 133$ m, three different time intervals are present, which is nicely illustrated by figure 5.28. The time between two subsequent slugs equals one of the for this experiment fixed values of 12 s, 35 s or 145 s. Some combinations of subsequent time intervals are possible (12-12), (35-12), while others (12-35) and (145-145) are not. After a long interval (145 s), only short intervals (12 s, 35 s) will occur. The long 145 s interval can only be present after a 12 s interval.

The three characteristic time intervals of 12 s, 35 s and 145 s can be related to the different slugs present. The 12 s corresponds to the time interval between the pairs of old slugs, as indicated in the middle of figure 5.26. The 35 s is the interval between the short hydrodynamic slugs, present at $x = 133$ m. The largest time interval is the time between the different sequences of slugs.

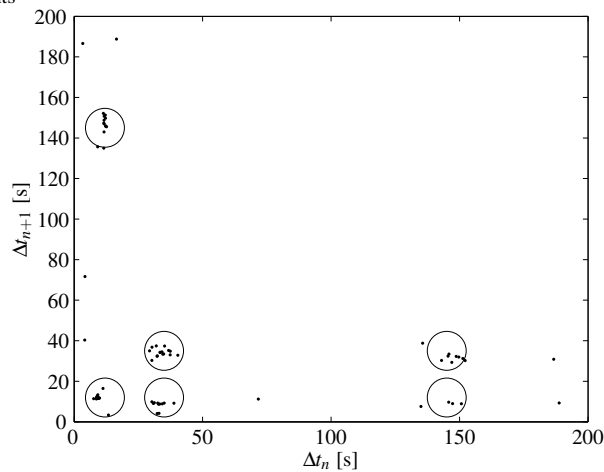


Figure 5.28: Slugs are being initiated after certain fixed time intervals. After an interval Δt_n on the horizontal axis, several, but not all values of Δt_{n+1} are possible after the next slug.

In table 5.1 the measured frequencies mentioned in the current section are compared with the Gregory and Scott (1969) relation, which is equal to the expression by Zabaras (2000) without angle correction term

$$f_s = 0.0226 \left[\frac{U_{sl}}{gD} \left(\frac{19.75}{U_m} + U_m \right) \right]^{1.2} . \quad (5.20)$$

It is clear from the numbers in the table, that only for the type E slugs (hydrodynamic), the measured frequencies are in agreement with the predicted value. For the D-type slugs close to the D-E boundary, the measurements and the prediction only differ by a factor of 2. For the long and growing slugs (B,C), the prediction is not valid. Since these slugs are much longer than the hydrodynamic slugs, it can easily be understood from the liquid mass balance that the frequency should be much lower for these long slugs.

| Figure | U_{sg} | U_{sl} | Slugtype | Δt_{meas} | Δt_{pred} |
|--------|----------|----------|----------|-------------------|-------------------|
| 5.19 | 0.496 | 0.104 | B,C | 175±25 | 4.2 |
| 5.21 | 1.072 | 0.071 | B,C | 145±10 | 13 |
| 5.22 | 1.5 | 0.18 | D,E | 13.5±2 | 6.5 |
| 5.23 | 2.0 | 0.18 | E | 10±5 | 8.0 |
| 5.25 | 2.513 | 0.071 | E,(BC) | 30,(>100) | 28 |
| 5.26* | 2.0 | 0.04 | - | 12,35,150 | 48 |

* For upward inclined flow

Table 5.1: Comparison between measured and predicted slug frequencies.

5.5 The relation between slug length and slug frequency

Combining the data from figures 5.3 and 5.14, a relation between slug length and slug frequency, here expressed by the slug time interval $\Delta t = f_s^{-1}$, can be obtained. In figure 5.29, the data is sorted for different velocity ranges U_{sl} . For each branch, a slope of 1.0 is obtained, indicated by the dashed lines. The most left dataset (o) corresponds to large values of $0.24 < U_{sl} \leq 0.27$ m/s, while the dataset on the right (x) represents the low liquid velocity range $0.09 < U_{sl} \leq 0.12$ m/s.

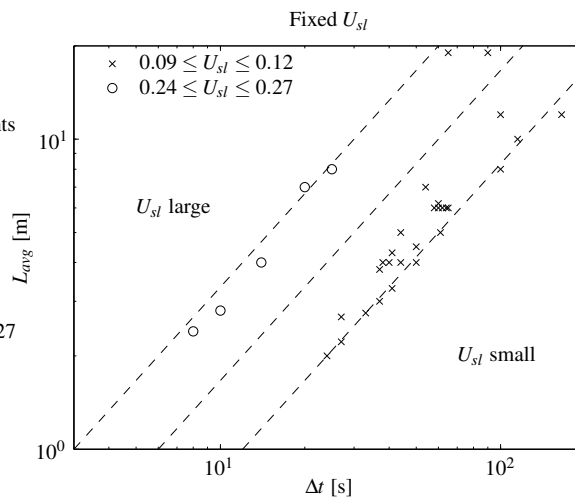


Figure 5.29: Relation between time interval and average slug length. The different symbols represent different liquid velocities U_{sl} . For each fixed liquid velocity, there is a log-log relation with 1.0 slope.

A similar exercise is done by grouping the gas velocities U_{sg} , which is shown in figure 5.30. A slope of 0.5 was obtained for all sets of equal gas velocity. The upper data set (o) was measured at $U_{sg} \leq 0.5$ m/s, the lower set of datapoints (\square) was obtained from the high velocity ($U_{sg} > 2.3$ m/s) experiments.

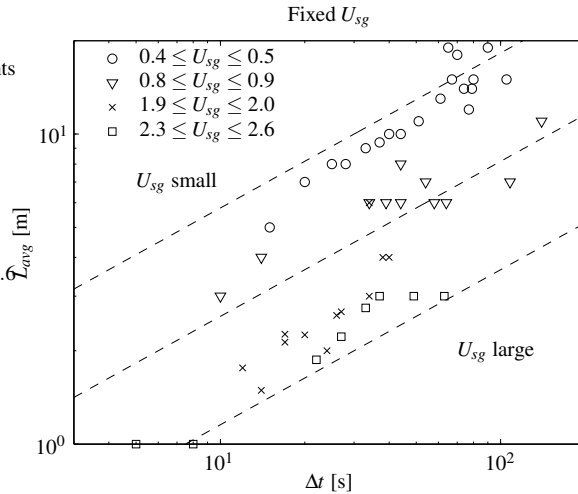


Figure 5.30: Relation between time interval and average slug length. The different symbols represent different gas velocities U_{sg} . For each fixed gas velocity, there is a log-log relation with 0.5 slope.

Woods et al. (2006) derived an expression for the hydrodynamic slug region, which relates the slug frequency to the slug length as

$$f_s = \frac{1.2U_{sl}}{L_s}, \quad (5.21)$$

which is in agreement with the linear relation between Δt and L_s as observed in figure 5.29. This relation by Woods et al. (2006) can also be expressed as

$$L_s \times f_s = 1.2U_{sl}, \quad (5.22)$$

which indicates that the product of length and frequency should be a linear function of the superficial liquid velocity. In figure 5.31, the experimental data is plotted, with the (+) signs indicating the short hydrodynamic slugs and long slugs represented by (o). It is clear that both types of slugs behave similar, and in agreement with the expression by Woods et al. (2006). Although it was derived for the hydrodynamic slug regime, it seems also to be valid for the long slugs.

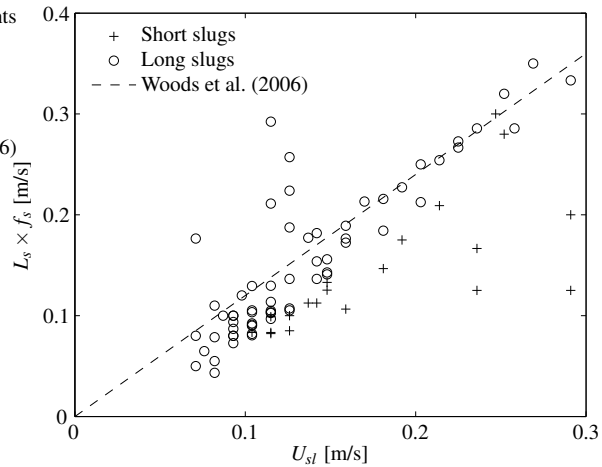


Figure 5.31: The relation by Woods et al. (2006) is also valid for the long slug region, as indicated by the circles.

As shown in (2.21) on page 23, the relation in (5.21) only holds for large liquid volume fractions $\lambda \geq 0.10$. The data shown in figure 5.31 covers the range $0.02 \leq \lambda \leq 0.35$. In figure 5.32, the data is split for values $\lambda \leq 0.10$ (a) and $\lambda \geq 0.10$ (b). From figure 5.32 it is clear that the constant 1.2 from (5.21) is on average correct for large liquid volume fractions (b), and gives an overestimate of the value $L \times f$ for lower liquid volume fractions $\lambda \leq 0.10$ (a).

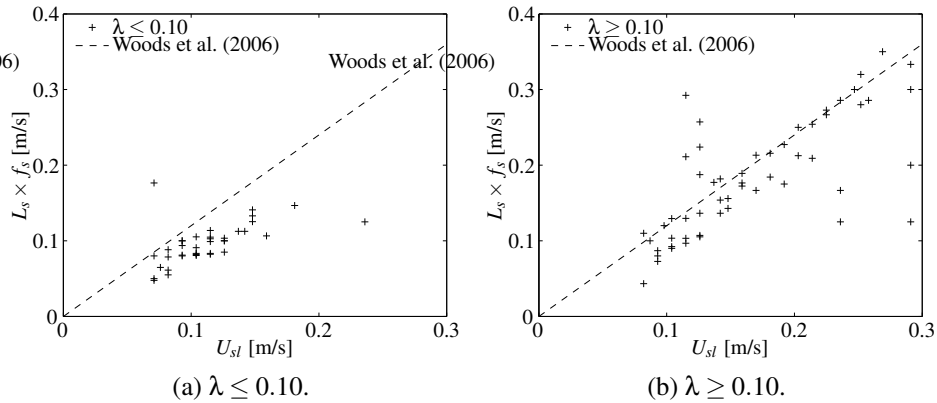


Figure 5.32: The relation (5.22) for liquid volume fractions $\lambda \leq 0.10$ (a) and $\lambda \geq 0.10$ (b).

5.6 Conclusions

The experiments described before are performed in a 137 m long 2-inch flowloop with air and water flowing at velocities ranging from 0.5 – 3.00 m/s and 0.04 – 0.30 m/s respectively. Different slug types are defined. Besides the short hydrodynamic slugs (type E), different types of long slugs were observed (types A-D).

The region of long slugs was shown to occur in the flow map for superficial gas velocities of $U_{sg} \leq 2.50$ m/s. In that region the transition from stratified flow to slug flow leads to hydrodynamic slugs via the long slug regime with sizes beyond $40D$. For a fixed gas velocity the lengths of the liquid slugs decrease with liquid velocity from values beyond $400D$ until values of about $40D$ on approaching the hydrodynamic slug boundary. Traversing the flow map along a horizontal line, *i.e.* with a fixed superficial liquid velocity and increasing gas velocity also leads to a decrease of the average length of the liquid slugs.

Slug length can increase when traveling downstream through the pipeline. This growth can be related to the difference in front and tail velocity. The tail velocity of the slug is constant for all slugs over all positions, the front velocity starts higher for growing slugs, and decreases gradually towards the value of the tail velocity. Going downstream, the difference between these velocities decreases, and the slug stops growing when both velocities are equal. All slugs for fixed inlet flow rates behave similarly with respect to length and velocity development as function of position. For constant gas velocities, a relation between slug length and liquid velocity was found. In a similar way, a relation between slug length and gas velocity for constant liquid velocity was obtained. The general expression for the slug length goes with power -1.5 for the gas velocity and -1.0 for the liquid phase. With this correlation, the

short hydrodynamic slugs as well as the long slugs are captured.

The only slug that differs from the rest is the first slug just after a change in the flowrates, because this slug encounters another environment, and shows different growth behavior. Usually, this single slug grows to much larger lengths compared to the rest of the slugs that follow afterwards. Based on the available amount of liquid in front of the slug, a certain part of the stratified layer is taken up by the slug. The slug length can be calculated considering mass conservation of the liquid phase.

The slug frequency is the other important parameter that was investigated in the current study. The lowest slug frequencies were obtained for the longest slugs, so for combinations of low gas and low liquid velocities. Like for the slug length, also the slug-slug time interval was determined as function of the gas (liquid) velocity for constant liquid (gas) velocity. The slug frequency increases linearly with gas velocity. The proportionality factor depends on the liquid velocity. When starting in the long slug region at a fixed liquid velocity, the slug frequency increases for increasing gas rate. After the transition to the hydrodynamic slug region, still at the same liquid flowrate, the frequency continues to increase with the gas flow rate. The correlation thus holds for both the long and the short slug regions.

This behavior differs from the observations by Fan (see Woods et al. (2006)), who states that for low gas velocities the frequency decreases as function of the gas velocity. Only at velocities $U_{sg} \geq 4$ m/s, the frequency starts increasing again. Their measurements also show that the frequency becomes constant for sufficiently high gas flows. In the current research, this regime was not observed, because the used gas velocities are too low.

Several experiments are shown, in which the frequency is calculated. One, or sometimes even more characteristic frequencies were found, which can be related to the flow conditions at the inlet by a power law correlation. The frequency goes linearly with the superficial gas velocity and with the superficial liquid velocity squared.

Depending on the flow conditions, different slug frequencies were found. The frequencies are comparable with the correlations by Gregory and Scott (1969) and Zabaras (2000) for the hydrodynamic slugs. For the longer slugs, both correlations result in far too high frequencies.

The last relation that was investigated is combination of slug length and slug frequency. According to the Woods et al. (2006) expression, the quantity $L \times f$ should be linearly related to the superficial liquid velocity U_{sl} , which was indeed also observed in the current series of experiments. Although the relation was originally derived for the short hydrodynamic slugs, the long slug data show better agreement than the results from the hydrodynamic slug experiments.

All correlations derived from the measurements are valid for both the short and the long slugs. At least for the length and frequency, both types of slugs can be treated in a similar way.

CHAPTER 6

Slug structure and initiation processes

In this chapter the focus is on the behavior and development of the slugs related to its properties and the local environment. The effect of the liquid hold-up is shown in section 6.1. This part also zooms in on the deviating behavior of the first slug. When looking at the extrema of the liquid hold-up, the transitions in the flowmap can be related to the values of the hold-up, as explained in section 6.2.

The sections 6.3 and 6.4 deal with the gas bubbles inside the liquid slug body. In the last section 6.5, the waves from which the slugs can be initiated are discussed. Different intermediate stages, roll waves and pseudo-slugs are shown. Although the slug initiation process can not be studied in detail with only 4 sensors distributed over the whole length of 137 m, some interesting patterns were observed, that can be related to stages of slug initiation.

6.1 Different growth behavior depending on the local hold-up environment

Slugs can occur from different environments, as discussed in section 2.4.2 in the theory. The local environment is defined by the hold-up in the stratified flow just before and after the liquid slug. For the flowconditions studied in the current research, the flowtypes observed are stratified(wavy) and slug flow, because the flow rates are relatively low.

Before a slug is initiated, the flow is stratified, so in that sense, all slugs come from a stratified environment. Still there can be a large difference between slugs based on the hold-up (or liquid level) of the stratified flow they were initiated from. In figure 6.1, several growing slugs are shown (type B), as measured at the 4 locations along the tube. The superficial velocities equal 0.865 m/s and 0.082 m/s for the gas and liquid, respectively.

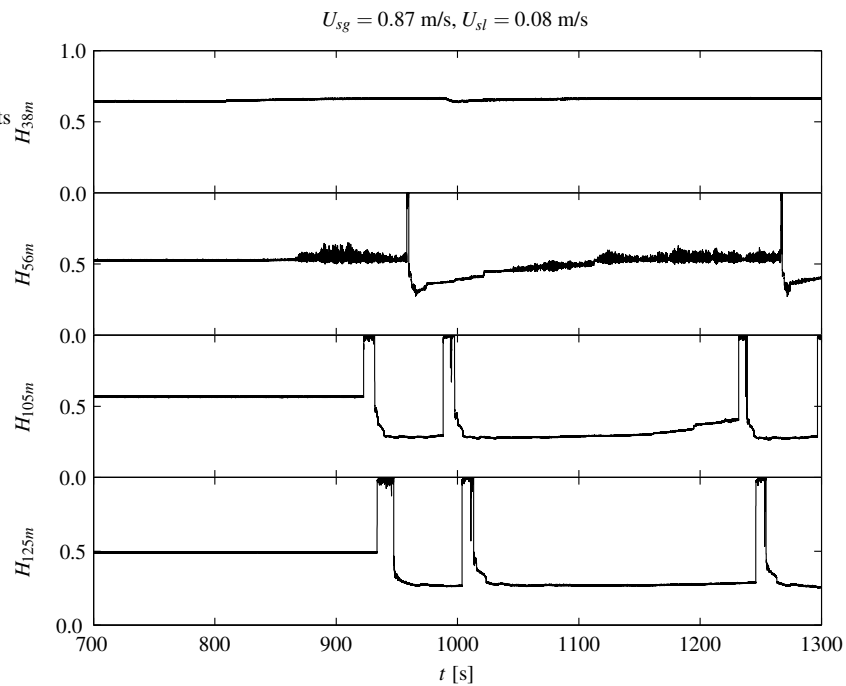


Figure 6.1: Slugs at different locations in the pipeline. The hold-up just in front of the slug varies between minimum and maximum hold-up, as shown in the pictures.

In the top image, only stratified flow is present, slugs were not initiated yet. In the second image, at $x = 56$ m from the inlet, waves occur after $t = 850$ s, and a slug is formed after $t = 950$ s. After the slug has passed, the liquid level has dropped. The next 150 s, the liquid level rebuilds to the original level as before the slug, and reached $H = 0.50$ again. At $t = 1260$, another slug is formed, and the whole process starts again.

The $t = 950$ s slug is not the first slug, since at $t = 920$ s, a slug was observed further downstream at $x = 105$ m. The first slug in the third image starts from a hold-up of about $H = 0.55$, while the next one arises from a stratified flow at $H = 0.25$. The 0.55 is indicated as maximum hold-up condition, the 0.25 as minimum hold-up. These numbers can vary, based on the flow conditions *i.e.* the superficial gas velocity U_{sg} .

The level of the stratified flow between the second and the third slug at $x = 105$ m is rising between $t = 1000$ s and $t = 1230$ s. The moment the third slug is formed, the hold-up is increasing. The hold-up has a value between $H = 0.25$ (minimum hold-up) and $H = 0.55$ (maximum hold-up). This situation is denoted by the growing hold-up environment. For the last measurement location at $x = 125$ m, the first slug comes from maximum hold-up, the other two from minimum hold-up.

In the experiment shown in figure 6.2, the different environments are indicated, again for growing long slugs of type B. The top image in (a) shows the stratified flow at $x = 38$ m. In (b) the corresponding histogram is shown, giving a peak at $H_{max} = 0.84$. By the second sensor, located at $x = 56$ m, several slugs are detected. The initial maximum hold up in this situation equals $H_{max} = 0.70$, and after each slug the liquid level rebuilds to this value. This is also observed in the histogram in (b), where there is a broad peak reaching from $H = 0.45$ till $H_{max} = 0.70$, indicating the growing hold-up environment. In the third image, representing the situation at $x = 105$ m, again a maximum hold-up of $H_{max} = 0.75$ is observed in the beginning, so before the first slug was created. After the first slug, the hold-up drops to $H = 0.35$, and only rebuilds to $H = 0.50$, which is much lower than the maximum hold-up of $H_{max} = 0.75$. This situation is also indicated as growing hold-up environment. In the last measurement point at $x = 125$ m, the hold-up is maximum in the beginning $H_{max} = 0.65$. After the first slug, the level drops till $H = 0.35$ and remains almost constant till the next slug arrives. This can also be seen with the narrow peak at $H = 0.35$ in the histogram, where for the two middle locations the peaks are much broader.

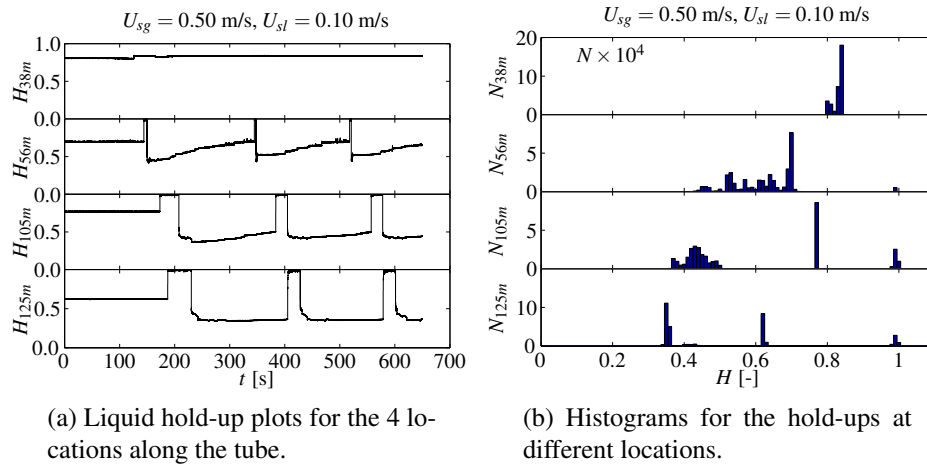


Figure 6.2: Liquid hold-up for the different environments. All graphs (a) start with maximum hold-up. The middle two show growing hold-up environment between successive slugs, where the hold-up in the last plot remains at minimum value after the first slug has passed. In (b) the histograms of (a) are shown.

The maximum hold-up at location $x = 105 \text{ m}$ ($H_{105m} = 0.75$) is higher than for the locations $x = 56 \text{ m}$ and $x = 125 \text{ m}$. This deviation is due to an error in that specific sensor, which causes a threshold value in (some of) the pixels. Since calibration is performed between zero and a time dependent maximum, the signal shows a too large value for hold-ups smaller than 1. This effect is also observed during some of the other experiments of the last runs. Since the value for $H = 1$ is correct (see the peak in figure 6.2(b)), all slug properties are reliable. The hold-up as shown in figure 6.2(a) is squeezed in vertical direction, the range is now e.g. $[0.2 \dots 1.0]$ instead of the $[0.0 \dots 1.0]$ as it should be. Since the slug length and velocity are calculated from the time information, these quantities are not effected by the squeezing of the signal. Only the value of the hold-up in stratified flow is slightly too high. Based on the hold-ups measured by the other sensors, a value of $H_{105m} \approx 0.65$ would be expected.

6.2 Liquid hold-up at flow transition, minimum and maximum hold-up situation

The liquid hold-up is an important parameter for the transition from stratified-wavy flow to the slug flow regime. As discussed in the previous section, different environments can be defined. The maximum hold-up environment, corresponding to the stratified flow situation, is the maximum hold-up for which the stratified flow is stable. A small increase in the hold-up, for example due to a change in the liquid flow rate will result in the formation of slugs. This maximum hold-up situation is shown in figure 6.1 for $x = 38$ m, the hold-up was over 0.65 and no slugs were observed. In the second image, a slug is created from a high hold-up, and after the slug, the hold-up drops to a lower value. This is even more clear in graphs from the last two sensors. At the locations $x = 56$ m and $x = 105$ m, the liquid level rebuilds (partially) toward the maximum hold-up before a second slug is created. For the last sensor at $x = 125$ m, only the first slug came from a stratified environment, while all other slugs move through the slug environment with a liquid layer equal to minimum hold-up. The values of these minimum and maximum hold-up depend mainly on the gas velocity in the system, and only very little on the liquid velocity.

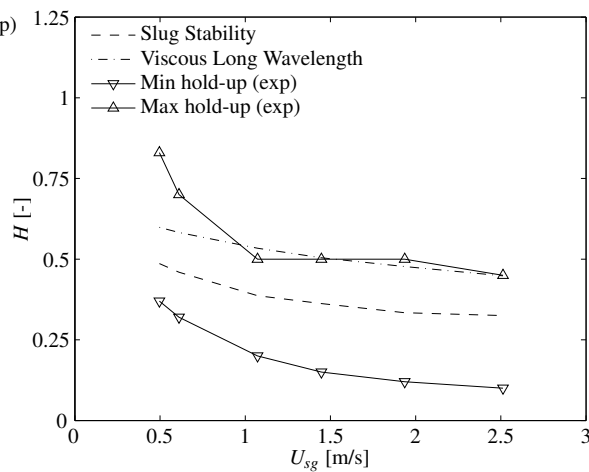


Figure 6.3: The minimum and maximum hold-ups as measured in the experiments. The maximum hold-up in stratified flow is indicated by the upper solid line, the lower solid line represents the minimum hold-up when in slug environment. The critical hold-ups as calculated with the slug stability model and the viscous long wavelength theory are also included in the figure.

In figure 6.3, the minimum and maximum hold-up values are shown for different superficial gas velocities. As mentioned before, the liquid velocity does not have large effect on the value of the minimum and maximum hold-ups. Both the lines show a decreasing trend for increasing gas velocities. As shown in figure 6.2(a), the hold-up changes continuously. From the histograms in figure 6.2(b), it is clear that the value of the hold-up is bounded by certain limits, the minimum and the maximum hold-up. From these histograms, the values shown in figure 6.3 can easily be extracted. The maximum hold-up is obtained just at the stratified to slug transition, so before the first slug is initiated. This hold-up value is thus obtained at the lowest liquid velocity for which slugs are present. The minimum hold-up is equal for all slugs (long and hydrodynamic) being formed at a fixed gas velocity, and independent of the liquid velocity.

The maximum hold-up line, indicated with the upward triangles, is in good agreement with the VLW-predicted hold-up for gas velocities $U_{sg} \geq 1.0$ m/s. For lower gas velocities, stable stratified flow was observed with hold-ups higher than expected based on the VLW-theory.

The slug stability theory predicts hold-ups that are higher than the minimum hold-up measured between the slugs. The shape of the lines of minimum hold-up and slug stability is similar. In minimum hold-up environment, the hold-up has dropped to the minimum level, such that the slug cannot take up any water from the stratified layer.

After a slug has passed, the hold-up at the tail equals the minimum hold-up. After that, the hold-up increases, and a new slug can be formed. Since the hold-up is only measured at 4 locations, the hold-up at slug initiation is not measured. Based on the experiments and the slug stability line in figure 6.3, the slugs can be initiated after the hold-up reached at least the slug stability level. The first slugs, as discussed in section 5.3.2, are initiated from maximum hold-up environment, which seems to be related to the VLW-calculated hold-up.

When predicting the critical liquid velocity for the transition between stratified and slug flow, the slug stability theory (SS) results in lower velocities for the liquid phase than observed in the experiments, as indicated in figure 6.4. The experiments were performed for increasing gas flow rate, from stratified flow into the slug flow regime, while SS determines the transition from slug to stratified flow. Therefore the experimental line shows higher liquid velocities than the SS-model.

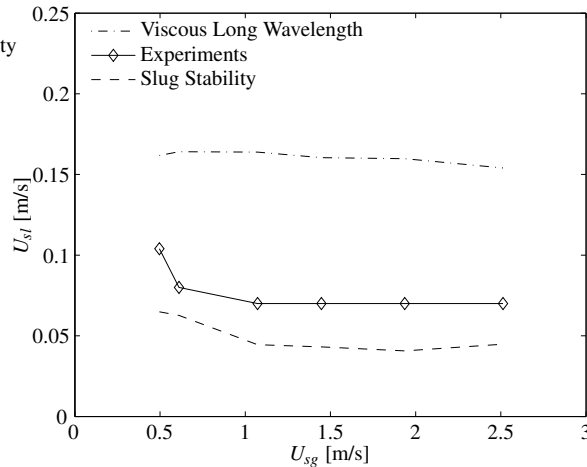


Figure 6.4: The critical liquid velocity for which the transition from stratified to slug flow occurs. The experimental data shows a similar trend as calculated with the SS-theory.

6.3 The effect of gas bubbles inside the liquid slug body

In 2-phase gas-liquid flows, the phases are separated as in stratified flow, or the liquid can be localized in slugs with the gas in between. There can also be an amount of gas inside the liquid slug body, which is called the gas-void fraction ϵ .

Bendiksen (1984); Nydal et al. (1992) state in their articles that the void fraction is only important higher mixture velocities. For $U_{mix} \leq 2\sqrt{gD}$ the amount of gas inside the liquid slug is assumed to be negligible. For higher mixture velocities, $U_{mix} \geq 2\sqrt{gD}$, Woods and Hanratty (1996, 1999) derived for air-water mixtures (see also section 2.2.3 on the slug stability)

$$\epsilon = 0.8 \left[1 - \frac{1}{1 + \left(\frac{U_{mix}}{8.66} \right)^{1.39}} \right]. \quad (6.1)$$

The expression is plotted in figure 6.5 for mixture velocities between 0 m/s and 5 m/s, showing void fractions upto 25%.

The hold-up inside the slug body is measured using the wire-mesh technique. Combining the local hold-up values of all measurement points over the cross-section of the tube results in the total liquid hold-up. For the low velocity measurements, the gas content is very small, but

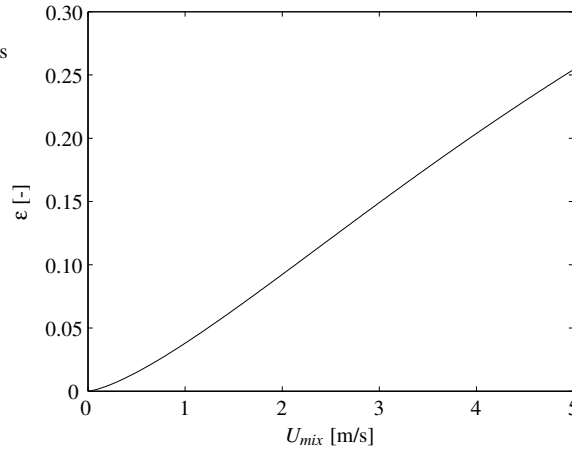


Figure 6.5: The void fraction ϵ for different mixture velocities U_{mix} , based on the model by Hurlburt and Hanratty (2002) and the experimental data by Woods and Hanratty (1996). For low mixture velocities, the void fraction increases almost linearly with the mixture velocity.

not equal to zero as proposed by Woods and Hanratty (1996). For higher mixture velocities, the presence of bubbles increased, as shown in figure 6.6. Based on the experiments done in the current study, the expression (6.1) seems to be valid for all velocities, and not only for $U_m > 2\sqrt{gD}$, which equals $U_m > 1.4$ m/s in the current experimental set-up.

Bonizzi and Issa (2003) also investigated the slug void fraction. Although the overlap in the range of mixture velocities is limited to $2.0 \leq U_{mix} \leq 3.0$ m/s, the observed trends are similar. The results for the current study are close to the observations by Manolis (see Bonizzi and Issa (2003)). The expression proposed by Bonizzi and Issa (2003) is similar to (6.1), but without the factor 0.8 in front. Both the Manolis data, as well as the void fractions obtained in the current research are overpredicted by the Bonizzi and Issa (2003) expression (without 0.8). Both datasets, Manolis and current, fit better with the 0.8 correction included, as also used by 6.1.

The values for the void fraction ϵ , were measured for different mixture velocities. In most cases, the gas fraction was lower than the value predicted with (6.1). The difference was in most cases less than 2%, as indicated with the dotted lines in figure 6.6(b). The long slugs, occurring at low gas and liquid velocities (see figure 5.2), result in slugs with little gas content, as shown in the lower left corner of figure 6.6(a) and (b). The short, hydrodynamic slugs are located in the upper right corners of the graphs at higher mixture velocities. There was no difference observed between the long and the hydrodynamic slugs, both slug types compare

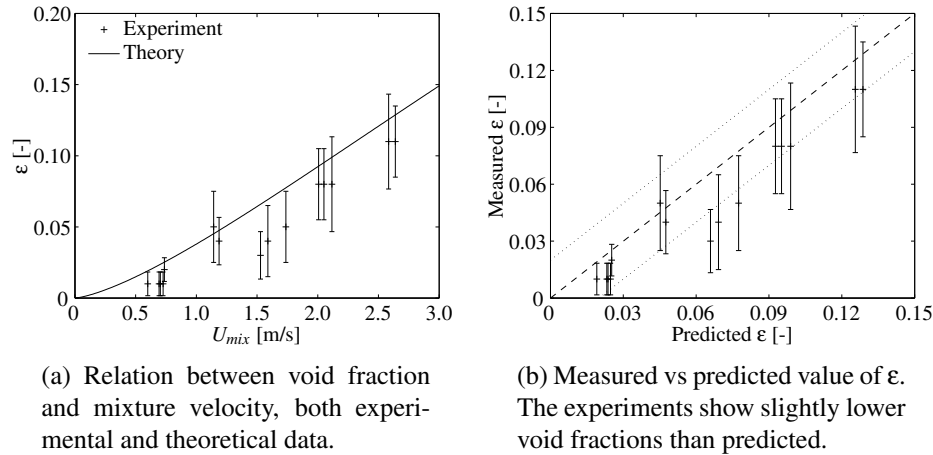


Figure 6.6: The experimental obtained values of ϵ for various mixture velocities U_{mix} . The experimental results are in reasonable agreement with the theoretical value as proposed by Hurlburt and Hanratty (2002).

well with the predicted void fractions by Hurlburt and Hanratty (2002); Woods and Hanratty (1996). When increasing the liquid velocity for constant gas velocity, see *e.g.* $U_{sg} = 2.0$ in figure 5.2, the flowtype changes from growing (B,C), via long slugs (D) into hydrodynamic slugs (E). The mixture velocity for all situations is approximately the same, since the liquid velocity is at least one order of magnitude smaller than the gas velocity. As a consequence, the predicted void fraction will also be more or less the same for all slugtypes (assuming that (6.1) is for all slugtypes), as also observed in the experiments.

Since the wire-mesh data are processed using a cubic region of interest (see section 4.2.2), the void fraction is underestimated, which is also observed when comparing the experiments with theory. Assuming a cubic cell to be completely filled with gas, no signal is to be expected for that particular cell in the wire-mesh. In reality, the active region is not simply cubic, but the surrounding liquid will give rise to some signal measured in the gridpoint, indicating the presence of liquid inside the cell. Therefore, the measured gas fraction will be lower than in reality.

6.4 The distribution of bubbles in the slug, front or tail bubbles

For higher (mixture) velocities, as shown in the previous section, small bubbles can be present in the liquid slug body. It is generally assumed that the majority of these bubbles are present in the head of the slug and that the bubble content in the rest of the slug body is much smaller, as indicated in figure 6.7.

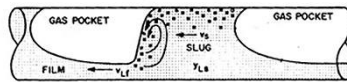


Figure 6.7: A schematic picture of a slug traveling to the left. In the front, a large amount of bubbles is present, while the back of the slug is pure liquid.
From : <http://www.pe.utexas.edu/>

This distribution of bubbles, mostly in the nose of the slug, is confirmed by the experiments, of which an example is shown in figure 6.8. The slug shown is one of a larger sequence of similar shaped liquid slugs. In the nose, which is measured first in time, shows a hold-up starting around $H \approx 0.97$, and after some larger bubbles which occupy almost 5% of space, in the tail a hold-up $H \approx 1.00$ is reached.

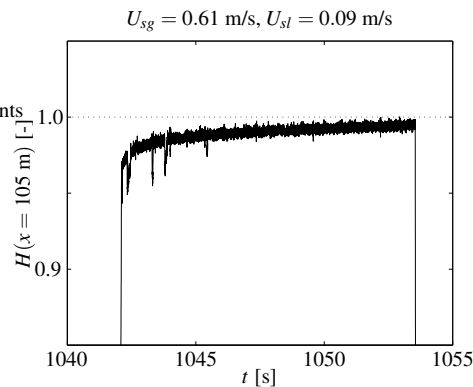


Figure 6.8: A single slug showing a lower hold-up (more gas voids) in the front. Towards the end, the slug becomes less aerated with a hold-up reaching unity.

Experiments showed that the bubbles can also be present at the back of the slugs, especially in fresh slugs. In figure 6.9, a slug is shown while moving through the set-up. In the first graph, corresponding to the most upstream location, the slugs are aerated, 15% – 20% gas hold-up locally at $x = 65$ m, which is much more than predicted ($\epsilon \approx 2\%$) for the mixture velocity of $U_{mix} = 0.70$ m/s. These peaks are not due to the dispersed bubbles in the slug body, but are large bubbles that separate different slugs, as will be explained in figure 6.10(a) which zooms in on the $x = 65$ m slug. Further downstream the slugs become more liquid, with only 2% of bubble fraction, which is equal to the predicted bubble concentration. The few bubbles remaining are mostly in the front of the slug, which is nicely illustrated in figure 6.10 which zooms in on the presence of gas in the first and last measurement section.

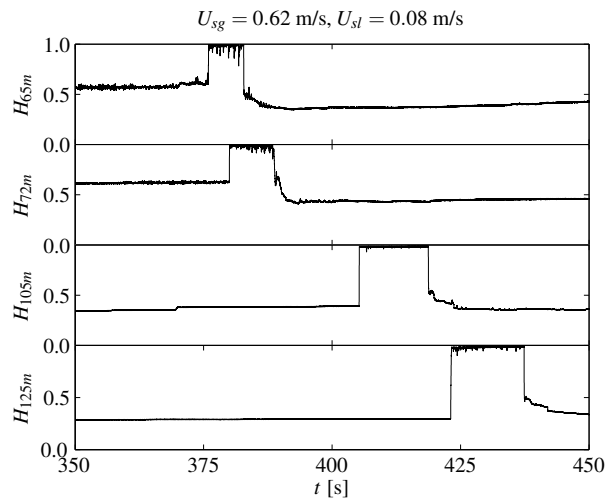


Figure 6.9: A single slug tracked along the length of the set-up. At four different positions, the hold-up is measured. Before and after the slug shown in the figure, other slugs were present. In the upper image, some large bubbles are present in the slug tail (dips in the hold-up). Towards the end of the tube, the slugs contain fewer gas.

The effect of gas bubbles is illustrated in figure 6.10(a), where the local dips down to 20% gas content are visible. These peaks are related to large bubbles in the top region of the tube and move with the slug. These large bubbles separate the subsequent slugs on the slug train, and are not related to the dispersed bubbles inside the liquid slug body. In the rest of the slug body, the hold-up reaches $H \approx 0.99$, indicating almost pure liquid with less than 1% bubbles. When having a closer look at the slug near the end of the set-up shown in (b), the sharp peaks of large bubbles are smaller, which means that the gas escaped from the liquid slug body. The bubbles are thinner (less deep peaks) compared to the $x = 65$ m position. The length of the bubbles is similar in both cases, since the width of the peaks is the same for the two locations. Since the right slug is much larger, the timescales in (a) and (b) are different. The actual width of the peaks is similar, and since all slugs move with the same velocity, the length of the bubbles is also comparable between the different positions. In (b), the maximum hold-up reaches $H \approx 0.975$ in the slug front to $H \approx 0.985$ in the tail of the slug. The void fraction in the front is larger ($\approx 2.5\%$) than in the back of the slug ($\approx 1.5\%$).

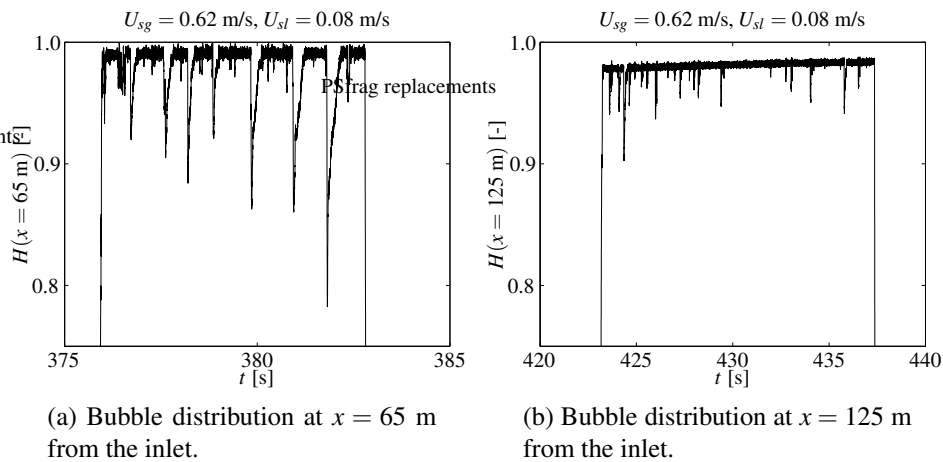


Figure 6.10: *There is a large difference in the shape of the slugs and the void distribution between the upstream section at $x = 65$ m and the downstream section at $x = 125$ m. The first contains several separate large bubbles near the tail, while in the last section, only in the front some, probably well-spread small bubbles are present. In (a) the bubbles are localized, while in (b) the voids are distributed through the whole slug body, since the maximum value of H is smaller for the latter case.*

From the slug in figure 6.10(a), it is clear that the largest bubbles (volume) are present in the tail of the slug. Further downstream, as shown in (b), the spread of bubble volumes changed, with the main contribution near the front of the slug. The slug length increased and the gas content decreased. The gas that is still present is mainly concentrated in the front of the liquid slug.

When series of small slugs merge into larger slugs, some of the gas from the bubbles between the slugs is captured inside the body of the new, large liquid slug, as illustrated by the experiment shown in figure 6.11.

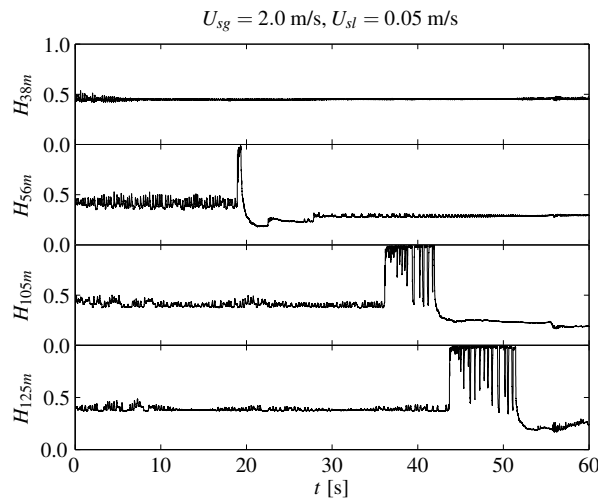


Figure 6.11: Development of a single slug. In the later stages, multiple slugs have merged into a larger structure, with large bubbles inside. Most of the captured bubbles are in the tail of the slug.

The slug shown in figure 6.11 grows considerably when flowing downstream. At $x = 56$ m, just after initiation, the slug is only 1 meter long, while near the end of the setup, 70 meters further downstream at $x = 125$ m, the total length of the slug is almost $L_{tot} = 19$ m ($L/D = 380$). The velocity of the slug can be calculated from the data, giving a front velocity of $v_f = (2.75 \pm 0.05)$ m/s and a tail velocity of $v_t = (2.2 \pm 0.03)$ m/s. These velocities, calculated between the different sections, are in agreement with the velocities obtained within the single measurement sections. It is clear that for growing slugs, the front moves faster than its tail. The growth rate, calculated as the ratio of velocities

$$\frac{v_f}{v_t} = \frac{2.75}{2.2} = 1.25 \quad (6.2)$$

which means that after each meter the slug traveled, the length increased with 25 cm. From the slug lengths, an increase from 1 m to 19 m was observed over a distance of 69 m, which results in a growth rate of 0.26 m/m.

6.5 Intermediate stages during slug formation : Waves and Pseudo slugs

Small disturbances in stratified wavy flow can grow into larger structures, called roll-waves. From these roll-waves pseudo-slugs can be formed. These pseudo-slugs look like real slugs, but are very small, just tipping the top wall in a single point. The experiment in figure 6.12 shows waves in the first measurement section at $x = 38$ m from the inlet for a high gasflow ($U_{sg} \approx 6$ m/s). There are several different wavelengths present in the flow. The long wave, in the order of 15 seconds in the graph and much shorter ones, which can not be seen separately in this image. The graph represents the signal of the liquid height as it is measured in time. The time it takes for a full wave to pass the sensor, is related to the actual wavelength of the waves and the velocity of the wave, assuming that the wave pattern does not deform in time.

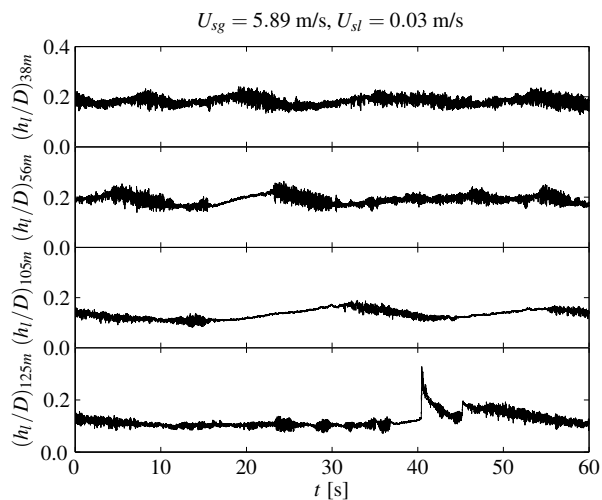


Figure 6.12: Interface waves are present on the stratified wavy flow, which move perpendicular to the main flow direction. In some regions, these waves are absent.

Further downstream, at $x = 56$ m, the upward part of the waves differs from the downward segment, when looking in streamwise direction. In the upward part, between $15 < t < 23$ s, there are hardly any waves on the interface. In the other parts in the flow, small waves are present on the interface, which are zig-zagging from left to right and back, so perpendicular to the stream wise direction.

When having a closer look at the individual points in the wire-mesh, these also show an oscillatory behavior. In the graph shown in figure 6.13, the wire-mesh signal is plotted for two meshpoints at the liquid surface. The upper curve corresponds with a point 2 cm from the center to the right, the lower curve at 2 cm left of the center. It is clear that the two curves are almost in opposite phase, where for pure longitudinal waves, the two graphs should be equal. This effect indicated the presence of a tangential component in the wave propagation. When calculating the total hold-up, all points of the wire-mesh are summed, and the waves shown in figure 6.13 are not visible any longer.

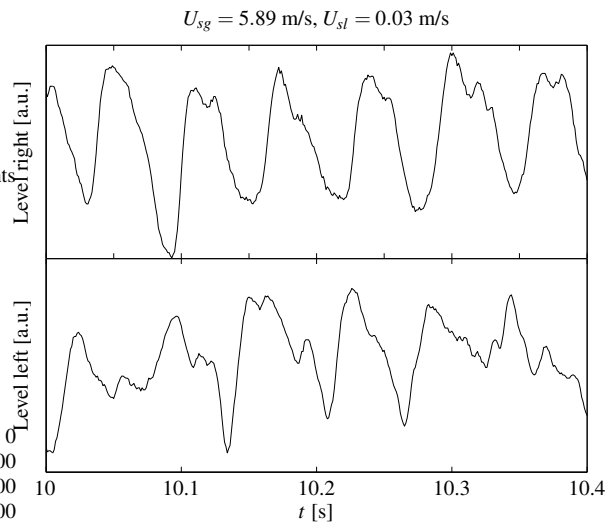


Figure 6.13: Interface waves measured with the wire-mesh for two points at the liquid surface, 2 cm left and right of the center of the tube.

The measurements shown in figure 6.12 represent the liquid level in the center of the tube, and not the total hold-up as usual. In the hold-up measurements, the whole cross section is taken into account, so that it is not possible to see the passing surface waves. For the hold-up, there is no difference whether the interface wave is near the left wall, in the middle or near the right wall. The total hold-up is constant and the same for all configurations. For the level measurements, the local liquid level in the center is measured, so the wave moving from one side to the other gives a varying liquid level in the center of the tube.

A similar pattern of flat and wavy surfaces is observed in the third measurement location positioned at $x = 105$ m. Finally, at $x = 125$ m, the first slug-like structure occurs, called a pseudo-slug. Based on the liquid volume fraction of $\lambda = 0.005$, which is much lower than the value of $\lambda \geq 0.10$ by Heywood and Richardson (1979), (long) slugs are unlikely to be present at these conditions. The pseudo-slug shown here also does not hit the upper wall of the tube, and can therefore not be treated as a real slug.

In figure 6.14, another example of slug formation is shown. Again, the slugs shown in the lower part of the image are not initiated from the waves shown in the upper part, but from similar wave-like structures earlier in time.

In the beginning, the surface is horizontal, and small disturbances are present. In the second image, measured at $x = 56$ m, a large wave is present, which for $t > 20$ shows some interface activity. Further downstream, (pseudo-)slugs are formed, and the stratified flow around the slugs is flat and without waves.

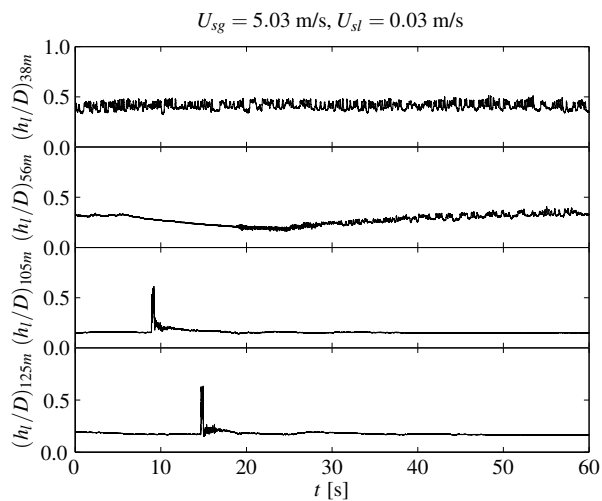


Figure 6.14: The wave pattern changes from small interface waves at $x = 38$ m as shown in the upper image into larger waves and finally slugs are formed further downstream.

6.6 Conclusions

The structure of the liquid slugs and the stratified layer have been measured with high accuracy using the wire-mesh sensors installed in the system. Different environments are observed, which are divided in 3 groups based on their hold-up. The maximum hold-up, the growing hold-up and the minimum hold-up environment. The maximum hold-up indicates the maximum liquid level for which the stratified flow is still stable. The minimum hold-up is defined as the situation at the tail of the slug. After a slug has passed, the liquid level can rebuild to the original maximum hold-up level. When a new slug passes before the liquid level has reached the maximum hold-up value, this environment is called growing hold-up.

A relation is presented between the growth behavior of the long slugs and the liquid hold-up environment. Whether a slug is able to grow or not depends on the the local hold-up. When sufficient liquid is available, *i.e.* the local hold-up is higher than the minimum hold-up, part of the liquid layer can be taken up by the liquid slug to feed its growth.

These minimum and maximum hold-up environments were measured, and proved to be strongly depending on the gas velocity and only little on the liquid velocity. Both hold-up curves are decreasing for increasing gas velocities.

An attempt is made to relate the measured maximum and minimum hold-up environments to the VLW and Slug Stability transition models, respectively. The measurements of maximum hold-up correspond with the values predicted with the VLW-theory for gas velocities $U_{sg} \geq 1$ m/s. For lower gas velocities, the experimentally observed hold-ups are higher than predicted based on the VLW-theory.

The lower limit, the minimum hold-up shows a similar trend as the Slug Stability hold-up, but the values do not agree. The theoretical values are larger than measured in the set-up. Slugs can thus be present for thinner stratified layers than predicted by the Slug Stability theory. The theory calculated the minimum hold-up for the initiation of new slugs. Slugs that are already formed can apparently also survive in situations with a lower hold-up.

A similar deviation is observed when comparing the critical superficial liquid velocities for the transition from stratified to slug flow. Here the values calculated with the slug stability theory are lower than observed in the experiments. The SS-theory predicts the transition from slug to stratified flow, while in the experiments the transition from stratified to slug flow is investigated. This explains the difference in the critical liquid velocities.

The bubbles that can be present inside the liquid slug body can be described as a function of the mixture velocity U_{mix} (6.1). The experimental data are in reasonable agreement with the predicted values, both for the long and the short hydrodynamic slugs. The deviation, the measured values are all lower than predicted, is probably a consequence of the reconstruction technique used when analyzing the data.

The bubbles, usually assumed to be mainly present in the front of the slug and less in the rest of the slug body, can also be accumulated in the tail of the slug, as observed in several experiments. No clear explanation was found why sometimes the bubbles are in the front, and for other situations in the tail of the slugs. The slugs that are formed from a train of smaller slugs can still contain the dividing gas bubbles in the top region. When the slugs continue developing, these bubbles gradually exit from the slug body, and the downstream slugs contain less gas.

The slug initiation process can, with the coarse measure grid of only four measurement locations, not be studied in detail. However, some intermediate stages were observed which are part of the initiation process. The rollwaves present on the gas-liquid interface can grow into pseudo-slugs, which look like ordinary slugs, but do not touch the upper pipe wall.

CHAPTER 7

Model comparison

In this chapter, the results obtained in the previous chapters are discussed, and compared with a theoretical model. Expressions for the slugging frequency and the maximum slug length are derived as function of the input parameters U_{sg} and U_{sl} . For the slug length, a model is derived, which only depends on the hold-up in the stratified layer between the slugs and the flowrates of both phases at the inlet.

7.1 Development of slug length and slug frequency

In section 5.3, relations were derived for the slug length and the slug interval or slug frequency. When one of the flowrates was fixed, there was a power law relation between the slug properties (L , Δt or f_{slug}) and the other varying flowrate.

Combining these relations results in an expression in the form $L \propto U_{sg}^p U_{sl}^q$. This is plotted for the maximum slug length in figure 7.1, which shows an upper limit given by the expression

$$L_{max} = 0.75 U_{sg}^{-1.5} U_{sl}^{-1}. \quad (7.1)$$

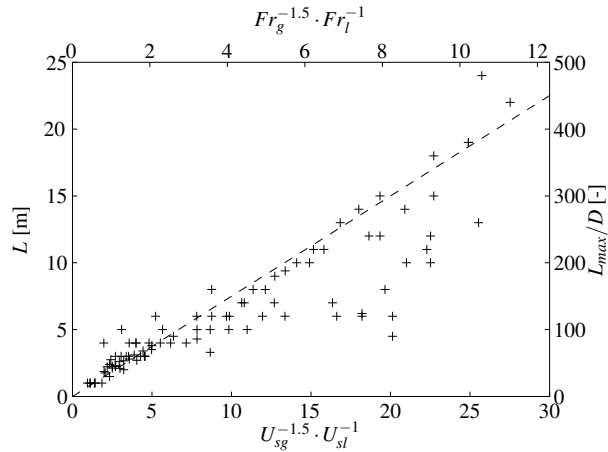


Figure 7.1: The maximum slug length that can occur is limited by $0.75U_{sg}^{-1.5}U_{sl}^{-1}$.

In the short slug region, the trend of the slug length follows the fitted line. For slugs with $L \geq 5$ m ($= 100D$), the line gives an estimation of the upper limit for the slug length that might occur at certain combinations of the gas and liquid flowrates. The points below the line indicate that not all slugs reached maximum length in the measurements. The points indicated are the average of the maximum length of each slug. Since there is a certain spread in the sluglengths, some points are just above the predicted line.

The maximum slug lengths, as earlier presented in figure 5.3 of function of the superficial gas and liquid velocities, can now be related to a single expression $0.75U_{sg}^{-1.5}U_{sl}^{-1}$.

The relation in (7.1) in dimensional form can also be expressed in the dimensionless Froude numbers ($Fr = U/\sqrt{gD}$) for the gas and the liquid velocities

$$\frac{L_{max}}{D} = 36.5Fr_g^{-1.5}Fr_l^{-1} \quad (7.2)$$

which results in the same plot as figure 7.1, but now with the dimensionless quantities L/D and Fr on the axes.

For the slug frequency, power law relations were derived in a similar way in section 5.4. For both the low frequencies, indicated in figure 7.2(a), and the high frequencies (small Δt) as shown in figure 7.2(b), the data can be fitted with

$$f_{slug} = \frac{4}{3} U_{sg} U_{sl}^2. \quad (7.3)$$

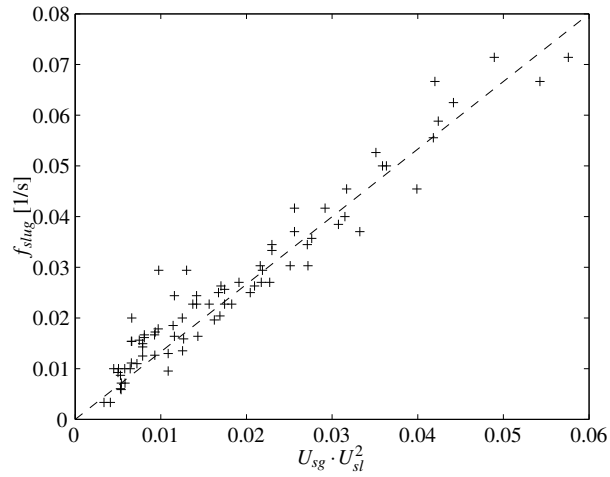
In dimensionless form, this can be written as

$$f_{slug} = f_0 Fr_g Fr_l^2, \quad (7.4)$$

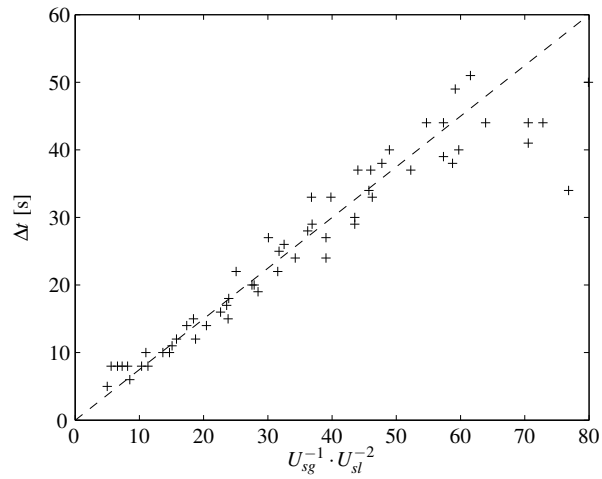
with the Froude number defined as $Fr = U/\sqrt{gD}$ and f_0 a characteristic frequency in the system. Based on the current set of experiments, this frequency equals

$$f_0 = 0.45 \text{ s}^{-1}. \quad (7.5)$$

The points, shown separately for low and high frequencies in figures 7.2(a) and (b), are in good agreement with the fitted line. In both figures, the deviation from the line is larger towards the right. For the low frequency region, $f_{slug} \leq 0.025 \text{ s}^{-1}$, the agreement is shown in the upper image. For higher frequencies $f_{slug} \geq 0.025 \text{ s}^{-1}$ ($\Delta t \leq 40 \text{ s}$), the relation is shown to be in agreement with the experimental data in the lower image. No difference is observed in the behavior of the long and the short hydrodynamic slugs. Both slug types are plotted in the graphs shown in figure 7.2, and a single correlation was obtained covering both regimes.



(a) For low frequencies, the slugging rate is linear with $U_{sg} U_{sl}^2$.



(b) At high slug rates (small Δt), the slug frequency also shows a straight line.

Figure 7.2: Both for the low (a) and high (b) slug frequencies, the slug rate f_{slug} is related to the superficial velocities as $f_{slug} = \frac{4}{3} U_{sg} U_{sl}^2$.

7.2 Simple slug length model

The slug length, as discussed in section 7.1 can also be calculated by using a simple model. From the experiments, the slug length is known for different combinations of superficial gas and superficial liquid velocity. For these velocities, the slug length is predicted using a model for completely developed slug flow.

The mixture velocity U_{mix} is calculated the usual way as

$$U_{mix} = U_{sg} + U_{sl}, \quad (7.6)$$

with U_{sg} and U_{sl} the superficial velocities for gas and liquid respectively.

The slug velocity is, in first approach, chosen constant for all slugs and equal to the mixture velocity (no slip)

$$u_{slug} = U_{mix}, \quad (7.7)$$

which also sets the actual gas velocity of the bubble between the slugs

$$u_g = u_{slug} = U_{mix}, \quad (7.8)$$

assuming that the bubbles are trapped between two subsequent slugs. The train of bubbles and slugs moves as a whole over the stratified layer. In a later stage, slip will be included.

For the region between the slugs, minimum hold-up is assumed. The only experimental input data is the minimum hold-up, which is fitted as a function on the superficial gas velocity, so independent of the liquid velocity. From experimental data, it is observed that the effect of the liquid velocity on the minimum hold-up levels is quite small, so for simplicity of the model, only the dependence on the gas velocity was taken into account. The fit derived from the experimental data is shown in figure 7.3.

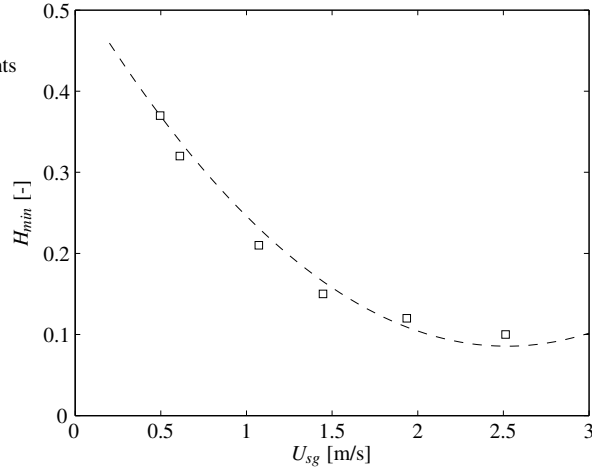


Figure 7.3: Minimum hold-up for different values of U_{sg} . The line is fitted through the experimental datapoints.

Since actual gas velocity ($u_g = u_{slug}$) and hold-up (figure 7.3) are known, the actual liquid velocity in the stratified liquid layer can be calculated by setting the pressure drops (see appendix B) in the gas and liquid phase in the stratified layer equal

$$\left(\frac{dp}{dx}\right)_g = \frac{1}{A_g} (\tau_{wg}P_g + \tau_iP_i), \quad (7.9)$$

$$\left(\frac{dp}{dx}\right)_l = \frac{1}{A_l} (\tau_{wl}P_l - \tau_iP_i), \quad (7.10)$$

with A the area of the phase, P the wetted perimeter and τ the shear stress. The values of τ are calculated as

$$\tau = \frac{1}{2}f\rho u^2 \quad (7.11)$$

with $f = 0.0791Re^{-0.25}$ according to Blasius law and u the velocity of the phase or the velocity difference at the gas-liquid interface. For the interface, the friction factor is multiplied by 5 to correct for the extra friction due to the wavy interface (Hurlburt and Hanratty (2002)).

When the actual liquid velocity in the stratified layer is known, the slug length can be calculated. The total amount of liquid transported by the slug and the liquid layer together should sum up to the total liquid flow given by the superficial liquid velocity.

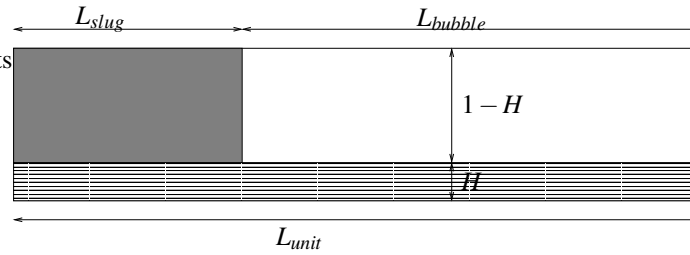


Figure 7.4: Definition of the slug length and the unit length.

From the liquid balance in figure 7.4, an expression for the slug length can be extracted. The slug body is in this figure defined as the part on top of the stratified layer. The stratified liquid layer continues below the slug over the whole unit length.

$$\frac{L_{slug}}{L_{unit}}(1-H)u_{slug} + \frac{L_{unit}}{L_{unit}}H \times u_{liq} = U_{sl}. \quad (7.12)$$

The length of the unit (slug + bubble) is equal to

$$L_{unit} = \frac{U_{mix}}{f_{slug}}. \quad (7.13)$$

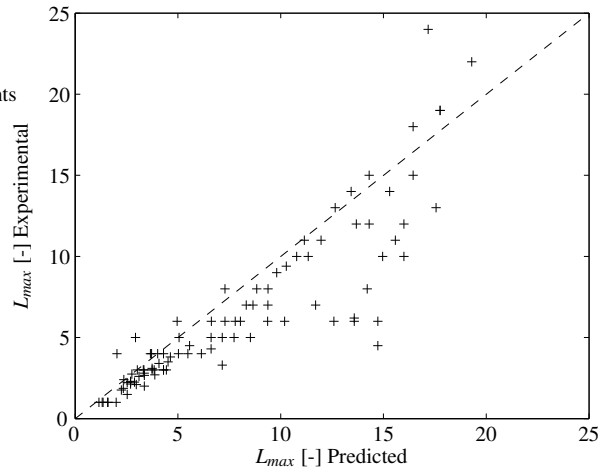
Substitution of (7.13) in (7.12) gives, with the $u_{slug} = U_{mix}$ from (7.7) the expression for the slug length

$$L_{slug} = \frac{1}{f_{slug}} \frac{U_{sl} - H \times u_{liq}}{1-H}. \quad (7.14)$$

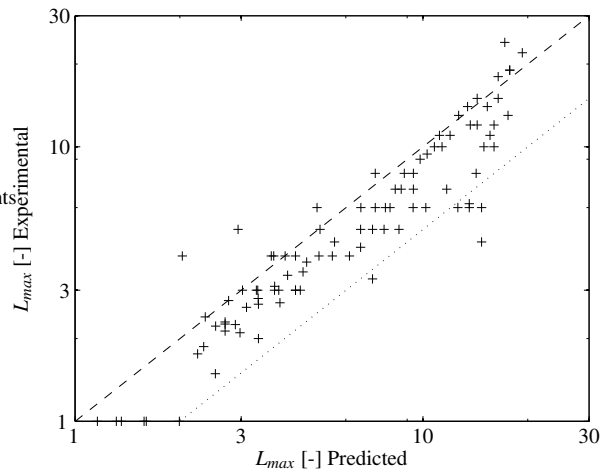
For the frequency, the expression from (7.3) is used

$$f_{slug} = \frac{4}{3} U_{sg} U_{sl}^2. \quad (7.15)$$

When plotting the experimental data versus the predicted values, as shown in figures 7.5(a) and (b), it is clear that the model predicts the maximum boundary quite well, since virtually all experimental points are below the line $y = x$.



(a) Experimental vs prediction on linear scale



(b) Experimental vs prediction on log-scale

Figure 7.5: Comparison between experimental and theoretical results on the maximum slug length. In the upper graph on a linear scale, in the lower graph as log-log. The experimental data are between 0.5 and 1.0 times the predicted value (dotted and dashed lines in plot (b)).

In figure 7.6, the experimental (circles) and predicted (stars) slug lengths are shown with $U_{sg}^{-1.5} \cdot U_{sl}^{-1}$ on the horizontal axis. The model predicts the maximum possible slug length based on (7.14). The dashed line shows the fit on the experimental data. The observed slug

lengths (circles) are smaller than or equal to the maximum predicted length. It is possible that these slugs did not yet reach their fully developed length when being measured in the experiments.

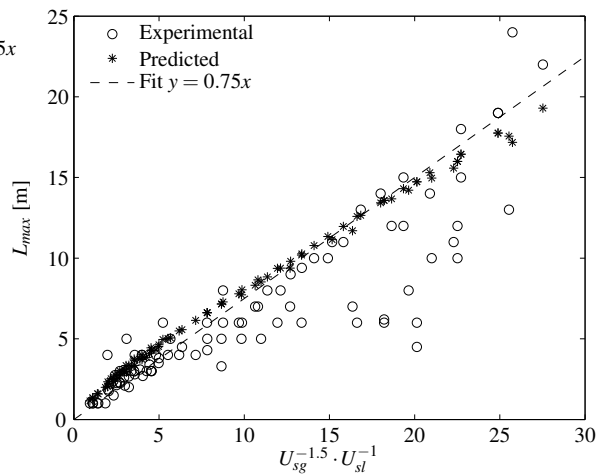


Figure 7.6: The experimental and predicted slug length expressed as function of $U_{sg}^{-1.5} \cdot U_{sl}^{-1}$. The straight line indicates the 0.75 constant from (7.1).

Because the slug frequency expression is derived from experimental data, the model is not pure theoretical any longer. By calculating the value of $L_{slug} \times f_{slug}$, no experimental input is needed. By multiplying the expression for the slug length (7.14) with the slug frequency f_{slug} the theoretical model now reads

$$L_{slug} \times f_{slug} = \frac{U_{sl} - H \times u_{liq}}{1 - H}, \quad (7.16)$$

which can directly be compared with the value of $L \times f$ from the experiments. No experimental fits on the slug length or the slug frequency are used in (7.16). The only experimental input is the relation for the minimum hold-up H which is derived from the experiments. When comparing the experimental results of $L \times f$ with the model predictions, a clear agreement is observed in figure 7.7.

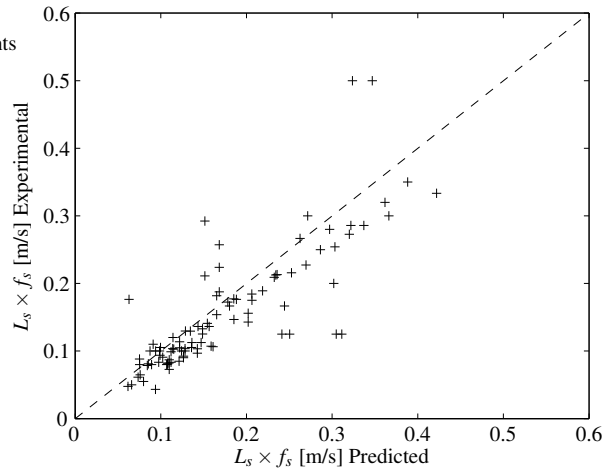


Figure 7.7: The slug length multiplied by the slug frequency shows good agreement with the model predictions. The model is free of any experimental input, and is compared with the raw experimental data.

In the model, the value of the minimum hold-up in the stratified flow between the slugs was chosen equal to the value observed during many experiments. The model is insensitive to the exact value of the chosen minimal hold-up, since the amount of liquid transported through the stratified layer is small compared to the transport by the liquid slug. For two different expressions of the minimum hold-up, the predicted L_{slug} is calculated. The first expression is based on the fitted experimental data, the second is the minimum critical hold-up for slug stability, as shown in figure 7.8. The value obtained for the slug stability approach is the critical minimum hold-up at the slug to stratified transition. For large gas velocities, the difference between the slug stability hold-up and the experimental hold-up is largest (see figure 7.8). This effect can be seen in figure 7.9 for the short slug region, for which the higher slug stability hold-up underpredicts the slug length compared to the experimental hold-up data. For the longer slugs, both approaches predict the same slug length.

For higher gas velocities, the difference between the two approaches (see figure 7.8) becomes larger. Since at higher flowrates, the slugs are shorter, this effect is seen in the deviation in figure 7.9 in the short slug region. The minimum hold-up for the SS was calculated at the critical liquid velocity of slug to stratified transition. For the minimum hold-up as obtained from the experiments, no dependence on the liquid velocity was observed. There is also no difference between the hold-up behind long slugs and the shorter hydrodynamic slugs.

In the first approach, the slug velocity was set equal to the mixture velocity (no-slip). Since

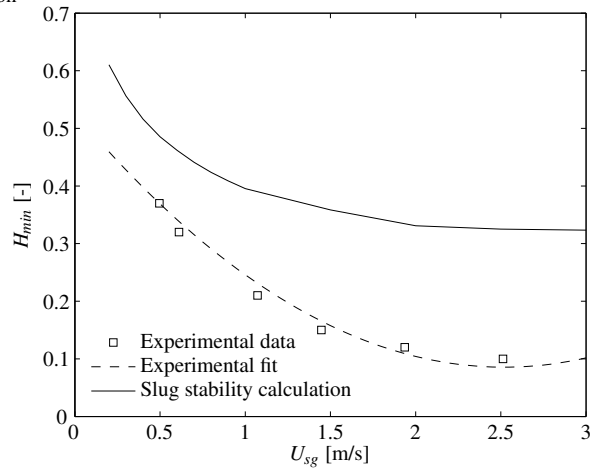


Figure 7.8: Two different relations for the minimum hold-up. The dashed line is from experimental data, the solid line is calculated using the slug stability criteria.

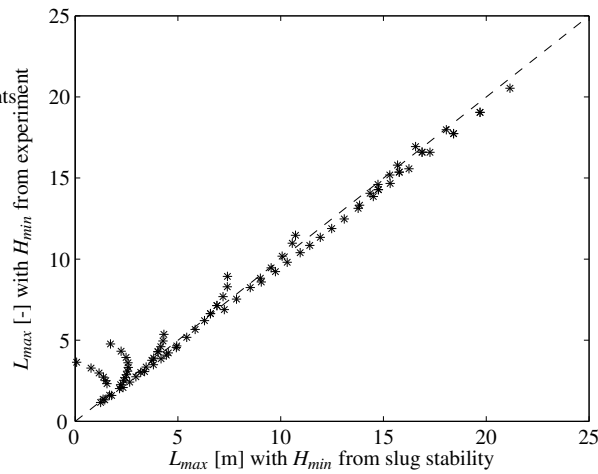


Figure 7.9: The predicted maximum slug length is hardly effected by the choice of H_{min} , as indicated by the almost straight line.

also liquid is transported through the stratified layer between the slugs, the slug velocity is higher than the mixture velocity.

In (7.12), only the liquid phase is considered. When also looking to the gas phase in figure 7.4, this results in

$$U_{sl} = \frac{L_{slug}}{L_{unit}}(1-H)u_{slug} + \frac{L_{unit}}{L_{unit}}H \times u_{liq}, \quad (7.17)$$

$$U_{sg} = \frac{L_{bubble}}{L_{unit}}(1-H)u_{slug}. \quad (7.18)$$

When adding (7.17) and (7.18), the left hand side results in the mixture velocity U_{mix} .

$$U_{mix} = U_{sl} + U_{sg} = \frac{L_{slug} + L_{bubble}}{L_{unit}}(1-H)u_{slug} + \frac{L_{unit}}{L_{unit}}H \times u_{liq} \quad (7.19)$$

$$U_{mix} = (1-H)u_{slug} + H \times u_{liq} \quad (7.20)$$

$$u_{slug} = \frac{1}{1-H} (U_{mix} - H \times u_{liq}) \quad (7.21)$$

$$u_{slug} = \frac{U_{mix}}{1-H} \left(1 - H \times \frac{u_{liq}}{U_{mix}} \right) \quad (7.22)$$

$$u_{slug} = U_{mix} \left(\frac{1 - \beta H}{1 - H} \right) \quad (7.23)$$

with β defined as the ratio between liquid velocity in the stratified layer and the mixture velocity

$$\beta = \frac{u_{liq}}{U_{mix}}. \quad (7.24)$$

In the first approach the slug velocity is calculated with $\beta = 1$, so the liquid is assumed to flow with the mixture velocity (no slip). This expression is only used for estimating the slug velocity, the actual liquid velocity is calculated accurately based on the pressure drop balance between the gas and liquid phase. The other extreme is the $\beta = 0$ situation, in which the stratified flow is at rest, and the virtual tube diameter is smaller, so velocity is increased by a factor $(1-H)^{-1}$.

The influence of the β is shown in the graphs 7.10. For values larger than 15 on the horizontal axis, the slug length tends to a constant length, which trend is captured in the $\beta = 0$ situation shown in the figure 7.10(b). The maximum line corresponds quite well with the $\beta = 1$ case, as shown in the upper figure.

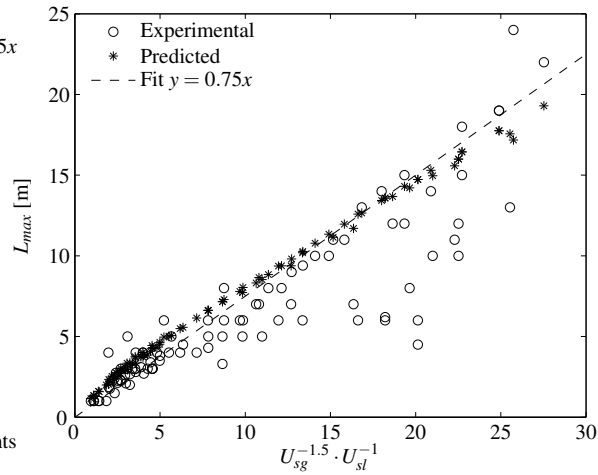
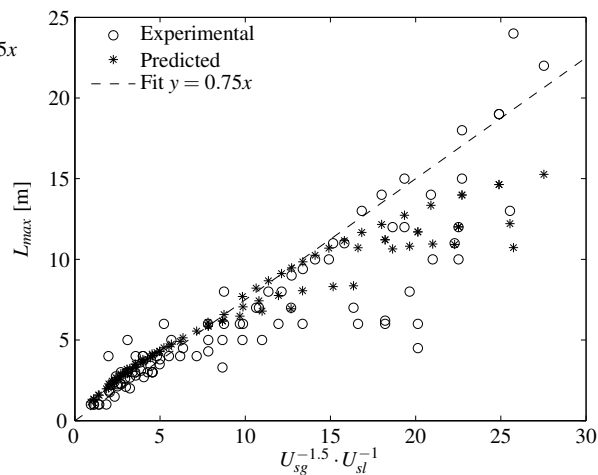
(a) $\beta = 1$ (b) $\beta = 0$

Figure 7.10: In the upper graph the situation for $\beta = 1$ is shown, which corresponds to the first approach with $u_{slug} = U_{mix}$. In the lower graph, the correction for the slower moving liquid layer (for $\beta = 0$ the liquid is stagnant) is applied, which increases the slug velocity.

The difference between figures 7.10(a) and (b) is very small. In the model, the actual liquid velocity is calculated from the pressuredrops in the gas and liquid phase (see page 132). The effect of β is only included in the approximation of the slug velocity.

From the calculations, it is observed that the values for the liquid velocity in the stratified layer between the slugs is much smaller than the velocity of the liquid slugs. For increasing mixture velocity, also the velocity of the liquid in the layer will increase. The ratio

$$\frac{u_{liq}}{U_{mix}} \leq 0.1, \quad (7.25)$$

remains small, which is valid for all the initial values of $0 \leq \beta \leq 1$. The transport capacity of liquid through the stratified layer is thus much smaller than the volume of liquid transported by the slugs.

CHAPTER 8

Conclusions and Recommendations

8.1 Conclusions

Set-up

The experiments in this study are performed in a 137 m long set-up with 2-inch inner diameter. This investigation gives a clear view on the behavior of 2 phase slug flow for air-water systems. With the air and water flowing at velocities ranging from 0.50 – 3.00 m/s and 0.04 – 0.30 m/s respectively, the liquid levels, slug lengths and frequencies and gas contents of the liquid are determined by electrical conductance techniques. With transparent pipes, it is quite easy to do visual observations on the flow, and the different sensors give quantitative results on the slug properties. The sensors, four in total distributed over the whole length of the tube, nicely capture the development of the liquid slugs which are present in the flowline. Because of the coarse measurement grid, slug initiation can not be studied in detail.

After alignment of the tubes, the effect of terrain induced slugging vanished. The slug propagation velocity, equal to the velocity of the slug tail, was constant over all positions. The length of the slugs was constant, or increased monotonically, depending on the flow conditions at the inlet. The effect of the bend halfway is visible as a disturbance on the gas-liquid interface of the stratified layer for the next several meters ($L_{disturbed}/D < 200$) after the turn, but has negligible effect on the development of the liquid slugs when looking to the whole tube length of $L/D = 2700$.

Instruments

During the experiments, several sets of sensors were used. The point-probe system measures the passing slugs, where length and velocity information can be extracted from. The wire-mesh system also measures the liquid level of the stratified layer between the slugs and gives a reasonable estimate on the average gas hold-up inside the liquid slug body and the distribution of the gas bubbles. Although a rough estimate of the grid cell volume was used, the results give a nice qualitative impressions of the gas bubble distribution. Single bubble measurements are not possible with the current reconstruction technique. The total hold-up is calculated over the whole cross-section of the tube, from which qualitative results are obtained.

Additional level indicators are installed in the flowloop, which measure the liquid level in the center of the tube. These sensors, one before and one after each wire-mesh sensor, are electrically connected to the wire-mesh data acquisition, so both the levels and the slug structure are measured simultaneously. These level signals are used for the calculation of the slug front and tail velocities.

The value of the wire-mesh signal, including the level indicators, change in time, which can be related to the temperature increase of the water. This temperature, which is linearly related to the conductivity and thus to the signal, shows an exponential behavior in time. The wire-mesh calibration is therefore also taken also an exponential function in time. The signal can change with 25% over a whole day, but after correction the difference between data and exponential fit is less than 0.65% of the value, which is small compared to the noise in the signal for a fully loaded pipe $\sigma/\mu \leq 1.2\%$.

Slug length and model prediction

The slugs present in the flowloop can grow if the local conditions allow. When sufficient liquid is available in front of the slug, the slug can take up an extra amount, and grow. This process will stop when there is no more liquid available to take up, *e.g.* the slug encounters a minimum hold-up environment. The maximum slug length that can be reached depends on the flowrates of the gas and liquid phases.

As shown in section 7.1, the maximum slug length can be accurately estimated by

$$L_{max} = 0.75U_{sg}^{-1.5}U_{sl}^{-1}, \quad (8.1)$$

or in dimensionless Froude numbers ($Fr = U/\sqrt{gD}$)

$$\frac{L_{max}}{D} = 36.5Fr_g^{-1.5}Fr_l^{-1}, \quad (8.2)$$

which is valid for the whole range from the short hydrodynamic slugs to the long and growing slugs.

With a simple model, only based on the superficial velocities of the gas and the liquid phase at the inlet and the minimum hold-up in the stratified layer between the slugs, the maximum length can also be predicted. These predictions are in good agreement with the results found in the experiments.

For the special situation of the first slugs that initiate from maximum hold-up, the length can be predicted using a simple mass balance on the liquid phase, which shows that all the liquid that is taken from the stratified layer is used to elongate the liquid slug.

Slug frequency

Similar to the slug length, a power law relation was derived for the slug frequency

$$f_{slug} = \frac{4}{3} U_{sg} U_{sl}^2, \quad (8.3)$$

which in dimensionless form equals

$$f_{slug} = 0.45 Fr_g Fr_l^2, \quad (8.4)$$

in which the characteristic frequency $f_0 = 0.45 \text{ s}^{-1}$ results from the fit on the experimental data. This correlation can be used for the short hydrodynamic slugs as well as for the long liquid slugs. In most of the experiments, a single frequency was obtained. For several conditions, multiple characteristic time intervals were observed. When looking at series of subsequent time intervals, some combinations of Δt_i and Δt_{i+1} are possible, while others are not.

For the hydrodynamic slugs, the frequency observed in the experiments is in reasonable agreement with the Gregory and Scott (1969) relation. The long slugs occur with much lower frequencies than would be predicted based on the relation by Gregory and Scott (1969), which clearly only holds for the hydrodynamic slugging region which it was originally derived for.

Hold-up

Based on the ranges of hold-ups that were observed during the experiments, the minimum and maximum hold-up values were determined. The maximum hold-up, for which the stratified flow is still stable and no slugs are initiated, agrees well with the hold-up predicted by the VLW-theory for gas velocities $U_{sg} \geq 1 \text{ m/s}$. The minimum hold-up is lower than the slug

stability line, but has similar shape. The minimum hold-up as measured is for slugs which are already present in the flow, while the SS-theory predicts the minimum hold-up for slug initiation. Apparently, a slug can, when being formed before, also survive in a hold-up environment that is lower than predicted by Slug Stability. The slugs leave a minimum hold-up environment behind. The growth of the slug is related to the amount of liquid that is available and can be taken from the environment in front of the slug. When the hold-up in this environment is higher than minimum, the slug can grow.

Voids

From the slug measurements, the amount of gas inside the slug body can be determined qualitatively. For a more detailed analysis of the size and distribution of the gas bubbles, a better non-linear reconstruction algorithm on the experimental data is required. The large bubbles, present in the top of the slug gradually shrink. The length of the bubbles is constant, but the thickness of the gas layer in the top part of the slug becomes thinner.

Just after initiation, the slug is highly aerated, with most of the gas content near the tail of the slug. While traveling downstream, the gas re-distributes and partially leaves the slug. The highest gas concentration is now observed near the front of the slug.

The average gas void fraction in the liquid slug can be related to the mixture velocity, which shows nice agreements with the relation derived by Hurlburt and Hanratty (2002). The systematic underprediction is due to the used reconstruction technique which was applied on the experimental wire-mesh data.

Waves

Different types of waves have been observed. The waves on the stratified flow, and the roll-waves all move in streamwise direction. From these waves, the (pseudo-)slugs can be initiated. Other small waves were observed in spanwise direction, which are only present in the downslope part of the wavecrest (looking in streamwise direction), while the upslope part of the wave is nearly flat.

8.2 Recommendations

In this study, the behavior of the slugs is investigated for the region where the long slugs exist. The experiments give good qualitative results of the slug length and slug frequency trends. Also for the interior of the slug, qualitative results were obtained for the amount and the spread of gas bubbles. For future research, it is interesting to have a closer, and more quantitative look at

- Several slugs had already reached their final length before being measured by the first sensor, and the length remained constant over all subsequent measurement locations. Redistribute the sensors, so that also the initiation phase and the initial hold-up are known for these kind of slugs.
- In the experiments, the tail velocity of the slugs was observed to be constant, while the front velocity changed with position, which can also be related to the growth rate. So far, it is not clear why the front velocity changes, and how this can be related to the length of the slug, the growth rate and the hold-up the slug encounters at the front. Investigation will give more insight in the relevant parameters which are responsible for the growth and the maximum length that can be reached before the front velocity has decreased and equals the tail velocity.
- Characteristic frequencies were observed, which are constant per experiment, but change for different inlet conditions. A general expression was derived which includes gas and liquid velocities. A further quantitative investigation on those frequencies is recommended, and also the pattern of slugs with multiple frequencies. In the upward flow experiment, several fixed time intervals were observed, which appeared in an alternating manner. Several subsequent combinations of these intervals were possible, others were not.
- In this research, the focus was on the development of the long slugs. An interesting question is whether there is a difference between the mechanisms initiating short hydrodynamic slugs and the long slugs. For that, the stratified flow conditions just before the transition to slug flow should be investigated.
- Besides the experiments in 2" horizontal facility, the scaling behavior could be tested with experiments in the 1" tube. Another parameter that can be varied is the angle to investigate the effect of upward and downward pipe geometries.

APPENDIX A

The length over which slug development can be measured

Slugs can travel through the set-up at different velocities. When the slug velocity is high, the time the slug is in the system is only short. For a fast moving, and growing slug, the change in length is measurable with the same accuracy as for a slow moving slug. This only holds for situations where both slugs have the same growth rate, so the ratio of front and tail velocity is the same. When only looking at the velocity difference between the front and tail velocity, the effective measurement length is shortened for fast moving slugs, *i.e.* only a small part of the growth can be measured.

Assume a slug moving from point A to B. The length in point A equals L_A , and the slug moves with velocities v_f at the front and v_t at the tail, both constant in time. The slug propagation velocity is chosen to be equal to tail velocity v_t . The time needed for a slug to move from A to B equals

$$\Delta t = \frac{\Delta x}{v_t} \quad (\text{A.1})$$

with $\Delta x = x_B - x_A$.

The length at position B is calculated as :

$$\begin{aligned} L_B &= L_A + \Delta t(v_f - v_t) \\ &= L_A + \Delta t \left(\frac{v_f}{v_t} - 1 \right) v_t \\ &= L_A + \left(\frac{v_f}{v_t} - 1 \right) \Delta x \end{aligned} \quad (\text{A.2})$$

The growth rate dL/dx can be expressed as

$$\frac{dL}{dx} = \frac{L_B - L_A}{\Delta x} = \frac{v_f}{v_t} - 1 \quad (\text{A.3})$$

which only depends on the velocity ratio in the segment between A and B.

Assume 2 different slugs with velocities v_1 and $v_5 = 5v_1$, both with the same velocity ratio v_f/v_t and equal initial length L_A

$$\Delta t_1 = \frac{\Delta x}{v_{1t}} \quad (\text{A.4a})$$

$$\begin{aligned} \Delta t_5 &= \frac{\Delta x}{v_{5t}} \quad (\text{A.4b}) \\ &= \frac{\Delta x}{5v_{1t}} \\ &= \frac{1}{5}\Delta t_1 \end{aligned}$$

For the length L_B at position B, the following expressions can be found :

$$\begin{aligned} L_{B1} &= L_A + \Delta t_1(v_{1f} - v_{1t}) \quad (\text{A.5a}) \\ &= L_A + \Delta t_1 \left(\frac{v_{1f}}{v_{1t}} - 1 \right) v_{1t} \end{aligned}$$

$$\begin{aligned} &= L_A + \left(\frac{v_{f1}}{v_{1t}} - 1 \right) \Delta t_1 v_{1t} \\ L_{B5} &= L_A + \Delta t_5(v_{5f} - v_{5t}) \quad (\text{A.5b}) \\ &= L_A + \Delta t_5 \left(\frac{v_{5f}}{v_{5t}} - 1 \right) v_{5t} \\ &= L_A + \left(\frac{v_{5f}}{v_{5t}} - 1 \right) \Delta t_5 v_{5t} \end{aligned}$$

Since

$$\Delta t_5 v_{5t} = \frac{1}{5} \Delta t_1 5v_{1t} = \Delta t_1 v_{1t} \quad (\text{A.6})$$

the expressions (A.5a) and (A.5b) give the same length at position B. The length of the slug at B is the same for both velocities, when the ratio is the same for both cases. No scaling of the position with the actual slug velocity is needed.

For the situation of a constant velocity difference, there is an effect that similar growth is only observed when the length of the set-up is scaled with velocity

APPENDIX B

Friction factors

In stratified and stratified wavy flow, there is an interaction force on the gas-liquid interface. Because of the difference in gas and liquid velocity, there will be a shear stress acting on the interface, as indicated in figure B.1. Based on the measured pressure drop over a pipe segment, this shear stress can be calculated. For a stationary situation, there is a balance between the driving force due to the pressure drop and the shear forces working in opposite direction. The shear represents the friction effect between two surfaces, $F = \tau A$, where the surface can be the wall or the gas-liquid interface.

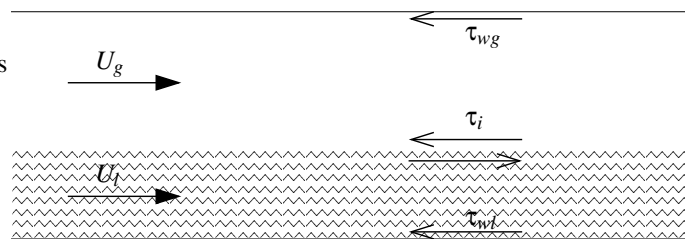


Figure B.1: *The forces acting on the gas and liquid phase for stratified flow.*

B.1 A simple case, friction at a smooth wall

When a fluid is flowing through a pipe (single phase), it will experience friction with the wall, denoted by wall shear stress τ . The value can be calculated from the properties of the fluid and flow quantities by

$$\tau = \frac{1}{2} f \rho u^2, \quad (\text{B.1})$$

with ρ the fluid density and u the fluid velocity. The value of the friction factor f depends on the type of flow (laminar or turbulent). For laminar flow the friction factor for a round tube is expressed by

$$f = \frac{16}{Re}, \quad (\text{B.2})$$

with Re the Reynolds number of the flow, defined as

$$Re = \frac{\rho U D_H}{\eta} = \frac{U D_H}{\nu}. \quad (\text{B.3})$$

In this expression, D_H is the (hydraulic) diameter of the tube, U the mean velocity in the tube and ν the kinematic viscosity of the fluid. The hydraulic diameter equals

$$D_H = 4 \frac{A}{P}, \quad (\text{B.4})$$

with A and P defined as indicated in figure B.2. When the flow is turbulent, the Blasius expression is used which equals

$$f = 0.0791 Re^{-0.25}. \quad (\text{B.5})$$

Both expressions for f assume a smooth wall. The Churchill relation, which is valid for all Reynolds number, also takes the effect of wall roughness into account, resulting in the following expression

$$f = 2 \left[\left(\frac{8}{Re} \right)^{12} + \left(\frac{1}{a+b} \right)^{3/2} \right]^{1/12}, \quad (\text{B.6})$$

with the coefficients a and b defined as

$$a = \left[2.547 \log \left(\frac{7}{Re} \right)^{0.9} + 0.27 \frac{\varepsilon}{D} \right]^{0.16}, \quad (\text{B.7})$$

$$b = \left[\frac{37530}{Re} \right]^{16}, \quad (\text{B.8})$$

with ε indicating the wall roughness.

B.2 Pressure drop and interfacial friction

The friction with the wall will give rise to a pressure drop over the pipe element.

For a stratified(-wavy) flow, the pressure drop in the gas-phase is expressed by

$$\left(\frac{dp}{dx}\right)_g = \frac{1}{A_g} (\tau_{wg}P_g + \tau_i P_i), \quad (\text{B.9})$$

with A_g the gas cross section area, P_g the length of the gas-wall interface and P_i the width of the gas-liquid interface as illustrated in figure B.2. The values τ_{wg} and τ_i indicate the wall shear stress and interface shear stress respectively.

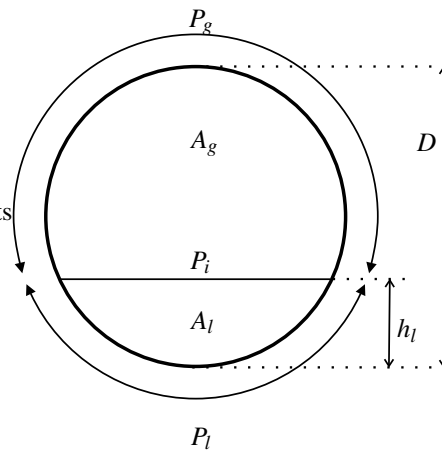


Figure B.2: Definition of lengths and surfaces in tube cross section. A indicates area, P the wall or gas-liquid interfaces.

The total pressure drop (B.9) is build from 2 separate contributions. The first is from the dry top wall of the tube. Using the Blasius equation, the friction factor (B.5) can be calculated based on the actual gas velocity. Combining with (B.1) gives the value of the wall shear stress. From the liquid level, the contact area between the gas and the tube P_g can be calculated, giving the first part of (B.9).

The second part of (B.9) can be calculated in a similar way. Since the contact interface between the gas and liquid phase is usually not a smooth as a solid wall, the roughness will result in a larger value of the friction factor f_i for the interface. In general, the friction factor is calculated with Blasius assuming a smooth wall, and corrected by a factor f_i/f_{wg} for the non-smoothness. For wavy flow, a correctionfactor of $f_i/f_{wg} = 5$ shows good agreements with the experiments by Hurlburt and Hanratty (2002)

APPENDIX C

Overview of the detector positions

| Sensor | | Position | Note |
|-------------|-----|----------|---------|
| Pointprobes | 1a | 28.55 m | |
| | 1b | 29.25 m | |
| Pressure | dp+ | 35.40 m | dx=0.7m |
| | dp- | 36.10 m | |
| Wiremesh | L1a | 38.00 m | |
| | WM1 | 38.20 m | |
| | L1b | 38.41 m | |
| Pointprobes | 2a | 42.40 m | |
| | 2b | 43.10 m | |
| Wiremesh | L2a | 55.40 m | |
| | WM2 | 55.60 m | |
| | L2b | 55.81 m | |

Table C.1: Positions of the detectors installed in the system. All distances are measured from the inlet of the set-up.

| Sensor | | Position | Note |
|-------------|-----|----------|----------|
| Pointprobes | 3a | 61.90 m | |
| | 3b | 62.60 m | |
| Pointprobe | 4a | 73.55 m | |
| | 4b | 74.25 m | |
| Pointprobe | 5a | 93.10 m | |
| | 5b | 93.80 m | |
| Pressure | PA | 100.47 m | dx=6.83m |
| Wiremesh | L3a | 104.58 m | |
| | WM3 | 104.78 m | |
| | L3b | 105.99 m | |
| Pressure | PB | 107.30 m | dx=6.83m |
| Pointprobe | 6a | 106.95 m | |
| | 6b | 107.65 m | |
| Pointprobe | 7a | 119.96 m | |
| | 7b | 120.66 m | |
| Wiremesh | L4a | 124.60 m | |
| | WM4 | 124.80 m | |
| | L4b | 125.01 m | |
| Pointprobe | 8a | 131.90 m | |
| | 8b | 132.60 m | |

Table C.2: Positions of the detectors installed in the system. All distances are measured from the inlet of the set-up (continued).

APPENDIX D

Calibration data

During the experiments, the flowrates of the gas and liquid phases are measured with a set of rotameters. In this appendix, the calibration data is shown.

D.1 Liquid flowmeters

The massflowrate of the water ϕ_m is determined by measuring the mass m of water that leaves the pump in a time Δt . The volumetric flowrate can now be determined by

$$\phi_v = \frac{\phi_m}{\rho_l} \quad (\text{D.1})$$

The superficial liquid velocity equals

$$U_{sl} = \frac{\phi_v}{A} = \frac{\phi_m}{\rho_l \frac{1}{4} \pi D^2} \quad (\text{D.2})$$

For the rotameters, a linear relation was assumed between the scale and the flowrate, which is linear related to the superficial liquid velocity.

The calibration experiments are fitted to the relation

$$U_{sl} = C_1 S + C_2, \quad (\text{D.3})$$

with S the value as read on the rotameter and $C_{1,2}$ the fitting parameters.

| Rotameter | C_1 | C_2 |
|-----------------|---------------------------------|---------------------------------|
| 1 (R-13M-20-3N) | $(1.37 \pm 0.31) \cdot 10^{-1}$ | $(2.06 \pm 1.01) \cdot 10^{-2}$ |
| 2 (R-12M-25-4) | $(1.15 \pm 0.01) \cdot 10^{-3}$ | $(5.40 \pm 0.05) \cdot 10^{-3}$ |
| 3 (R-10M-25-1) | $(5.17 \pm 0.09) \cdot 10^{-4}$ | $(2.47 \pm 0.08) \cdot 10^{-3}$ |
| 4 (R-8M-24-4) | $(1.24 \pm 0.07) \cdot 10^{-4}$ | $(8.32 \pm 0.32) \cdot 10^{-4}$ |

Table D.1: Results of calibrations for the four liquid rotameters.

D.2 Gas flowmeters

For the gas flow meters, a also a linear relation was fitted. In this case, the volumetric flowrate ϕ_v was measured using a calibrated gas flowmeter.

The values for $C_{1,2}$ in the relation

$$U_{sg} = C_1 S + C_2, \quad (\text{D.4})$$

are shown in table D.2.

| Rotameter | C_1 | C_2 |
|----------------|---------------------------------|----------------------------------|
| 1 (R-10M-25-3) | $(6.48 \pm 0.02) \cdot 10^{-2}$ | $(-4.42 \pm 0.86) \cdot 10^{-2}$ |
| 2 (R-12M-25-4) | $(3.29 \pm 0.02) \cdot 10^{-2}$ | $(2.01 \pm 0.21) \cdot 10^{-1}$ |
| 3 (R-8M-25-2) | $(4.18 \pm 0.01) \cdot 10^{-3}$ | $(4.78 \pm 0.11) \cdot 10^{-2}$ |
| Electronic | $(7.01 \pm 0.12) \cdot 10^{-1}$ | $(6.22 \pm 0.38) \cdot 10^{-2}$ |

Table D.2: Results of calibrations for the three gas rotameters.

For the electronic gas flow meter, the input S is the voltage in [V].

APPENDIX E

Wire mesh electronics : details and schemes

In this appendix, the technical details on the wire-mesh system are discussed.

E.1 Electronics device for measurement control and data logging

The electronics are combined in a central unit, as shown in figure E.1. The DSP modules produces the pulses for the transmitting wires. The signals collected by the receiving wires are send to the ADC modules, which convert the analogue signal to a digital signal. These digital signals are send to the computer via Ethernet (ETH) and stored on a local hard drive. There is also a local memory available in the central unit, which acts as a FIFO buffer for the Ethernet connection. For small measurements, the whole measurement can be stored in the local memory, and transferred to the computer afterwards. Since most of the measurements were longer than 87 s (which is the maximum measurement time in the local memory at a framerate of $f = 1$ kHz), the system was used in continuous mode and data was directly send to the computer during the measurement.

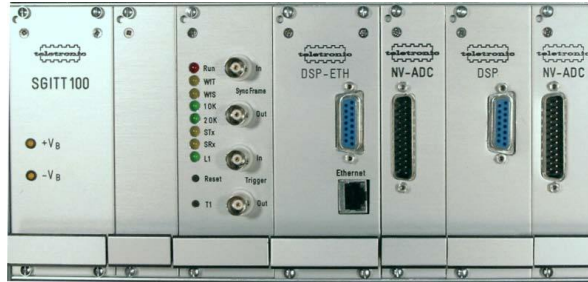


Figure E.1: The central unit of the wire-mesh system. The right four modules perform the measurements. The DSP modules control the transmitting side of the wire-mesh. The ADC modules collect the data from the receiving wires. All modules have 16 channels each. From *Manual for Wire-Mesh-System 32x32 V 1.0.5 (2004)*.

The pulse on the transmitting wire and the signal amplification after the receiver wire are shown in figure E.2. The three amplifiers indicated in figure E.2(b) can be set individually with the control software. The values of the individual points in the matrix can be read out on the screen of the computer.

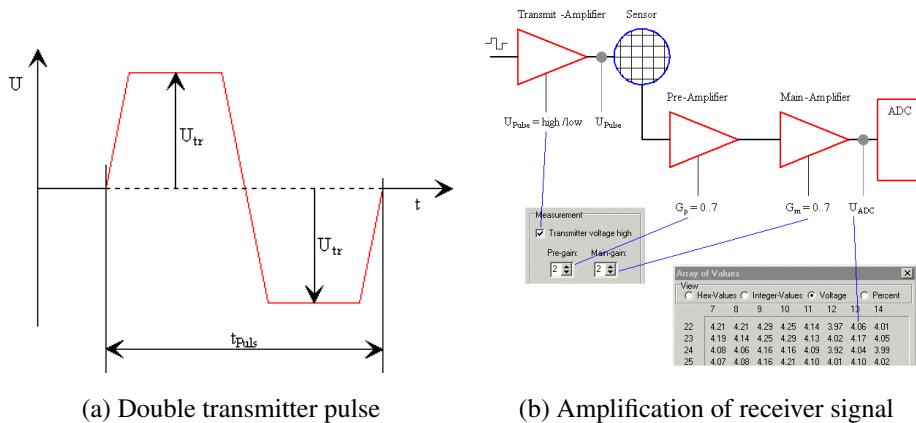


Figure E.2: The pulse send by the DSP to the transmitter wire (a) has a positive and negative part, to prevent any DC-component in the signal. The pulse is send to the mesh (b) and, after amplification, read by the ADC. From *Manual for Wire-Mesh-System 32x32 V 1.0.5 (2004)*.

E.2 Measurement principle

The wire-mesh measures the local electrical conductivity of the fluid that is in the sensors. Therefore, an electric pulse is sent to one of the horizontal transmitting wires, as indicated in figure E.3 for a simple 4x4 sensor. In the current study 4 sensors were used with 16x16 points each, working in a similar way.

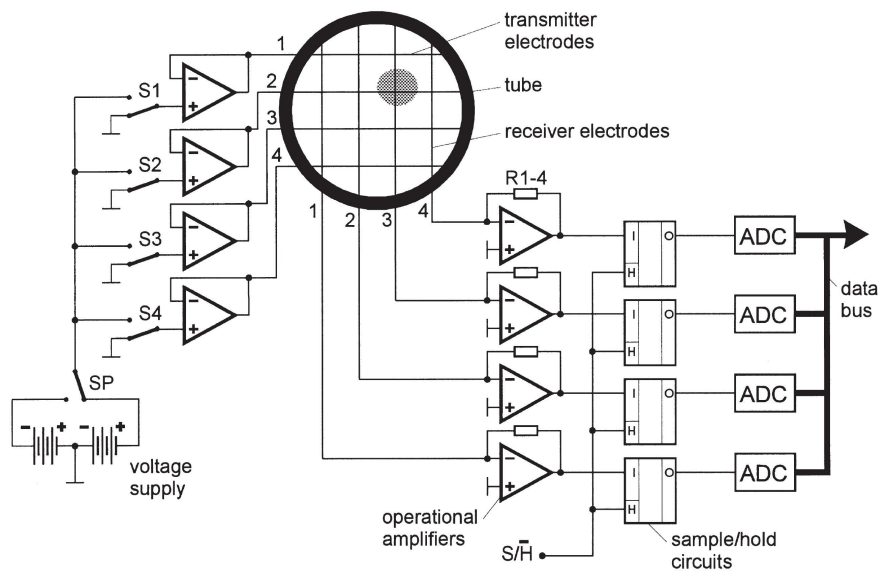


Figure E.3: The electronic structure behind the wire-mesh system. The sensor, here for simplicity only containing 4x4 wires, is controlled by the voltage supply and the switches SW and S1..S4. On the other side, the signals from the receiving lines are amplified and stored in a sample-hold circuit, and later converted to a digital signal for the computer by the ADC. From Prasser et al. (1998)

With switch SW a positive-negative pulse (see figure E.2(a)) is created. This pulse is set on one of the horizontal wires by closing one of the switches S1..S4 as shown in figure E.4. In the figure, one whole cycle of measuring is shown, comparable to one single frame.

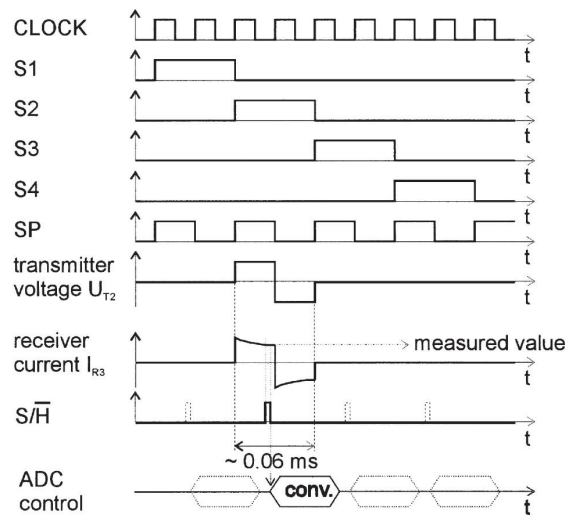


Figure E.4: The timing signals of the wire-mesh, shown for the 4x4 sensor of figure E.3. The pulses are set to the different wires by switches S1..S4 one after each other. The signals of the receiving wires are stored at the same moment for all wires, and converted by the ADC later on. From Prasser et al. (1998).

The pulse, U_{T2} in figure E.4, is set to wire T2 by closing switch S2. This results in a signal in all the crossing receiver lines, depending on the conductivity of the surrounding fluid. For the third line, this signal is plotted as I_{R3} , which is sampled just before the flip in the pulse. This is also done for all other receiving lines at the same moment, and data is stored in separate sample-hold circuits. The next step is to read out the values from the sample-hold circuits by the ADC. In this timestep, all receiver lines crossing transmitter line T2 are processed. This is also done for the other wires T1..T4 by closing the switches S1..S4. After the whole cycle, a single frame is recorded, and the 16 local conductivity values of the 4x4 matrix are known.

In the used set-up, sensors with 16x16 wires are mounted. For each 4 lines there is one ADC-chip, so in each timestep the ADC reads and converts the signals of 4 separate sample-hold circuits. The ADC-module, with 16 channels thus contains 4 separate ADC-chips to process the 16 channels. Since all channels are sampled at the same moment in time, there are 16 separate sample-hold circuits, one for each channel.

With the current central unit, sample frequencies up to 5 kHz are possible. That means that in each $\Delta t = 0.2$ ms, a whole frame is sampled. Within this single frame, 32 individual transmitter pulses are given (2 DSP modules with 16 channels each), which means that the pulses are much shorter than the $\Delta t = 0.2$ ms based on the framerate. The length of a single pulse equals $\delta t = 5.3 \mu s$ for the 5 kHz sampling rate. Within this $\delta t = 5.3 \mu s$, the 16 sample-hold circuits are processed by the 4 ADC-chips, leaving only less than $1.5 \mu s$ for a single ADC-conversion. For lower frequencies, the pulses are longer. For most of the experiments a framerate of 1 kHz is used which corresponds to a pulse length of $\delta t = 20.3 \mu s$.

The central box, with two DSP modules (16 channels each) and two ADC modules (16 channels each) is able to measure a 32x32 array of signals in each frame. This large 32x32 array is divided into 4 separate 16x16 sensors, which each occupy a quadrant in the larger 32x32 matrix. The connection of the 4 sensors to the central unit is shown in figure E.5. Some signals are combined with adders or split by driver modules.

Each sensor has its own set of amplifiers, as shown previously in figure E.2(b). The transmit amplifier and the pre amplifier are connected directly to the sensor, as shown in figure E.5. The main amplifier is in the central unit just before the analogue to digital conversion (ADC). All three amplifiers are software controlled. The extra power modules installed are to increase signal strength (not signal value) since the long cables used might suffer from signal strength losses.

The drivers and adders are included because there are 4 sensors and only two DSP modules and two ADC modules. The pulse train from the DSP modules goes from DSP1 row 1..16 to DSP2 row 17..32, so the whole vertical axis of the 32x32 matrix from top to bottom. Sensors 2 and 4 are controlled by DSP1 and after that DSP2 activates the wires in sensors 1 and 3.

Within each pulse of a DSP, the whole horizontal axis is read by the ADC modules ADC1 (column 1..16) and ADC2 (column 17..32) from left to right. Since the DSP modules are never active at the same moment in time, there is always only 1 side of the adder modules receiving a signal which is send to the ADC. The control software determines which DSP is active at the moment, and so whether the signal measured by ADC1 comes from sensor 2 (DSP1 active) or sensor 1 (DSP2 active). The same holds for ADC2 which reads sensor 4 when DSP1 is active and sensor 3 for an active DSP2.

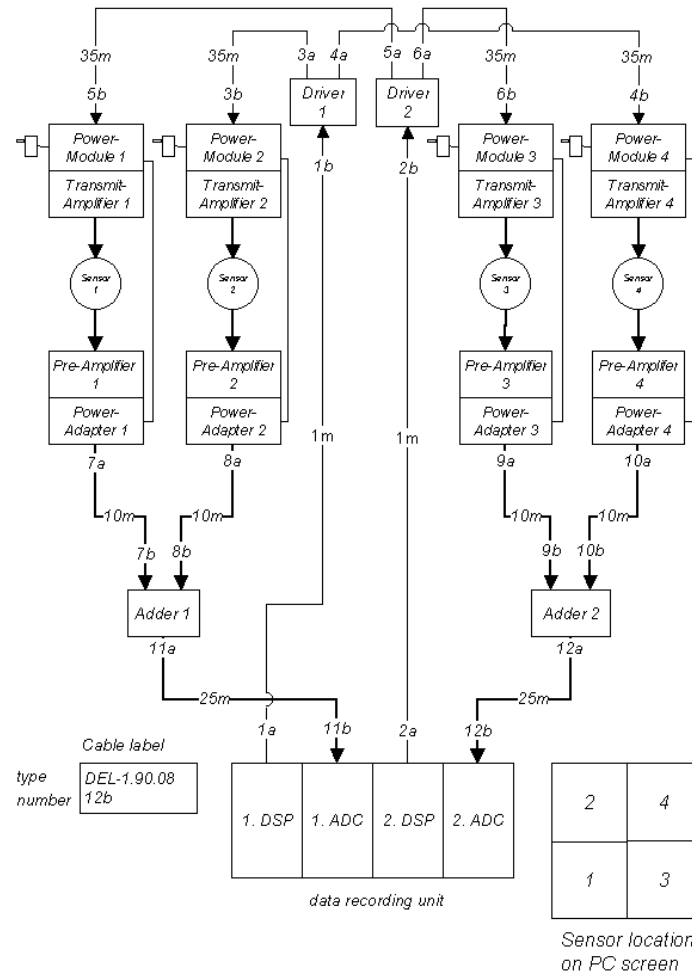


Figure E.5: Wiring scheme of the 4 16x16 wire-mesh sensors. The 32x32 image on the screen, shown in the lower right corner, is divided in 4 parts, each corresponding to a single 16x16 sensor. From Manual for Wire-Mesh-System 32x32 V 1.0.5 (2004).

E.3 Measurement data, different data formats and conversion

The standard file format for the wire-mesh data files is 12 bits. These 12 bits measurement values are packed in long integer words of 32 bits, as shown in table E.1. The values along a single wire (32 values of 12 bits each) are packed in 12 following 32 bits words.

File format of the measured data in packed form:

| File Offset | Bits 31..20 | | Bits 19..16 | | Bits 15..04 | | Bits 03..00 | |
|-------------------|-------------|----------|-------------|----------|-------------|----------|-------------|----------|
| <i>First row</i> | | | | | | | | |
| 0 | Col 10 | [11..00] | Col 09 | [03..00] | Col 02 | [11..00] | Col 01 | [03..00] |
| 1 | Col 11 | [11..00] | Col 09 | [07..04] | Col 03 | [11..00] | Col 01 | [07..04] |
| 2 | Col 12 | [11..00] | Col 09 | [11..08] | Col 04 | [11..00] | Col 01 | [11..08] |
| 3 | Col 14 | [11..00] | Col 13 | [03..00] | Col 06 | [11..00] | Col 05 | [03..00] |
| 4 | Col 15 | [11..00] | Col 13 | [07..04] | Col 07 | [11..00] | Col 05 | [07..04] |
| 5 | Col 16 | [11..00] | Col 13 | [11..08] | Col 08 | [11..00] | Col 05 | [11..08] |
| 6 | Col 26 | [11..00] | Col 25 | [03..00] | Col 18 | [11..00] | Col 17 | [03..00] |
| 7 | Col 27 | [11..00] | Col 25 | [07..04] | Col 19 | [11..00] | Col 17 | [07..04] |
| 8 | Col 28 | [11..00] | Col 25 | [11..08] | Col 20 | [11..00] | Col 17 | [11..08] |
| 9 | Col 30 | [11..00] | Col 29 | [03..00] | Col 22 | [11..00] | Col 21 | [03..00] |
| 10 | Col 31 | [11..00] | Col 29 | [07..04] | Col 23 | [11..00] | Col 21 | [07..04] |
| 11 | Col 32 | [11..00] | Col 29 | [11..08] | Col 24 | [11..00] | Col 21 | [11..08] |
| <i>Second row</i> | | | | | | | | |
| 12 | Col 10 | [11..00] | Col 09 | [03..00] | Col 02 | [11..00] | Col 01 | [03..00] |
| 13 | Col 11 | [11..00] | Col 09 | [07..04] | Col 03 | [11..00] | Col 01 | [07..04] |
| 14 | Col 12 | [11..00] | Col 09 | [11..08] | Col 04 | [11..00] | Col 01 | [11..08] |
| 15 | Col 14 | [11..00] | Col 13 | [03..00] | Col 06 | [11..00] | Col 05 | [03..00] |

Table E.1: The 12 bits wire-mesh data stored in 32 bits longint words.

The values of the 1st, 5th, 9th, 13th, 17th, 21st, 25th and 29th column are shared into three parts each 4 bits long. The part with the lower 4 bits [03..00] is stored first. The second part with the middle 4 bits [07..04] is stored in the following 32 bits word in the file and the part with the highest 4 bits [11..08] is written into the 3rd 32 bits word.

The values of the columns 9, 13, 25 and 29 are split in a similar way, but now shifted 16 bits to left.

The values of the columns 2, 3, 4, 6, 7, 8, 18, 19, 20, 22, 23 and 24 are not split and stored as 12 bits values which are shifted 4 bits to left. These values are on the [15..04] positions of the 32 bits longint word. The values of the columns 10, 11, 12, 14, 15, 16, 26, 27, 28, 30, 31 and 32 are stored as 12 bits values, but now shifted 20 bits to the left, resulting in positions [31..20] of the 32 bits longint word.

The data can also be exported to a 16 bits file format, which is shown in table E.2. In this case, each 12 bits value of a single measurement point is stored in its own 16 bit word. The value is stored in the first 12 bits [11..00], the 4 highest bits [15..12] are set equal to 0.

| File offset | 16 Bit word | | |
|-------------|-------------|--------|---------|
| 0 | Column 1 | Row 1 | Frame 1 |
| 1 | Column 2 | Row 1 | Frame 1 |
| 2 | Column 3 | Row 1 | Frame 1 |
| 31 | Column 32 | Row 1 | Frame 1 |
| 32 | Column 1 | Row 2 | Frame 1 |
| 33 | Column 2 | Row 2 | Frame 1 |
| 1023 | Column 32 | Row 32 | Frame 1 |
| 1024 | Column 1 | Row 1 | Frame 2 |
| 1025 | Column 2 | Row 1 | Frame 2 |

Table E.2: *The 16 bits wire-mesh data stored in 16 bits words.*

References

- Al-Sarkhi, A. & Hanratty, T.J. Effect of drag-reducing polymers on annular gas-liquid flow in a horizontal pipe. *Int. J. Multiphase Flow*, 27(7):1151–1162, 2001.
- Andritsos, N. & Hanratty, T.J. Influence of interfacial waves in stratified gas-liquid flows. *AIChE J.*, 33(3):444–454, 1987.
- Barnea, D. & Taitel, Y. A model for slug length distribution in gas-liquid slug flow. *Int. J. Multiphase Flow*, 19(5):829–838, 1993.
- Bendiksen, K.H. An experimental investigation of the motion of the long bubbles in inclined tubes. *Int. J. Multiphase Flow*, 10(4):467–483, 1984.
- Bendiksen, K.H. & Malnes, D. Experimental data on inlet and outlet effects on the transition from stratified to slug flow in horizontal tubes. *Int. J. Multiphase Flow*, 13(1):131–135, 1987.
- Bonizzi, M. & Issa, R.I. A model for simulating gas bubble entrainment in two-phase horizontal flow. *Int. J. Multiphase Flow*, 29:1685–1717, 2003.
- Cook, M. & Behnia, M. Slug length prediction in near horizontal gas-liquid intermittent flow. *Chem. Eng. Sci.*, 55:2009–2018, 2000.
- De Henau, V. & Raithby, G.D. A study of terrain-induced slugging in two-phase flow pipelines. *Int. J. Multiphase Flow*, 21(3):365–379, 1995.
- Dukler, A.E. & Hubbard, M.G. A model for gas-liquid slug flow in horizontal and near horizontal tubes. *Ind. Eng. Chem. Fundam.*, 14(4):337–347, 1975.
- Dukler, A.E., Maron, D.M. & Brauner, N. A physical model for predicting the minimum stable slug length. *Chem. Eng. Sci.*, 20(8):1379–1385, 1984.
- Fan, Z., Lusseyran, F. & Hanratty, T.J. Initiation of slugs in horizontal gas-liquid flows. *AIChE J.*, 39(3):1741–1753, 1993.

- Gregory, G.A. & Scott, D.S. Correlation of liquid slug velocity and frequency in horizontal cocurrent gas-liquid flow. *AIChE J.*, 15(6):933–935, 1969.
- Greskovich, E.J. & Shrier, A.L. Slug frequency in horizontal gas-liquid slug flow. *Ind. Eng. Chem. Proc. Des. Dev.*, 11(2):317–318, 1972.
- Heywood, N.I. & Richardson, J.F. Slug flow in air-water mixtures in a horizontal pipe : Determination of the liquid holdup using γ -ray absorption. *Chem. Eng. Sci.*, 34(1):17–30, 1979.
- Hoogendoorn, C.J. Gas-liquid flow in horizontal pipes. *Chem. Eng. Sci.*, 40:205, 1957.
- Hurlburt, E.T. & Hanratty, T.J. Prediction of the transition from stratified to slug and plug flow for long pipes. *Int. J. Multiphase Flow*, 28(5):707–729, 2002.
- Kadri, U., Mudde, R.F. & Oliemans, R.V.A. On the development of waves into roll waves and slugs in gas-liquid horizontal pipe flow. *Proc. ICMF Conf. Leipzig, Germany*, 2007a.
- Kadri, U., Mudde, R.F. & Oliemans, R.V.A. On the prediction of the transition from stratified flow to waves and slugs flow in horizontal pipes. *BHRA Conf. Edinburgh, Scotland*, pages 65–78, 2007b.
- Kordyban, E. & Ranov, T. Mechanism of slug formation in horizontal two-phase flow. *J. Basic Eng.*, 92(4):857–864, 1970.
- Kristiansen, O. Experiments on the transition from stratified to slug flow in multiphase pipe flow. PhD thesis, Norwegian University of Science and Technology, 2004.
- Lin, P.Y. & Hanratty, T.J. Prediction of the initiation of slugs with linear stability theory. *Int. J. Multiphase Flow*, 12(1):79–98, 1986.
- Lin, P.Y. & Hanratty, T.J. Effect of pipe diameter on flow patterns for air-water flow in horizontal pipes. *Int. J. Multiphase Flow*, 13(4):549–563, 1987.
- Mandre, S. Effect of bottom topography on roll wave instabilities. *Woods Hole Oceanographic Institution*, 1:279–295, 2001.
- Manual for Wire-Mesh-System 32x32 V 1.0.5. Teletronic Rossendorf GmbH, 2004.
- Mishima, K & Ishii, M. Theoretical prediction of onset of horizontal slug flow. *J. Fluids Eng.*, 102(4):441–445, 1980.
- Moissis, R. & Griffith, P. Entrance effects in a two-phase slug flow. *J. Heat Transfer*, 84: 29–39, 1962.
- Nydal, O.J. & Andreussi, P. Gas entrainment in a long liquid slug advancing in a near horizontal pipe. *Int. J. Multiphase Flow*, 17(2):179–189, 1991.

- Nydal, O.J. & Banerjee, S. Dynamic slug tracking simulations for gas-liquid flow in pipelines. *Chem. Eng. Commun.*, 141-142:13–39, 1996.
- Nydal, O.J., Pintus, S. & Andreussi, P. Statistical characterization of slug flow in horizontal pipes. *Int. J. Multiphase Flow*, 18(3):439–453, 1992.
- Oliemans, R.V.A., 2001. Applied Multiphase Flows. Delft University of Technology.
- Pols, R.M. & Oliemans, R.V.A. Liquid slug generator for separated gas/liquid flow in pipes. *BHR Conf. Cannes, France*, 1995.
- Prasser, H.-M., 2000. High-speed measurement of the void fraction distribution in ducts by wire-mesh sensors. Proceedings of IMORN-28, Greece.
- Prasser, H.-M., Böttger, A. & Zschau, J. A new electrode-mesh tomograph for gas-liquid flows. *Flow measurement and Instrumentation*, 9:111–119, 1998.
- Prasser, H.-M., Scholz, D. & Zippe, C. Bubble size measurement using wire-mesh sensors. *Flow measurement and Instrumentation*, 12:299–312, 2001.
- Richter, A., Aritomi, M., Prasser, H.-M. & Hampel, R. Approach towards spatial phase reconstruction in transient bubbly flow using wire-mesh sensor. *Int. J. Heat Mass Transfer*, 45:1063–1075, 2002.
- Ruder, Z. & Hanratty, T.J. A definition of gas-liquid plug flow in horizontal pipes. *Int. J. Multiphase Flow*, 26(2):233–242, 1990.
- Simmons, Mark J.H. & Hanratty, Thomas J. Transition from stratified to intermittent flows in small angle upflows. *Int. J. Multiphase Flow*, 27:599–616, 2001.
- Smeets, P.T.M., 2007. Spatially resolved phase distributions in a vertical gas-liquid-liquid flow. Master's thesis, Delft University of Technology.
- Soleimani, A., Al-Sarkhi, A. & Hanratty, T.J. Effect of drag-reducing polymers on pseudo-slugs—interfacial drag and transition to slug flow. *Int. J. Multiphase Flow*, 28(12):1191–1927, 2002.
- Soleimani, A. & Hanratty, T.J. Critical liquid flows for the transition from the pseudo-slug and stratified patterns to slug flow. *Int. J. Multiphase Flow*, 29(1):51–67, 2003.
- Taitel, Y. & Barnea, D. Simplified transient simulation of two phase flow using quasi-equilibrium momentum balances. *Int. J. Multiphase Flow*, 23(3):493–501, 1997.
- Taitel, Y. & Dukler, A.E. A model for predicting flow regime transitions in horizontal and near horizontal gas-liquid flow. *AIChE J.*, 22(1):51–67, 1976.

- Taitel, Y. & Dukler, A.E. A model for slug frequency during gas-liquid flow in horizontal and near horizontal pipes. *Int. J. Multiphase Flow*, 3(6):585–596, 1977.
- Tronconi, Enrico. Prediction of slug frequency in horizontal two-phase slug flow. *AIChE J.*, 36(5):701–709, 1990.
- Ujang, P.M., Lawrence, C.J., Hale, C.P. & Hewitt, G.F. Slug initiation and evolution in two-phase horizontal flow. *Int. J. Multiphase Flow*, 32(5):527–552, 2006.
- Weisman, J., Duncan, D., Gibson, J. & Crawford, T. Effect of fluid properties and pipe diameter on two-phase flow patterns in horizontal lines. *Int. J. Multiphase Flow*, 5(6): 437–462, 1979.
- Woods, B.D. & Hanratty, T.J. Relation of slug stability to shedding rate. *Int. J. Multiphase Flow*, 22(5):809–828, 1996.
- Woods, B.D. & Hanratty, T.J. Influence of the froude number on physical processes determining frequency of slugging in horizontal gas-liquid flows. *Int. J. Multiphase Flow*, 25 (6-7):1195–1223, 1999.
- Woods, B.D., Hurlburt, E.T. & Hanratty, T.J. Mechanism of slug formation in downwardly inclined pipes. *Int. J. Multiphase Flow*, 26:977–998, 2000.
- Woods, Bennett D., Fan, Zhongkiang & Hanratty, Thomas J. Frequency and development of slugs in a horizontal pipe at large liquid flows. *Int. J. Multiphase Flow*, 32:902–925, 2006.
- Zabaras, G.J. Prediction of slug frequency for gas/liquid flows. *SPE Journal*, 5(3):252–258, 2000.
- Zheng, G., Brill, J.P. & Taitel, Y. Slug flow behavior in a hilly terrain pipeline. *Int. J. Multiphase Flow*, 20(1):63–79, 1993.
- Zitha, P.L.J., 2000. Well treatment and water shutoff by polymer gels. Delft University Press, Delft.

Dankwoord

Dit is het dan, het boekje dat staat voor de afsluiting van een periode, de afronding van mijn promotie onderzoek. Dit is dan ook het moment om een aantal mensen te bedanken die hebben bijgedragen aan de tot standkoming van dit proefschrift. Want ook al prijkt alleen mijn naam op de cover van dit boekwerkje, ik heb het zeker niet allemaal in mijn eentje gedaan.

Ten eerste wil ik mijn promotoren, René en Rob, bedanken voor de vele verhelderende gesprekken over mijn onderzoek. Ondanks jullie andere bezigheden en de zomervakantie hebben jullie toch tijd vrij gemaakt om kritisch door mijn proefschrift heen te gaan, om na een paar correctieslagen tot dit eindresultaat te kunnen komen.

Binnen het project hebben ook Herman, Pieter, Usama en Bart hun steentje bij gedragen. Eén voor één hadden jullie allemaal je eigen idee en visie over de sluggies, zoals ze soms liefkozend werden genoemd. Het was bijzonder inspirerend om met jullie samen te mogen werken.

Bij een experimenteel onderzoek heb je een opstelling nodig, en die had ik, enkele honderden meters aan buizen, slangen en kabels stonden tot mijn beschikking. En dan moet alles nog naar behoren gaan functioneren. Aangezien er nog wel eens iets aangepast, of vaker nog, gerepareerd moest worden, zijn technici daarbij onontbeerlijk. Ab, Jaap B, Jaap K, Jaap v R, Evert en Wouter, jullie stonden altijd klaar met een praktische oplossing voor mijn soms onmogelijke wensen. Op het gebied van computers wist Peter overal wel een scrijpie voor te bedenken en kon hij zoekgeraakte bestanden weer voor je terugvinden.

In de loop der jaren heb ik heel wat kamergenoten gehad, die voor de nodige gezelligheid zorgden tijdens de soms lange dagen in het Kramerslab. Ruurd, Martin, Wouter, Hugo, Jos, Özgür, Annekatrien, Maria en Zaki, het was een onvergetelijke tijd. Naast mijn kamergenoten mogen ook Roel en Volkert niet ontbreken, voor de vele nuttige tips over GnuPlot en L^AT_EX. En niet te vergeten de appeltaarten, brownies, speculaas en andere lekkernijen die Annekatrien van tijd tot tijd meebracht voor bijzondere gelegenheden, danwel om de technici te stimuleren om haar project wat meer prioriteit te geven. We hebben er met z'n allen heerlijk van gesmuld.

Voor de papierwinkel en de meest uiteenlopende vragen kon ik altijd terecht bij de dames van het secretariaat. Er zijn in de loop van de jaren vele gezichten voorbij gekomen, Karin, Thea, Gulizar, Janice, Mirjam en momenteel wordt het secretariaat bevrouwd door Amanda en Angela. Bedankt voor jullie hulp.

Ook buiten het lab zijn een aantal mensen heel bijzonder voor me geweest. Bedankt allemaal voor de gezellige momenten de afgelopen jaren. Hopelijk zullen er in de toekomst nog vele volgen.

Dankzij de creatieve visie van Cees heeft dit boekje een kaft die alles behalve standaard is.

Tot slot wil ik mijn familie en in het bijzonder mijn ouders bedanken. Jullie hebben me altijd gesteund in mijn keuze voor dit project, ook al hadden jullie er vaak geen idee van waar ik mee bezig was.

Curriculum Vitae

De auteur is geboren op 6 augustus 1978 in Goes. In 1996 behaalde hij zijn diploma Voorbereidend Wetenschappelijk Onderwijs (VWO) aan de Stedelijke Scholen Gemeenschap Het Goese Lyceum.

Daarna begon hij aan de Technische Universiteit Eindhoven aan de gecombineerde opleiding Technische Wiskunde en Technische Natuurkunde. Hij behaalde van beide opleidingen de propedeuse. De studie Technische Natuurkunde werd volledig doorlopen en in 2002 afgerond met een diploma. Tijdens deze studie heeft de auteur een interne stage opdracht uitgevoerd bij de groep Toepassing van Ionen Bundels (TIB) van Martien de Voigt aan stromingsvisualisatie met radioactieve tracers. Via dezelfde groep heeft hij een externe stage gedaan bij Themphos International in Vlissingen op het gebied van aerosolen detectie. Het afstudeeronderzoek op het gebied van 2-dimensionale turbulentie is uitgevoerd binnen de groep Turbulentie en Weveldynamica (WDY) van Gert-Jan van Heijst.

Na een kort project bij het IRI, het huidige R3 van de Technische Universiteit Delft, is in 2003 een start gemaakt met een promotieonderzoek bij de faculteit Technische Natuurwetenschappen (TNW) van de Technische Universiteit Delft. Het onderzoek op het gebied van tweefasenstroming is begeleid door de promotoren René Oliemans en Rob Mudde. De resultaten van het onderzoek zijn beschreven in dit proefschrift. Na het afronden van dit project in 2007 is de auteur begonnen als innovator bij de business unit Industrial Modelling and Control van TNO in Delft.

